

# Benchmarking Di-Higgs Production in Various Extended Higgs Sector Models

Hamza Abouabid<sup>1\*</sup>, Abdesslam Arhrib<sup>1†</sup>, Duarte Azevedo<sup>3,4‡</sup>, Jaouad El Falaki<sup>5§</sup>,  
Pedro. M. Ferreira<sup>2,6¶</sup>, Margarete Mühlleitner<sup>3||</sup>, Rui Santos<sup>2,6\*\*</sup>

<sup>1</sup>*Abdelmalek Essaadi University, Faculty of Sciences and Techniques  
Ancienne route de l'aéroport, Ziaten, B.P. 416, Tangier, Morocco*

<sup>2</sup>*ISEL - Instituto Superior de Engenharia de Lisboa,  
Instituto Politécnico de Lisboa 1959-007 Lisboa, Portugal*

<sup>3</sup>*Institute for Theoretical Physics, Karlsruhe Institute of Technology,  
Wolfgang-Gaede Str. 1, 76128 Karlsruhe, Germany*

<sup>4</sup>*Institute for Astroparticle Physics, Karlsruhe Institute of Technology,  
Hermann-von-Helmholtz-Platz 1, 76344 Eggenstein-Leopoldshafen, Germany*

<sup>5</sup>*LPTHE, Physics Department, Faculty of Science, Ibn Zohr University,  
P.O.B. 8106, Agadir, Morocco*

<sup>6</sup>*Centro de Física Teórica e Computacional, Faculdade de Ciências,  
Universidade de Lisboa, Campo Grande, Edifício C8 1749-016 Lisboa, Portugal*

## Abstract

We present a comprehensive study on Higgs pair production in various archetypical extended Higgs sectors such as the real and the complex 2-Higgs-Doublet Model, the 2-Higgs-Doublet Model augmented by a real singlet field and the Next-to-Minimal Supersymmetric extension of the Standard Model. We take into account all relevant theoretical and experimental constraints, in particular the experimental limits on non-resonant and resonant Higgs pair production. We present the allowed cross sections for Standard Model (SM)-like Higgs pair production and the ranges of the SM-like Yukawa and trilinear Higgs self-coupling that are still compatible with the applied constraints. Furthermore, we give results for the pair production of a SM-like with a non-SM-like Higgs boson and for the production of a pair of non-SM-like Higgs bosons. We find that di-Higgs production in the models under investigation can exceed the SM rate substantially, not only in the non-resonance region but also due to resonant enhancement. We give several benchmarks with interesting features such as large cross sections, the possibility to test CP violation, Higgs-to-Higgs cascade decays or di-Higgs production beating single Higgs production. In all of our benchmark points, the next-to-leading order QCD corrections are included in the large top-mass limit. For these points, we found that, depending on the model and the Higgs pair final state, the corrections increase the leading order cross section by a factor of 1.79 to 2.24. We also discuss the relation between the description of Higgs pair production in an effective field theory approach and in the specific models investigated here.

---

\*E-mail: aabouabid@uae.ac.ma

†E-mail: aarhrib@uae.ac.ma

‡E-mail: duarte.azevedo@kit.edu

§E-mail: jaouad.elfalaki@gmail.com

¶E-mail: pmmferreira@fc.ul.pt

||E-mail: margarete.muehlleitner@kit.edu

\*\*E-mail: rasantos@fc.ul.pt

# Contents

<b>1</b>	<b>Introduction</b>	<b>2</b>
<b>2</b>	<b>The Models</b>	<b>4</b>
2.1	The Real and Complex 2HDM . . . . .	4
2.2	The N2HDM . . . . .	7
2.3	The NMSSM . . . . .	7
<b>3</b>	<b>Scans and Theoretical and Experimental Constraints</b>	<b>9</b>
<b>4</b>	<b>Numerical Results for SM-Like Higgs Pair Production</b>	<b>11</b>
4.1	Gluon Fusion into Higgs Pairs . . . . .	12
4.2	The Impact of Di-Higgs Constraints . . . . .	14
4.3	Parameter Dependences . . . . .	17
4.3.1	Distributions of the Mass Spectra . . . . .	18
4.3.2	Higgs Couplings . . . . .	18
4.3.3	Allowed Coupling Ranges and Impact of Di-Higgs Constraints . . . . .	19
4.4	SM-Like Higgs Pair Production . . . . .	22
<b>5</b>	<b>Benchmarks for SM-Like Higgs Pair Production</b>	<b>26</b>
5.1	Resonant SM-like $H_1 H_1$ Production in the R2HDM-I . . . . .	27
5.2	Resonant SM-like $H_1 H_1$ Production in the R2HDM-II . . . . .	28
5.3	Resonant SM-like $H_1 H_1$ Production in the C2HDM-I . . . . .	29
5.4	Resonant SM-like $H_2 H_2$ Production in the C2HDM-I . . . . .	30
5.5	Resonant SM-like $H_1 H_1$ Production in the C2HDM-II . . . . .	30
5.6	Resonant SM-like $H_1 H_1$ Production in the N2HDM-I . . . . .	31
5.7	Resonant SM-like $H_2 H_2$ Production in the N2HDM-I . . . . .	32
5.8	Resonant SM-like $H_1 H_1$ Production in the N2HDM-II . . . . .	33
5.9	Resonant SM-like $H_2 H_2$ Production in the N2HDM-II . . . . .	34
5.10	Resonant SM-like $H_1 H_1$ Production in the NMSSM . . . . .	34
5.11	Resonant SM-like $H_2 H_2$ Production in the NMSSM . . . . .	36
<b>6</b>	<b>Constraining Model Parameters</b>	<b>37</b>
<b>7</b>	<b>Effective Field Theory versus Specific Models</b>	<b>38</b>
<b>8</b>	<b>Mixed Higgs Pair Final States - <math>H_{\text{SM}} + \Phi</math></b>	<b>42</b>
8.1	The $(b\bar{b})(b\bar{b})$ Final State . . . . .	43
8.2	The $(b\bar{b})(WW)$ Final State . . . . .	43
8.3	The $(b\bar{b})(t\bar{t})$ Final State . . . . .	45
8.4	Multi-Higgs Final States . . . . .	46
8.4.1	Non-SM-like Higgs Search: Di-Higgs beats Single Higgs . . . . .	46
<b>9</b>	<b>Non-SM-Like Higgs Pair Final States</b>	<b>50</b>
<b>10</b>	<b>Conclusions</b>	<b>50</b>
<b>A</b>	<b>Resonant and Non-Resonant Production Cross Sections</b>	<b>53</b>
<b>B</b>	<b>Alignment Limit in the C2HDM</b>	<b>54</b>

## 1 Introduction

The discovery of the Higgs boson in 2012 by the ATLAS [1] and CMS [2] collaborations at the Large Hadron Collider (LHC) structurally completes the Standard Model (SM) of particle physics. The subsequent investigation of its properties revealed the Higgs boson to be very SM-like [3–6]. In order to verify that the Brout-Englert-Higgs mechanism [7–10] is indeed responsible for the generation of elementary particle masses we not only need to measure the Higgs couplings to massive SM particles at the highest precision but we also need to reconstruct the Higgs potential itself to establish experimentally whether indeed its Mexican hat shape is responsible for the Brout-Englert-Higgs mechanism of spontaneous symmetry breaking [11, 12]. Moreover, despite the success of the SM, which has been tested very accurately at the quantum level, some open problems remain that cannot be solved by the SM, like *e.g.* the nature of Dark Matter (DM) or why there is more matter than antimatter in the universe. Extensions of the Higgs sector beyond the SM can provide a DM candidate [13–22]. Electroweak baryogenesis provides a mechanism to dynamically generate the matter-anti-matter asymmetry if the three Sakharov conditions [23] are fulfilled. This may be possible within extended Higgs sectors with additional scalar degrees of freedom and new sources of CP violation. In summary, the investigation of the Higgs potential itself will provide deep insights into the mechanism underlying electroweak symmetry breaking and into the possible landscape of new physics extensions of the Higgs sector. Understanding the Higgs potential will help us to answer some of the open questions of contemporary particle physics.

In the SM the trilinear and quartic Higgs self-couplings are given in terms of the Higgs boson mass. This is not the case in extended Higgs sectors. Experimentally, the Higgs self-interactions are accessible in multi-Higgs production, the trilinear Higgs self-coupling in double and the quartic Higgs self-coupling in triple Higgs production. At the LHC the dominant di-Higgs production process is given by gluon fusion into Higgs pairs [24–26]. At leading order the process is mediated by heavy quark triangle and box diagrams [27–29], implying a small SM cross section of 31.05 fb at  $\sqrt{s} = 13$  TeV. At  $\text{FT}_{\text{approx}}$  [30] and for a c.m. energy of  $\sqrt{s} = 13$  TeV. At  $\text{FT}_{\text{approx}}$ , the cross section is computed at next-to-next-to-leading order (NNLO) QCD in the heavy-top limit with full leading order (LO) and next-to-leading order (NLO) mass effects and full mass dependence in the one-loop double real corrections at NNLO QCD. Note that the NLO cross section in the heavy top limit was first presented in [31] supplemented by a large-top-mass expansion [32, 33] and the inclusion of the full real corrections [34, 35]. The NLO result including the full top-quark mass dependence has been calculated by [36–40] and confirmed in [41, 42] by applying suitable expansion methods. The NNLO corrections in the large  $m_t$  limit have been calculated in [43–45], the results at next-to-next-to-leading logarithmic accuracy (NNLL) became available in [46, 47]. And the corrections up to next-to-next-to-next-to leading order ( $\text{N}^3\text{LO}$ ) were presented in [48–50] for the heavy top-mass limit. Note that these corrections apply to the SM case and cannot necessarily be taken over to extended Higgs sectors where *e.g.* the bottom loops may play an important role or additional diagrams are involved.

In the SM the process suffers from a destructive interference between the triangle and box diagrams which makes its observation very challenging at the LHC. In extended Higgs sectors SM-like di-Higgs production can be enhanced because Yukawa and trilinear Higgs self-couplings are modified relative to the SM. This can result in altering the interference structure between

the various diagrams. Additional Higgs bosons can enhance the cross section resonantly and new colored particles that run in the loops can also lead to an increased cross section. Therefore, extended Higgs sectors not only answer some of the open questions but they can possibly also facilitate access to di-Higgs production. Furthermore, the additional Higgs states lead to a large variety of di-Higgs final states implying a plethora of multi-particle final state signatures. To get a comprehensive picture of which final state signatures in Higgs pair production processes are possible and to be able to give a meaningful guideline to experimentalists in their searches for Higgs pair production, we have to take into account all available experimental and theoretical constraints on beyond-the-SM (BSM) extensions. Since the discovered Higgs boson behaves very SM-like, new physics extensions become increasingly constrained. The trilinear Higgs self-coupling, however, is not as constrained as single Higgs couplings yet [51, 52] and we may still expect some distinctive signatures from Higgs pair production.

The goal of this paper is to investigate Higgs pair production in some archetypical BSM extensions. Imposing all available constraints - also from recent di-Higgs searches - we derive the parameter space of these models that is still allowed. Based on this data set we will derive limits on the involved couplings in Higgs pair production, namely the trilinear Higgs self-coupling and the Higgs-Yukawa coupling, investigate the possible enhancement (or also suppression) of SM-like Higgs pair production and investigate what kind of non-SM-like signatures might appear. We provide benchmark points so that experimentalists can match their derived limits on specific models for further interpretation. Since the experiments derive limits from non-resonant and resonant Higgs pair production and our extended Higgs sector models include both effects, we derive a strategy on how we can apply the available di-Higgs limits on our models. We included for all benchmark scenarios and parameter points fulfilling the applied constraints the information on the resonant part of the cross section, where applicable. Our aim is to give a global and comprehensive overview on Higgs pair production in BSM Higgs sectors.

The models that we consider are both non-supersymmetric and supersymmetric ones. Supersymmetry (SUSY) [53–66] is able to solve many of the open problems of the SM. The non-minimal supersymmetric extension (NMSSM) [67–78] solves the little hierarchy problem and more easily complies with the discovered SM-like Higgs mass after inclusion of the higher-order corrections [79]. The Higgs sector consists of two Higgs doublets to which a complex singlet superfield is added so that after electroweak symmetry breaking (EWSB) we have three neutral CP-even, two neutral CP-odd and two charged Higgs bosons in the spectrum. Supersymmetric relations constrain the Higgs potential parameters in a different way than non-SUSY models. Therefore, we also investigate non-SUSY Higgs sector extensions where the trilinear couplings are less constrained from a theoretical point of view. This way we make sure not to miss some possibly interesting di-Higgs signatures. We start with one of the most popular extensions complying with  $\rho = 1$  at tree level, the CP-conserving 2-Higgs doublet model (R2HDM) [80, 81] where a second Higgs doublet is added to the SM sector. Incorporating a minimal set of BSM Higgs bosons (five in total, three neutral and two charged ones) allows for resonant di-Higgs enhancement. We additionally take into account the possibility of CP violation (which is required for electroweak baryogenesis) by investigating the CP-violating 2HDM (C2HDM) [81–84] which consists of three CP-mixed and two charged Higgs bosons. In this case the SM-like Higgs couplings can be diluted by CP admixture, the same happens through singlet admixture. Thus, light Higgs bosons may not be excluded yet because they may have escaped discovery through small couplings to the SM particles. Such a singlet admixture is realized in the next-to-2HDM (N2HDM) [18, 85, 86]. By adding a real singlet field to the 2HDM Higgs sector the Higgs spec-

trum then consists of three neutral CP-even Higgs bosons, one neutral CP-odd and two charged Higgs bosons, allowing for the possibility of Higgs-to-Higgs cascade decays. This is also possible in the C2HDM and the NMSSM. For simplicity, we will focus on the type I and II versions of the R2HDM, C2HDM and N2HDM. With the models investigated in this paper<sup>1</sup> we cover a broad range of interesting new physics and in particular a large variety of possible new physics signatures in di-Higgs production. In turn, we provide guidelines to the experiment. We also take the occasion to confront our models with a simple effective field theory (EFT) approach and investigate to which extent this model-independent parametrisation of new physics, becoming effective at high scales, can describe the effects in our investigated specific UV-complete models.

The paper is organised as follows. In Sec. 2, we briefly introduce our models. In Sec. 3, we present the regions which we scanned for each model and the theoretical and experimental constraints that we take into account. After a brief re-capitulation of the di-Higgs production process through gluon fusion, we explain in detail in Sec. 4 how we apply the experimental limits from resonant and non-resonant di-Higgs searches on our models. We then investigate the impact of the di-Higgs constraints on our parameter sample. We present the distributions of the Higgs mass spectra in the different models and give the ranges for the SM-like Higgs top-Yukawa and Higgs self-couplings that are still allowed after considering all constraints. Subsequently, we present scatter plots for all models showing the cross section values for SM-like Higgs pair production that are compatible with the constraints, and we list the maximum values for resonant and non-resonant Higgs pair production possible in each model. In Sec. 5 we present the maximum values from resonant SM-like di-Higgs production and present the corresponding benchmark points along with their specific features. In Sec. 6 we investigate to which extent di-Higgs production can constrain the parameter values of the models. Section 7 is devoted to the comparison of the EFT description of BSM Higgs pair production with the results in specific UV-finite models. The last two sections, 8 and 9, are devoted to the pair production of a SM-like Higgs together with a non-SM-like Higgs, of a pair of non-SM-like Higgs bosons and to the cascade decays leading to multi-Higgs final states. We also present benchmark points where di-Higgs production beats single Higgs production. We conclude in Sec. 10. In the Appendix we present cross sections for resonant and non-resonant production and discuss the conditions for alignment in the C2HDM and the N2HDM.

## 2 The Models

In this section we provide a very brief description of the different models we will be studying, highlighting the diverse scalar spectra of each model as well as the different input parameter sets for each of them.

### 2.1 The Real and Complex 2HDM

The 2HDM is one of the simplest extensions of the SM, where instead of a single Higgs doublet we now have two, carrying identical hypercharges. The model was first proposed by Lee in 1973 [80] to provide an extra source of CP violation via spontaneous symmetry breaking, and has a rich phenomenology (for a review, see [141]). We considered the 2HDM version with a softly broken discrete  $\mathbb{Z}_2$  symmetry of the form  $\Phi_1 \rightarrow \Phi_1$  and  $\Phi_2 \rightarrow -\Phi_2$ . In terms of the two

---

<sup>1</sup>For a selection of further works on Higgs pair production and the Higgs self-coupling in the framework of BSM Higgs sectors in non-SUSY models, see *e.g.* [87–128], and in SUSY models, see *e.g.* [94, 120, 129–140].

	$u$ -type	$d$ -type	leptons	$Q$	$u_R$	$d_R$	$L$	$l_R$
type I	$\Phi_2$	$\Phi_2$	$\Phi_2$	+	−	−	+	−
type II	$\Phi_2$	$\Phi_1$	$\Phi_1$	+	−	+	+	−
flipped (FL)	$\Phi_2$	$\Phi_1$	$\Phi_2$	+	−	−	+	+
lepton-specific (LS)	$\Phi_2$	$\Phi_2$	$\Phi_1$	+	−	+	+	−

Table 1: Four left rows: The four Yukawa types of the  $\mathbb{Z}_2$ -symmetric 2HDM, stating which Higgs doublet couples to the different fermion types. Five right columns: Corresponding  $\mathbb{Z}_2$  assignment for the quark doublet  $Q$ , the up-type quark singlet  $u_R$ , the down-type quark singlet  $d_R$ , the lepton doublet  $L$ , and the lepton singlet  $l_R$ .

$SU(2)_L$  Higgs doublets  $\Phi_{1,2}$  with hypercharge  $Y = +1$ , the most general scalar potential which is  $SU(2)_L \times U(1)_Y$  invariant and possesses a softly broken  $\mathbb{Z}_2$  symmetry is given by

$$\begin{aligned}
V_{(C)2\text{HDM}} = & m_{11}^2 |\Phi_1|^2 + m_{22}^2 |\Phi_2|^2 - m_{12}^2 (\Phi_1^\dagger \Phi_2 + h.c.) + \frac{\lambda_1}{2} (\Phi_1^\dagger \Phi_1)^2 + \frac{\lambda_2}{2} (\Phi_2^\dagger \Phi_2)^2 \\
& + \lambda_3 (\Phi_1^\dagger \Phi_1) (\Phi_2^\dagger \Phi_2) + \lambda_4 (\Phi_1^\dagger \Phi_2) (\Phi_2^\dagger \Phi_1) + \left[ \frac{\lambda_5}{2} (\Phi_1^\dagger \Phi_2)^2 + h.c. \right]. \quad (2.1)
\end{aligned}$$

The  $\mathbb{Z}_2$  symmetry is introduced in the model in order to avoid dangerous flavour-changing neutral currents (FCNCs) mediated by the neutral scalar. Since the  $\mathbb{Z}_2$  symmetry is extended to the fermion sector, it will force all families of same-charge fermions to couple to a single doublet which eliminates tree-level FCNCs [141, 142]. This implies four different types of doublet couplings to the fermions listed in Tab. 1.

The dimension-2 coefficient  $m_{12}^2$  which breaks the  $\mathbb{Z}_2$  symmetry softly, is introduced to allow for the existence of a *decoupling limit*, in which all scalars other than the SM-like one have very large masses, with suppressed couplings to fermions and gauge bosons. Furthermore, in the case where all parameters in Eq. (2.1) are real we are in the CP-conserving 2HDM, which we will call R2HDM from now on. In the case of complex  $m_{12}^2$  and  $\lambda_5$  parameters<sup>2</sup> the model explicitly breaks the CP symmetry. This is the CP-violating version of the 2HDM, called C2HDM. The two complex doublet fields can be parametrised as

$$\Phi_i = \begin{pmatrix} \phi_i^+ \\ \frac{1}{\sqrt{2}}(v_i + \rho_i + i\eta_i) \end{pmatrix}, \quad i = 1, 2, \quad (2.2)$$

with  $v_{1,2}$  being the vacuum expectation values (VEVs) of the two doublets  $\Phi_{1,2}$ . After EWSB three of the eight degrees of freedom initially present in  $\Phi_{1,2}$  are taken by the Goldstone bosons to give masses to the gauge bosons  $W^\pm$  and  $Z$ , and we are left with five physical Higgs bosons. In the CP-conserving case, these are two neutral CP-even Higgs bosons,  $h$  and  $H$ , where by convention  $m_h < m_H$ , one neutral CP-odd  $A$  and a pair of charged Higgs bosons  $H^\pm$ . In the following we will denote  $h$  and  $H$  by  $H_1$  and  $H_2$ , respectively, in order to standardise the notation for all considered models. The CP-even neutral Higgs mass matrix is diagonalised by a mixing angle  $\alpha$ , whereas both the neutral CP-odd and charged mass matrices are diagonalised by a mixing angle  $\beta$ , such that

$$\tan \beta = \frac{v_2}{v_1}. \quad (2.3)$$

<sup>2</sup>The phases of these two parameters must be such that  $\arg(m_{12}^2) \neq \arg(\lambda_5)/2$ , otherwise a trivial field rephasing would render the potential real.

In the C2HDM, the three neutral Higgs bosons mix, resulting in three neutral Higgs mass eigenstates  $H_i$  ( $i = 1, 2, 3$ ) with no definite CP quantum number and which by convention are ordered as  $m_{H_1} \leq m_{H_2} \leq m_{H_3}$ . The rotation matrix  $R$  diagonalising the neutral Higgs sector can be parametrised in terms of three mixing angles  $\alpha_i$  ( $i = 1, 2, 3$ ) as

$$R = \begin{pmatrix} c_1 c_2 & s_1 c_2 & s_2 \\ -(c_1 s_2 s_3 + s_1 c_3) & c_1 c_3 - s_1 s_2 s_3 & c_2 s_3 \\ -c_1 s_2 c_3 + s_1 s_3 & -(c_1 s_3 + s_1 s_2 c_3) & c_2 c_3 \end{pmatrix}, \quad (2.4)$$

where  $s_i \equiv \sin \alpha_i$ ,  $c_i \equiv \cos \alpha_i$ , and, without loss of generality, the angles vary in the range

$$-\frac{\pi}{2} \leq \alpha_i \leq \frac{\pi}{2}. \quad (2.5)$$

The CP-conserving limit of the C2HDM is obtained by setting  $\alpha_2 = \alpha_3 = 0$  and  $\alpha_1 = \alpha + \pi/2$  [83]. The shift by  $\pi/2$  in this limit is necessary to match the usual 2HDM convention. We discuss the alignment limit, where the C2HDM approaches the SM in Appendix B.

By identifying

$$v = \sqrt{v_1^2 + v_2^2}, \quad (2.6)$$

where  $v$  is the SM VEV,  $v \approx 246$  GeV, and using the two minimisation conditions, the scalar sector of the 2HDM can be described by eight independent input parameters. For convenience in the parameter scans, *cf.* Sec. 3, we replace the mixing angle  $\alpha$  by the coupling of the  $H_2$  state to massive gauge bosons ( $V = Z, W^\pm$ ), which we represent by  $c_{H_2 V V}$ . Thus we have as input parameter set

$$v, \quad \tan \beta, \quad c_{H_2 V V}, \quad m_{H_1}, \quad m_{H_2}, \quad m_A, \quad m_{H^\pm} \quad \text{and} \quad m_{12}^2. \quad (2.7)$$

In the C2HDM, as stated above, the parameters  $\lambda_5$  and  $m_{12}^2$  can be complex so that the C2HDM Higgs sector at tree level is described by ten parameters. Notice that it is always possible to perform a basis change to make one of these phases vanish so that we end up with nine independent parameters. In the C2HDM the three neutral Higgs boson masses are not independent. The third neutral Higgs mass is a dependent quantity and is obtained from the input parameters, *cf.* [143]. We hence choose two of the three neutral Higgs boson masses as input values and calculate the third one. The chosen input masses are called  $m_{H_i}$  and  $m_{H_j}$  with  $H_i$  per default denoting the lighter one, *i.e.*  $m_{H_i} < m_{H_j}$ . They denote any two of the three neutral Higgs bosons among which we take one to be the 125 GeV SM-like scalar. We furthermore replace the three mixing angles  $\alpha_{1,2,3}$  by two coupling values of  $H_i$  and by a matrix element of our rotation matrix. These are the squared  $H_i$  couplings to the massive gauge bosons  $V$  and to the top quarks  $t$ ,  $c_{H_i V V}^2$  and  $c_{H_i t t}^2$ , respectively, and the neutral mixing matrix entry  $R_{23}$ . We furthermore fix the sign of  $R_{13}$ ,  $\text{sg}(R_{13})$ , to either +1 or -1 in order to lift the degeneracy that we introduce by specifying only the squared values of the  $H_i$  couplings. This choice of input parameters complies with the input parameters of the program code **ScannerS** that we will use for our parameter scans as explained below. We hence have the input parameter set

$$v, \quad \tan \beta, \quad c_{H_i V V}^2, \quad c_{H_i t t}^2, \quad R_{23}, \quad m_{H_i}, \quad m_{H_j}, \quad m_{H^\pm} \quad \text{and} \quad \text{Re}(m_{12}^2). \quad (2.8)$$

## 2.2 The N2HDM

In the following, we give a brief introduction to the N2HDM and refer to [85] for more details. The scalar potential of the N2HDM is obtained from the 2HDM potential by adding a real singlet field  $\Phi_S$ . In terms of the two  $SU(2)_L$  Higgs doublets  $\Phi_1$  and  $\Phi_2$ , defined in Eq. (2.2), and the singlet field, defined as

$$\Phi_S = v_S + \rho_S , \quad (2.9)$$

the N2HDM potential is given by

$$V_{\text{N2HDM}} = V_{\text{2HDM}} + \frac{1}{2}m_S^2\Phi_S^2 + \frac{\lambda_6}{8}\Phi_S^4 + \frac{\lambda_7}{2}(\Phi_1^\dagger\Phi_1)\Phi_S^2 + \frac{\lambda_8}{2}(\Phi_2^\dagger\Phi_2)\Phi_S^2 . \quad (2.10)$$

The above scalar potential is obtained by imposing two  $\mathbb{Z}_2$  symmetries,

$$\begin{aligned} \Phi_1 &\rightarrow \Phi_1 , & \Phi_2 &\rightarrow -\Phi_2 , & \Phi_S &\rightarrow \Phi_S & \text{ and} \\ \Phi_1 &\rightarrow \Phi_1 , & \Phi_2 &\rightarrow \Phi_2 , & \Phi_S &\rightarrow -\Phi_S . \end{aligned} \quad (2.11)$$

The first (softly-broken)  $\mathbb{Z}_2$  symmetry is the extension of the usual 2HDM  $\mathbb{Z}_2$  symmetry to the N2HDM which, once extended to the Yukawa sector, will forbid FCNCs at tree level, implying four different N2HDM versions just like in the 2HDM, *cf.* Tab. 1. The second  $\mathbb{Z}_2$  symmetry is an exact symmetry which will be spontaneously broken by the singlet VEV and as such does not allow the model to have a DM candidate. Other versions of the model choose parameters such that  $v_S = 0$  yielding very interesting DM phenomenology, but in the current work we will not consider these possibilities.

After EWSB, we have three neutral CP-even Higgs bosons  $H_{1,2,3}$  with masses ranked as  $m_{H_1} < m_{H_2} < m_{H_3}$ , one neutral CP-odd boson  $A$  and a pair of charged Higgs bosons  $H^\pm$ . The physical states  $H_{1,2,3}$  are obtained from the weak basis  $(\rho_1, \rho_2, \rho_S)$  by an orthogonal transformation  $R$  which is defined by 3 mixing angles  $\alpha_{1,2,3}$  that are in the same range as in the C2HDM. After exploiting the minimisation conditions, we are left with twelve independent input parameters for the N2HDM. For the scan, we will again replace the three mixing angles  $\alpha_{1,2,3}$  by the squared  $H_1$  couplings to massive gauge bosons  $V$  and the top quarks  $t$ ,  $c_{H_1VV}^2$  and  $c_{H_1tt}^2$ , respectively, and the neutral mixing matrix element  $R_{23}$ , so that our input parameters read

$$\tan\beta , c_{H_1VV}^2 , c_{H_1tt}^2 , R_{23} , m_{H_1} , m_{H_2} , m_{H_3} , m_A , m_{H^\pm} , v , v_S , \text{ and } m_{12}^2 . \quad (2.12)$$

Like in the 2HDM, we fix  $\text{sg}(R_{13})$  to either +1 or -1 in order to lift the introduced degeneracy through the squared values of the  $H_1$  couplings. The limit of the real 2HDM with an added decoupled singlet field is obtained from the N2HDM spectrum by letting  $\alpha_{2,3} \rightarrow 0$  and  $\alpha_1 \rightarrow \alpha + \pi/2$ . Again, the shift by  $\pi/2$  in this limit is necessary to match the usual 2HDM convention. The alignment limit for the N2HDM is discussed in Appendix C.

## 2.3 The NMSSM

As a supersymmetric benchmark model, we consider the Next-to Minimal Supersymmetric SM (NMSSM) [69–78]. It extends the two doublet fields  $\hat{H}_u$  and  $\hat{H}_d$  of the MSSM by a complex superfield  $\hat{S}$ . When the singlet field acquires a non-vanishing VEV, this not only solves the  $\mu$  problem [144] but, compared to the MSSM, it also relaxes the tension on the stop mass values that need to be large for the SM-like Higgs boson mass value to be compatible with the measured

125.09 GeV. Indeed in supersymmetry the neutral Higgs masses are given in terms of the gauge parameters at tree level so that there is an upper mass bound on the lightest neutral scalar which, in the MSSM, is given by the  $Z$  boson mass. Substantial higher-order corrections to the Higgs boson mass are therefore required to obtain phenomenologically valid mass values for the SM-like Higgs boson. The additional singlet contribution to the tree-level mass of the lightest neutral Higgs boson shifts its mass to larger values compared to the MSSM prediction, thus no longer requiring large radiative corrections. The scale-invariant NMSSM superpotential that is added to the MSSM superpotential  $W^{\text{MSSM}}$  reads

$$\begin{aligned} W^{\text{NMSSM}} &= -\lambda \hat{S} \hat{H}_u \cdot \hat{H}_d + \frac{\kappa}{3} \hat{S}^3 + W^{\text{MSSM}}, \quad \text{with} \\ W^{\text{MSSM}} &= -y_t \hat{Q}_3 \hat{H}_u \hat{t}_R^c + h_b \hat{Q}_3 \hat{H}_d \hat{b}_R^c + y_\tau \hat{L}_3 \hat{H}_d \hat{\tau}_R^c, \end{aligned} \quad (2.13)$$

where for simplicity we only included the third generation fermion superfields, given by the left-handed doublet quark ( $\hat{Q}_3$ ) and lepton ( $\hat{L}_3$ ) superfields, and the right-handed singlet quark ( $\hat{t}_R^c, \hat{b}_R^c$ ) and lepton ( $\hat{\tau}_R^c$ ) superfields. The NMSSM-type couplings  $\lambda$  and  $\kappa$  are dimensionless and taken real since we consider the CP-conserving NMSSM. The Yukawa couplings  $y_t, y_b, y_\tau$  can always be taken real. The scalar part of  $\hat{S}$  will develop a VEV  $v_S/\sqrt{2}$ , which dynamically generates the effective  $\mu$  parameter  $\mu_{\text{eff}} = \lambda v_S/\sqrt{2}$  through the first term in the superpotential. The second term, cubic in  $\hat{S}$ , breaks the Peccei-Quinn symmetry and thus avoids a massless axion, and  $W^{\text{MSSM}}$  contains the Yukawa interactions. The symplectic product  $x \cdot y = \epsilon_{ij} x^i y^j$  ( $i, j = 1, 2$ ) is built by the antisymmetric tensor  $\epsilon_{12} = \epsilon^{12} = 1$ . The soft SUSY breaking Lagrangian reads

$$\begin{aligned} \mathcal{L}_{\text{soft, NMSSM}} &= -m_{H_u}^2 |H_u|^2 - m_{H_d}^2 |H_d|^2 - m_{\tilde{Q}_3}^2 |\tilde{Q}_3|^2 - m_{\tilde{t}_R}^2 |\tilde{t}_R|^2 - m_{\tilde{b}_R}^2 |\tilde{b}_R|^2 - m_{\tilde{L}_3}^2 |\tilde{L}_3|^2 \\ &\quad - m_{\tilde{\tau}_R}^2 |\tilde{\tau}_R|^2 + (y_t A_t H_u \cdot \tilde{Q}_3 \tilde{t}_R^c - y_b A_b H_d \cdot \tilde{Q}_3 \tilde{b}_R^c - y_\tau A_\tau H_d \cdot \tilde{L}_3 \tilde{\tau}_R^c + \text{h.c.}) \\ &\quad - \frac{1}{2} \left( M_1 \tilde{B} \tilde{B} + M_2 \sum_{a=1}^3 \tilde{W}^a \tilde{W}_a + M_3 \sum_{a=1}^8 \tilde{G}^a \tilde{G}_a + \text{h.c.} \right) \\ &\quad - m_S^2 |S|^2 + (\lambda A_\lambda S H_d \cdot H_u - \frac{1}{3} \kappa A_\kappa S^3 + \text{h.c.}), \end{aligned} \quad (2.14)$$

where again only the third generation of fermions and sfermions have been taken into account. The tilde over the fields denotes the complex scalar component of the corresponding superfields. The soft SUSY breaking gaugino parameters  $M_k$  ( $k = 1, 2, 3$ ) of the bino, wino and gluino fields  $\tilde{B}$ ,  $\tilde{W}$  and  $\tilde{G}$ , as well as the soft SUSY breaking trilinear couplings  $A_x$  ( $x = \lambda, \kappa, t, b, \tau$ ) are in general complex, whereas the soft SUSY breaking mass parameters of the scalar fields,  $m_X^2$  ( $X = S, H_d, H_u, \tilde{Q}, \tilde{u}_R, \tilde{b}_R, \tilde{L}, \tilde{\tau}_R$ ) are real. Since we consider the CP-conserving NMSSM, they are all taken real. In what follows, we will use conventions such that  $\lambda$  and  $\tan \beta$  are positive, whereas  $\kappa, A_\lambda, A_\kappa$  and  $\mu_{\text{eff}}$  are allowed to have both signs.

After EWSB, we expand the Higgs fields around their VEVs  $v_u, v_d$ , and  $v_S$ , respectively, which are chosen to be real and positive

$$H_d = \begin{pmatrix} (v_d + h_d + i a_d)/\sqrt{2} \\ h_d^- \end{pmatrix}, \quad H_u = \begin{pmatrix} h_u^+ \\ (v_u + h_u + i a_u)/\sqrt{2} \end{pmatrix}, \quad S = \frac{v_s + h_s + i a_s}{\sqrt{2}}. \quad (2.15)$$

This leads to the mass matrices of the three scalars  $h_d, h_u, h_s$ , the three pseudoscalars  $a_d, a_u, a_s$ , and the charged Higgs states  $h_u^\pm, h_d^\mp$ , obtained from the second derivatives of the scalar potential.

The mass matrix is diagonalised with orthogonal rotation matrices, mapping the gauge eigenstates to the mass eigenstates. These are the three neutral CP-even Higgs bosons  $H_1, H_2, H_3$  that are ordered by ascending mass with  $m_{H_1} \leq m_{H_2} \leq m_{H_3}$ , the two CP-odd mass eigenstates  $A_1$  and  $A_2$  with  $m_{A_1} \leq m_{A_2}$ , and a pair of charged Higgs bosons  $H^\pm$ .

After applying the minimisation conditions, we choose as independent input parameters for the tree-level NMSSM Higgs sector the following,

$$\lambda, \kappa, A_\lambda, A_\kappa, \tan\beta = v_u/v_d \quad \text{and} \quad \mu_{\text{eff}} = \lambda v_s/\sqrt{2}. \quad (2.16)$$

The sign conventions are chosen such that  $\lambda$  and  $\tan\beta$  are positive, while  $\kappa, A_\lambda, A_\kappa$  and  $\mu_{\text{eff}}$  are allowed to have both signs. Further parameters will become relevant upon inclusion of the higher-order corrections to the Higgs boson mass that are crucial to shift the SM-like Higgs boson mass to the measured value.

### 3 Scans and Theoretical and Experimental Constraints

Our goal is to investigate the landscape of Higgs pair production in extended Higgs sectors by taking into account the relevant theoretical and experimental constraints. In order to do so, we performed a scan in the various parameter spaces of the models and checked each parameter point for compatibility with our applied constraints. In this section, we briefly describe the constraints used in our study. For details, we refer to our previous papers on the different models [85, 94, 145–149].

We performed the scans with the help of the program **ScannerS** [150–152] for all models except for the NMSSM. In Tables 2, 3, and 4, we list the scan ranges of the R2HDM, the C2HDM, and the N2HDM, respectively. We give them for the various set-ups with respect to which neutral Higgs boson takes the role of the SM-like Higgs which we will denote  $H_{\text{SM}}$  from now on. We distinguish the cases “light” where the lightest of the neutral Higgs bosons is SM-like ( $H_1 \equiv H_{\text{SM}}$ ), “medium” with  $H_2 \equiv H_{\text{SM}}$ , and “heavy” with the heaviest being SM-like ( $H_3 \equiv H_{\text{SM}}$ ). In the R2HDM, with only two neutral Higgs bosons, we have the cases “light” ( $H_1 \equiv H_{\text{SM}}$ ) and “heavy” ( $H_2 \equiv H_{\text{SM}}$ ) only. Note that in the C2HDM, only two of the three neutral Higgs boson masses are independent input quantities whereas the third one is dependent and computed from the input parameters. Therefore, in the generation of the data points two cases are considered, namely  $H_1/H_2 \equiv H_{\text{SM}}$ . The third one is calculated and all three masses are subsequently ordered by ascending mass so that all three set-ups, with either of the  $H_i$  ( $i = 1, 2, 3$ ) representing the  $H_{\text{SM}}$ , are covered by the two scans described in Tab. 3. Note also that we restrict ourselves to the type I and II models. For all these models, the R2HDM, the C2HDM and the N2HDM, we apply the same theoretical constraints, which have different expressions for each model, requiring that all potentials are bounded from below, that perturbative unitarity holds and that the electroweak vacuum is the global minimum. In the R2HDM we use for the latter the discriminant from [153] and for the C2HDM the one from [154].

As for experimental constraints, we impose compatibility with the electroweak precision data by demanding the computed  $S$ ,  $T$  and  $U$  values to be within  $2\sigma$  of the SM fit [155], taking into account the full correlation among the three parameters. We require one of the Higgs bosons to have a mass of [156]

$$m_{H_{\text{SM}}} = 125.09 \text{ GeV}, \quad (3.17)$$

$m_{H_1}$ [GeV]	$m_{H_2}$ [GeV]	$m_A$ [GeV]	$m_{H^\pm}$ [GeV]	$\tan \beta$	$c_{H_2 VV}$	$m_{12}^2$ [GeV <sup>2</sup> ]
R2HDM I/II (light)						
125.09	130...3000	30...3000	85/800...3000	0.8...30	-0.3...0.3	$10^{-3}...10^7$
R2HDM I/II (heavy)						
30...120	125.09	30...3000	85/800...3000	0.8...30	0.8...1	$10^{-3}...10^7$

Table 2: Scan ranges of the R2HDM input parameters, *cf.* Eq. (2.7), where light (heavy) refers to the set-up where the lightest (heaviest) of the two CP-even neutral Higgs bosons is the SM-like Higgs  $H_{\text{SM}}$ , *i.e.*  $H_1(H_2) \equiv H_{\text{SM}}$ .

$m_{H_i}$ [GeV]	$m_{H_j}$ [GeV]	$m_{H^\pm}$ [TeV]	$\tan \beta$	$c_{H_i VV}^2$	$c_{H_i tt}^2$	$\text{sg}(R_{13})$	$R_{23}$	$\text{Re}(m_{12}^2)$ [GeV <sup>2</sup> ]
C2HDM I/II (light)								
125.09	130...3000	0.08/0.8...3	0.8...30	0.8...1	0.7...1.3	-1/1	-1...1	$10^{-3}...10^7$
C2HDM I/II (medium/heavy)								
30...120	125.09	0.08/0.8...3	0.8...30	0...0.1	0...1.2	-1/1	-1...1	$10^{-3}...5 \cdot 10^5$

Table 3: Scan ranges of the C2HDM input parameters, *cf.* Eq. (2.8), where light/medium/heavy refers to the set-up where the lightest/medium/heaviest of the three CP-mixed neutral Higgs bosons is the SM-like Higgs  $H_{\text{SM}}$ , *i.e.*  $H_1/H_2/H_3 \equiv H_{\text{SM}}$ .

$m_{H_1}$ [GeV]	$m_{H_2}$ [GeV]	$m_{H_3}$ [GeV]	$m_A$ [GeV]	$m_{H^\pm}$ [GeV]	$m_{12}^2$ [GeV <sup>2</sup> ]
$\tan \beta$	$c_{H_1 VV}^2$	$c_{H_1 tt}^2$	$\text{sg}(R_{13})$	$R_{23}$	$v_S$ [GeV]
N2HDM I/II (light)					
125.09	130...2995	130...3000	30...3000	85/800...3000	$10^{-3}...10^7$
0.8...30	0.9...1	0.8...1.2	-1/1	-1...1	0...10000
N2HDM I/II (medium)					
30...120	125.09	135...3000	30...3000	85/800...3000	$10^{-3}...5 \cdot 10^5$
0.8...30	0...0.1	0...1.2	-1/1	-1...1	0...5000
N2HDM I/II (heavy)					
30...115	35...120	125.09	30...3000	85/800...3000	$10^{-3}...5 \cdot 10^5$
0.8...30	0...0.1	0...1.2	-1/1	-1...1	0...5000

Table 4: Scan ranges of the N2HDM input parameters, *cf.* Eq. (2.12), where light/medium/heavy refers to the set-up where the lightest/medium/heaviest of the three neutral Higgs bosons is the SM-like Higgs  $H_{\text{SM}}$ , *i.e.*  $H_1/H_2/H_3 \equiv H_{\text{SM}}$ .

and to behave SM-like. Compatibility with the Higgs signal data is checked through **HiggsSignals** version 2.6.1 [157] which is linked to **ScannerS**. We furthermore suppress interfering Higgs signals by forcing any other neutral scalar mass to deviate by more than  $\pm 2.5$  GeV from  $m_{H_{\text{SM}}}$ . Scenar-

ios with neutral Higgs bosons that are close in mass are particularly interesting for non-resonant di-Higgs production as they may have discriminating power with respect to the SM case. The appearance of non-trivial interference effects requires, however, a dedicated thorough study that is beyond the focus of this study and is left for future work. We require 95% C.L. exclusion limits on non-observed scalar states by using `HiggsBounds` version 5.9.0 [158–160]. Additionally, we checked our sample with respect to the recent ATLAS analyses in the  $ZZ$  [161] and  $\gamma\gamma$  [162] final states that were not yet included in `HiggsBounds`. Consistency with recent flavour constraints is ensured by testing for the compatibility with  $\mathcal{R}_b$  [163, 164] and  $B \rightarrow X_s \gamma$  [164–169] in the  $m_{H^\pm} - \tan\beta$  plane. For the non-supersymmetric type II models, we imposed the latest bound on the charged Higgs mass given in [169],  $m_{H^\pm} \geq 800$  GeV for essentially all values of  $\tan\beta$ , whereas in the type I models this bound is much weaker and is strongly correlated with  $\tan\beta$ . Lower values for  $m_{H^\pm}$  allow, via electroweak precision constraints, different ranges for the masses of the neutral Higgs bosons, which will therefore affect our predictions for di-Higgs production.

In the C2HDM, we additionally have to take into account constraints on CP violation in the Higgs sector arising from electric dipole moment (EDM) measurements. Among these, the data from the EDM of the electron imposes the strongest constraints [170], with the current best experimental limit given by the ACME collaboration [171]. We demand compatibility with the values given in [171] at 90% C.L.

In the NMSSM, we use the program `NMSSMCALC` [172, 173] and compute the Higgs mass corrections up to  $\mathcal{O}((\alpha_t + \alpha_\lambda + \alpha_\kappa)^2 + \alpha_t \alpha_s)$  [174–176] with on-shell renormalisation in the top/stop sector. We demand the computed SM-like Higgs boson mass to lie in the range 122 GeV...128 GeV which accounts for the present typically applied theoretical error of 3 GeV [79]. We use `HiggsBounds` and `HiggsSignals` to check for compatibility with the Higgs constraints. Furthermore, we omit parameter points with the following mass configurations for the lightest chargino  $\tilde{\chi}_1^\pm$  and the lightest stop  $\tilde{t}_1$ ,

$$m_{\tilde{\chi}_1^\pm} < 94 \text{ GeV}, \quad m_{\tilde{t}_1} < 1 \text{ TeV}, \quad (3.18)$$

to take into account lower limits on the lightest chargino and the lightest stop mass. The experimental limits given by the LHC experiments ATLAS and CMS rely on assumptions on the mass spectra and are often based on simplified models. The quotation of a lower limit therefore necessarily requires a scenario that matches the assumptions made by the experiments. For our parameter scan we therefore chose a conservative approach to apply limits that roughly comply with the recent limits given by ATLAS and CMS [177, 178]. For further details of the Higgs mass computation and of the input parameters as well as their scan ranges, we refer to [176].

## 4 Numerical Results for SM-Like Higgs Pair Production

In this section, we will present our numerical results for Higgs pair production at the LHC with the dominant process given by gluon fusion [24]. After recapitulating the details of the process, we will outline how we applied the experimental limits on resonant and non-resonant di-Higgs production. We will subsequently present the mass values allowed in the various models as well as the ranges of the SM-like top-Yukawa and trilinear Higgs self-coupling that are still compatible with the data. Finally we will show our results for SM-like Higgs pair production in all discussed models that are in accordance with the applied constraints.

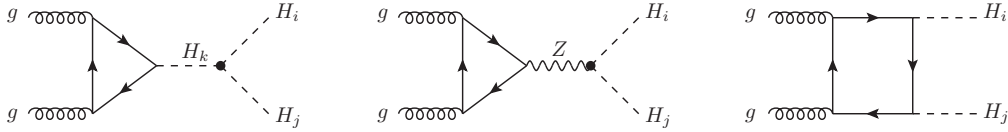


Figure 1: Generic diagrams contributing to leading-order C2HDM Higgs  $H_i H_j$  ( $i, j, k = 1, 2, 3$ ) pair production in gluon fusion.

## 4.1 Gluon Fusion into Higgs Pairs

All our di-Higgs production cross sections through gluon fusion have been computed by adapting the public code `HPAIR` [179] to the R2HDM, the C2HDM [106,109], the N2HDM and the NMSSM [109,131]. The process is mediated through heavy quark loops already at leading order (LO). Generic diagrams are shown for the example of  $H_i H_j$  ( $i, j = 1, 2, 3$ ) production in the C2HDM in Fig. 1. The diagrams that contribute are triangle diagrams and box diagrams. The first triangle diagram contains a Higgs boson  $H_k$  ( $k = 1, 2, 3$ ) in the  $s$ -channel that couples to the final state Higgs bosons  $H_i$  and  $H_j$  through the trilinear coupling  $\lambda_{H_i H_j H_k}$ . The box diagrams (third diagram) are proportional solely to the Yukawa couplings of  $H_i$  and  $H_j$  to the top and bottom quarks. In the C2HDM, which is CP-violating, we additionally have a  $Z$  boson exchange in the  $s$ -channel (second diagram) which couples to the CP-mixed Higgs boson final states. This diagram also has to be taken into account in the CP-conserving models when the production of a mixed pair of one CP-even and one CP-odd Higgs boson in the final state is considered. Note that the contribution of the  $Z$  boson exchange diagram to the overall cross section is small. Furthermore, the QCD corrections from the SM cannot be taken over here. Our implementation of the BSM models in `HPAIR` allows us to take the QCD corrections (in the heavy top limit) correctly into account also for this diagram.

In extended Higgs sectors we have several modifications compared to the SM. The additional Higgs bosons  $H_k$  can lead to resonant enhancement of the di-Higgs cross section compared to the SM in case  $m_{H_k} > m_{H_i} + m_{H_j}$ . In Higgs pair production we will call parameter configurations where the resonant rates makes up for a significant part of the cross section “resonant production”. For mediator masses of  $m_{H_k} < m_{H_i} + m_{H_j}$  resonant enhancement is kinematically not possible. This is a clear case of “non-resonant” production. However, note that, for parameter configurations with  $m_{H_k} > m_{H_i} + m_{H_j}$ , the resonance contribution may be very suppressed if the involved couplings are small, the mediator mass is very heavy, its total width is large, or if there are destructive interferences between different diagrams. From an experimental point of view, the cross section would not be distinguishable from “non-resonant” production then. The transition between “resonant” and “non-resonant” is of course fluid. We will address this in detail in the discussion of our application of the experimental limits from resonant and non-resonant di-Higgs production. Further differences from the SM case arise from Higgs-Yukawa and trilinear Higgs couplings deviating from those of the SM Higgs boson and from additional particles running in the loop. The latter is the case for the NMSSM where supersymmetric partners of the top and bottom quark contribute to the loop. An interesting feature is that in the SM we have a destructive interference between the triangle and the box diagrams, implying

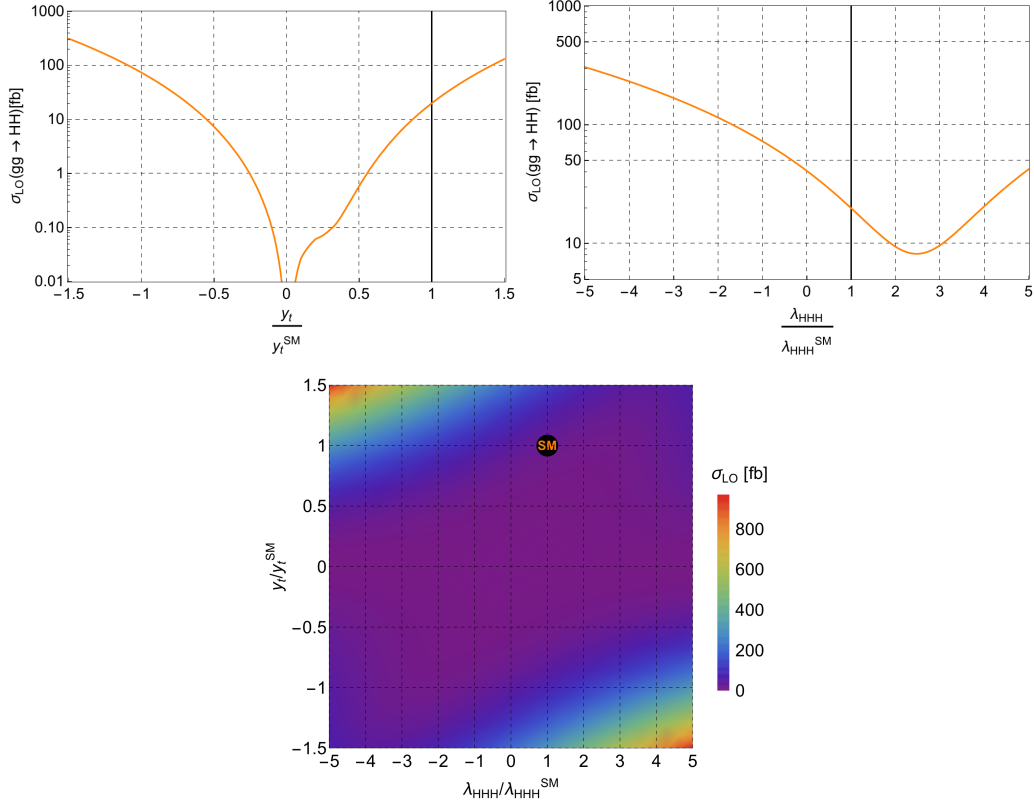


Figure 2: Leading-order SM Higgs pair production in gluon fusion at  $\sqrt{s} = 14$  TeV as function of the Higgs top-Yukawa coupling  $y_t$  normalized to the SM value  $y_t^{\text{SM}}$  for the trilinear coupling fixed to the SM value (upper left); as a function of the trilinear coupling  $\lambda_{HHH}$  normalized to the SM value  $\lambda_{HHH}^{\text{SM}}$  for the top Yukawa coupling fixed to the SM value (upper right); as a function of the trilinear and the top-Yukawa couplings in terms of the respective SM values (lower). The color code indicates the size of the LO cross section in fb. The SM point is marked in orange.

possible enhancements in extended Higgs sectors where the couplings differ from the SM case. This can be inferred from Fig. 2, where we show the LO Higgs pair production cross section when we vary the SM Higgs top-Yukawa coupling (upper left), the trilinear Higgs self-coupling (upper right) and both couplings (lower) while keeping all other couplings fixed to the SM values. Note, that for the sake of illustration we varied the top-Yukawa coupling in ranges beyond the experimental exclusion limits.<sup>3</sup> We see the destructive interference which becomes largest for  $\lambda_{HHH}/\lambda_{HHH}^{\text{SM}} = 2.48$ . The cross section drops to zero (modulo the small bottom quark contribution) for the top-Yukawa coupling  $y_t = 0$  as the Higgs does not couple to the top quarks any more. Note finally that the di-Higgs cross section values through the  $s$ -channel exchange triangle diagrams are sensitive to the total widths of the exchanged Higgs bosons as well, that have to be provided for the computation of the cross section.

For the calculation of the gluon fusion di-Higgs cross section shown here and in the following, we use the following input values for the c.m. energy  $\sqrt{s}$ , the top and bottom quark mass values  $m_t$  and  $m_b$ , the  $Z$  boson mass  $m_Z$ , the strong coupling constant  $\alpha_s$  at  $m_Z$ , the renormalisation

<sup>3</sup>In the subsequently presented analyses, the experimental limits on the couplings are taken into account.

and factorisation scale  $\mu$  at which the cross section is evaluated, and the pdf set,

$$\begin{aligned}\sqrt{s} &= 14 \text{ TeV}, \quad m_t = 173.2 \text{ GeV}, \quad m_b = 4.75 \text{ GeV}, \\ m_Z &= 91.187 \text{ GeV}, \quad \alpha_s(m_Z) = 0.118, \quad \mu = 0.5 m_{HH}, \quad \text{pdfset: CT14lo/nlo},\end{aligned}\tag{4.19}$$

where  $m_{HH}$  denotes the invariant Higgs pair mass and where we take the corresponding CT14 pdf set [180] for the LO and the next-to-leading order (NLO) computation. The NLO QCD corrections which are of two-loop order are computed in the limit of heavy loop particle masses. When we explicitly present NLO results we consistently set the bottom-quark mass to zero both at LO and at NLO. For presented  $K$ -factors, *i.e.* the ratio of the NLO to the LO cross section, we consistently set the pdf sets to LO and NLO for the LO and the NLO calculation, respectively.

Note that, in order to keep our scans economic in time, we compute the Higgs pair production cross sections for the results covering the whole scanned parameter space of the models at leading order. The NLO QCD corrections are roughly taken into account by applying a factor of two. This rough approximation works reasonably well for SM-like Higgs pair production [31, 36–40, 106, 131]. When we present specific benchmark scenarios, however, we compute the cross sections explicitly at NLO QCD in the heavy loop particle limit for the considered model by using our adapted HPAIR codes. Be aware, however, that the QCD corrections should be taken with caution for scenarios with large values of  $\tan\beta$ . In this case the bottom loop contributions become more important so that the limit of heavy loop particle masses cannot be applied any more.

## 4.2 The Impact of Di-Higgs Constraints

We first want to discuss how we take into account the already available results from the experimental SM-like di-Higgs searches, resonant and non-resonant. Since the experimental limits in the two cases rely on different topologies, the question arises how these limits can be applied in our cases where both resonant and non-resonant production are included in the evaluated cross sections. Moreover, in some of the models we can have more than one resonance decaying into a SM-like Higgs pair. In the following, we will outline our applied strategy.

For the generation of the data we turned off in **HiggsBounds** the experimental limits from resonant di-Higgs production while applying all other constraints described above. We then computed, for each data point that fulfils the kinematic constraint  $m_{H_k} > 2m_{H_{\text{SM}}}$ , the production cross section  $\sigma(H_k)$ , for all possible intermediate resonances  $H_k$ . The latter has been obtained with the code **SusHi v1.6.1** [181–183] at NNLO QCD and it includes both production in gluon fusion and in association with a  $b$ -quark pair. Note, however, that associated production with a  $b$ -quark pair does not play an important role for our scenarios. This production cross section is subsequently multiplied with the branching ratio of the  $H_k$  decay into  $H_{\text{SM}}H_{\text{SM}}$ . The branching ratio has been obtained for the R2HDM, C2HDM, N2HDM, and NMSSM by using the public codes **HDECAY** [184–186], **C2HDM\_HDECAY** [84], **N2HDECAY** [85, 86], and **NMSSMCALC** [172], respectively. We then compare the cross section  $\sigma(H_k) \times \text{BR}(H_k \rightarrow H_{\text{SM}}H_{\text{SM}})$  for each possible intermediate resonance<sup>4</sup> with the experimental limits on resonant di-Higgs production. Since these limits are obtained from the LHC run at  $\sqrt{s} = 13 \text{ TeV}$ , we also compute the **SusHi** cross sections at this c.m. energy (in contrast to the Higgs pair production cross sections that are all evaluated at  $\sqrt{s} = 14 \text{ TeV}$ ). We took into account the experimental limits that were the stringest

---

<sup>4</sup>In the case of the N2HDM *e.g.* with three neutral Higgs bosons  $H_{1,2,3}$  for scenarios with  $H_1 \equiv H_{\text{SM}}$  both  $H_2$  and  $H_3$  could be resonantly produced and decay into an  $H_{\text{SM}}$  pair provided they fulfill the kinematic constraint.

ones at the time of the production of our plots. They are given in Refs. [187] for the  $4b$ , [188,189] for the  $(2b)(2\tau)$ , [190] for the  $(2b)(2\gamma)$ , [191] for the  $(2b)(2W)$ , [192] for the  $(2b)(ZZ)$ , [193] for the  $(2W)(2\gamma)$  and [194] for the  $4W$  final state.<sup>5</sup> We furthermore included the recently published results on  $4b$  by ATLAS [196] and CMS [197],  $(2b)(2\tau)$  [198] and  $(2b)(2\gamma)$  [199]. Parameter points where at least for one possible resonance  $H_k$  the experimental limit for any of the final state signatures is exceeded, are rejected. Nevertheless, there is one exception. Since the experimental limits are given assuming narrow resonances, we do not reject points where the ratio of the total width  $\Gamma_{\text{tot}}(H_k)$  of  $H_k$  and its mass  $m_{H_k}$  exceeds the value  $(\Gamma_{\text{tot}}(H_k)/m_{H_k})_{\text{limit}} = 5\%$ .<sup>6</sup>

For illustration, we show the impact of the limits from resonant searches for the N2HDM type I (N2HDM-I) where the lightest CP-even scalar  $H_1$  is the SM-like Higgs boson  $H_{\text{SM}}$ . The yellow points in Fig. 3 (left) show for the points of our scan in the N2HDM-I parameter space that pass the constraints described in Sec. 3, the single production cross sections of the heavy Higgs boson  $H_2$ , computed with **SusHi**, and multiplied with the branching ratio into a pair of two SM-like Higgs bosons  $H_1$ . In other words, they represent one of the resonant production modes of a SM-like Higgs pair. The dashed line and the dot-dashed line are the experimental limits obtained from resonant di-Higgs production searches in the  $4b$  final state [196] and the  $(2b)(2\tau)$  final state [198], respectively. These limits are now applied on all yellow points. Note, however, that we not only apply them on resonant  $H_2$  but also on resonant  $H_3$  production. The right plot in Fig. 3 shows the situation after applying the aforementioned experimental constraints plus the bounds from  $(2b)(2\gamma)$  [199] and the CMS bounds from  $4b$  [197], which only affect the very low and heavy mass region, respectively, and, due to better visibility, were not added in the plot. All previous experimental results are weaker in the whole heavy resonance mass range and thus automatically satisfied. We see that some of the yellow points above the experimental limits are left over. Here we do not fulfil our criteria of  $(\Gamma_{\text{tot}}(H_k)/m_{H_k})_{\text{limit}} < 5\%$  so that the experimental limits cannot be applied and, thus, no statement about the validity of these points can be made.

The red points in Fig. 3 (left) show for all parameter scenarios passing the constraints of Sec. 3, the cross sections for SM-like Higgs pair production as a function of the mass of the non-SM-like Higgs boson  $H_2$ . As described above, the cross section is calculated at LO and multiplied by a factor two to approximately take into account NLO QCD corrections. The constraints from resonant di-Higgs searches are taken into account by referring to the yellow points. Only those scenarios where the yellow points passed the resonant search limits are retained for the di-Higgs cross sections and result in the allowed red points presented in Fig. 3 (right). The comparison of the left and right plot in Fig. 3 clearly shows that the present di-Higgs searches are already sensitive to the N2HDM parameter space and exclude parts of it beyond single Higgs data constraints.

From the right plot, we infer that there are many points left after application of the resonant search limits. In many of them, the contribution from resonant diagrams is suppressed or kinematically forbidden.

Looking only at the total cross section values, as we do it here, and not at distributions, the sizes of the resonant Higgs pair production cross sections in the suppressed cases are similar

<sup>5</sup>Combinations of all searches have been published in [51] and [195]. We, however, only place limits on the individual final states as the correct combination of all limits would require a sophisticated treatment that goes beyond the rough estimate of the experimental results on our channels applied in this paper.

<sup>6</sup>Note that by default, *i.e.* independently of the applied experimental constraints, we rejected all parameter points with  $\Gamma_{\text{tot}}(H_i)/m_{H_i} > 50\%$ .

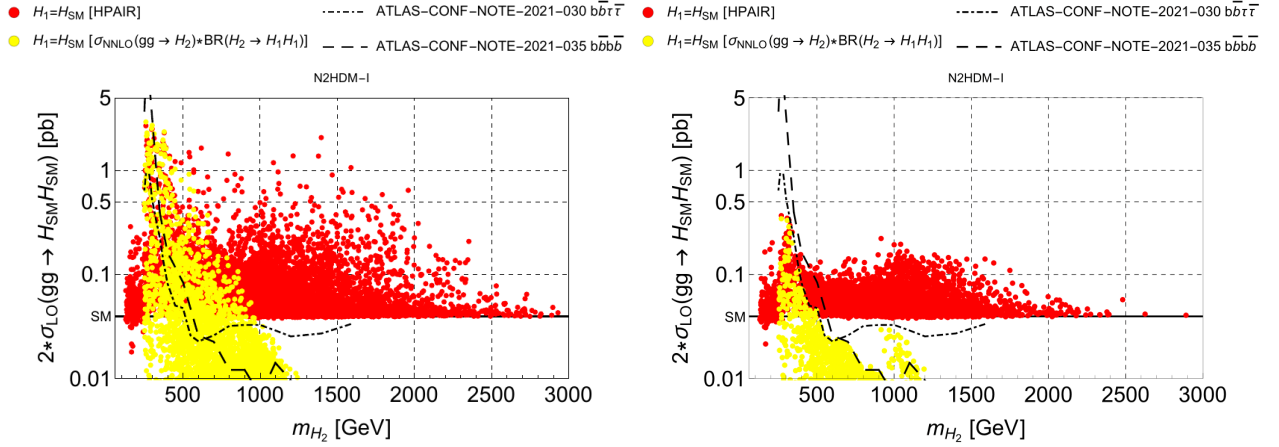


Figure 3: N2HDM-I: Yellow points:  $\sigma(pp \rightarrow H_2)_{\text{NNLO}}^{\text{SusHi}} \times \text{BR}(H_2 \rightarrow H_1 H_1)$ . Red points:  $2 \times \sigma_{\text{LO}}^{\text{HPAIR}}(gg \rightarrow H_{\text{SM}} H_{\text{SM}})$ , with  $H_{\text{SM}} \equiv H_1$ , as function of  $m_{H_2}$ . Left (right) panel without (with) the constraints from experimental resonant di-Higgs searches, *cf.* text for details. The dashed (dot-dashed) line denotes the ATLAS limit from the  $(b\bar{b})(b\bar{b})$  ( $(b\bar{b})(\tau\tau)$ ) final state. Horizontal line: Higgs pair production cross section in the SM.

to the non-resonant ones or even smaller, so that they cannot be distinguished based on the total rates. Also, invariant mass distributions barely change as we explicitly verified, since the contributions from the resonances are largely suppressed w.r.t. to those from the non-resonant parts. We therefore applied on these points the corresponding non-resonant limits. We come back to this point below. One can also see from this plot that for  $m_{H_2} \lesssim 2m_{H_1}$  the cross section can be suppressed relative to the SM value. This is to be attributed to destructive interferences between the various diagrams contributing to the di-Higgs cross section.

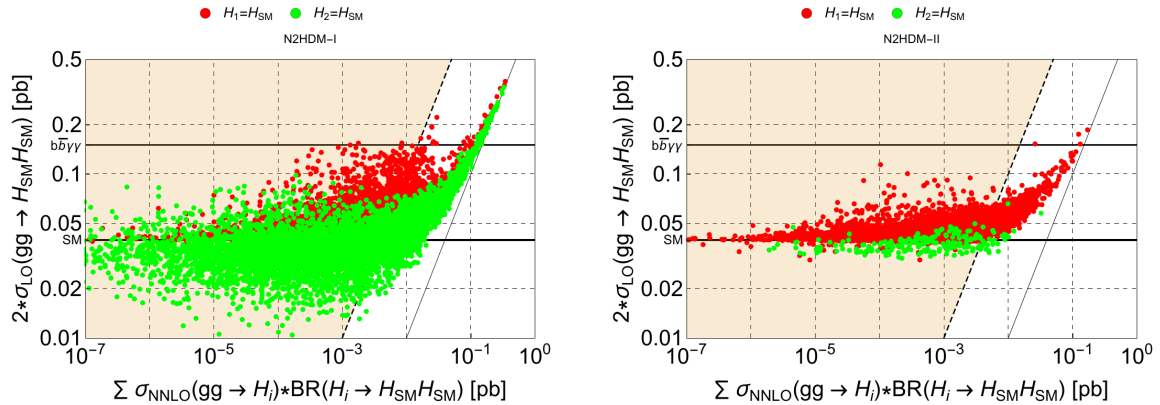


Figure 4: N2HDM: LO gluon fusion cross sections, multiplied by a factor 2 to approximate the NLO QCD corrections, into a SM-like Higgs pair with  $H_1 \equiv H_{\text{SM}}$  (red) and  $H_2 \equiv H_{\text{SM}}$  (green) for all points passing our constraints, as a function of the NNLO cross section for resonant heavy Higgs  $H_i$  production with subsequent decay into a SM-like Higgs pair. For  $H_1 \equiv H_{\text{SM}}$  (red points) we sum up the single Higgs production cross sections of  $H_2$  and  $H_3$ . Left: type I, right: type II. The horizontal line denoted by SM corresponds to the SM Higgs pair production value, and the one denoted by  $b\bar{b}\gamma\gamma$  to the limit from non-resonant di-Higgs searches in the  $2b2\gamma$  final state. For the shaded region, see text.

As for the experimental limits from non-resonant searches, they mostly do not constrain our models. The latest results in  $(b\bar{b})(\gamma\gamma)$  [199], however, start cutting on the N2HDM-I (with

$H_1 \equiv H_{\text{SM}}$ ) parameter space as is illustrated in Fig. 4 for type I (left) and type II (right). For all points passing our constraints, we plot the NLO QCD (approximated by a factor 2) gluon fusion SM-like Higgs pair production cross sections for the N2HDM-I (left) and II (right), versus the NNLO QCD gluon fusion production cross section of a heavy non-SM-like Higgs  $H_i$  that subsequently decays into the SM-like Higgs pair. For  $H_2 \equiv H_{\text{SM}}$ , we have  $H_i = H_3$ , for  $H_1 \equiv H_{\text{SM}}$  we sum over the two possibilities  $H_i = H_2, H_3$ . From the plot, we can infer that for parameter points where  $H_{\text{SM}}H_{\text{SM}}$  production from resonant heavy Higgs production dominates the di-Higgs process, both cross sections, di-Higgs and single Higgs times Higgs-to-Higgs decay, approach each other (see diagonal line in the plot).<sup>7</sup> For the smaller cross sections, resonant production stops playing a significant role and the experimental limits from non-resonant di-Higgs searches can be applied. The most stringent one among the various final states is presently given by the  $(2b)(2\gamma)$  final state [199]<sup>8</sup>, which is visualized in the plots by the horizontal lines. We see that in the N2HDM-I this already cuts into the parameter space so that non-resonant Higgs search constraints start to play a role for certain models.<sup>9</sup> The transition between non-resonant and resonant production is fluid of course. In order to be able to apply the experimental limits we are forced to define a separation between the two cases which is arbitrary. We define a cross section to be resonantly dominated when the single non-SM Higgs production with subsequent decay into SM-like Higgs bosons makes up for more than 10% of the di-Higgs result and accordingly apply the resonant limits. This region separation is shown by the diagonal dashed line in each plot. The shaded region is hence the region where we apply the non-resonant search limits. Apart from the N2HDM-I case, we found that non-resonant searches do not constrain the investigated models at present. The previous definition is arbitrary and a sophisticated experimental analysis taking into account distributions would be required. This is beyond the scope of this paper. Since at present the non-resonant searches are not very sensitive, this approach is good enough for our purpose of drawing an overall phenomenological picture.

### 4.3 Parameter Dependences

The size of the cross section for SM-like Higgs pair production depends on the SM-like Higgs values of the trilinear Higgs self-couplings and of the top and bottom Yukawa couplings. The influence of the latter is only relevant for BSM models in the case of large values of  $\tan\beta$ . The cross section value furthermore depends on the masses of all additionally involved non-SM-like Higgs bosons  $H_k$ , their total widths, their Yukawa couplings and the trilinear Higgs self-couplings  $\lambda_{H_k H_{\text{SM}} H_{\text{SM}}}$ . In this subsection we present the distributions of the mass spectra of the non-SM-like neutral Higgs bosons and discuss the allowed sizes of the trilinear Higgs self-coupling and top-Yukawa coupling of the SM-like Higgs boson in our investigated BSM models.

<sup>7</sup>Note that the di-Higgs and single Higgs cross sections are not exactly the same for several reasons. The **SusHi** single Higgs gluon fusion results are computed at NNLO QCD and  $\sqrt{s} = 13$  TeV whereas **HPAIR** for di-Higgs production is run at  $\sqrt{s} = 14$  TeV for LO QCD and multiplies the result afterwards by a factor of two. (The SM Higgs pair production cross sections at **FT<sub>approx</sub>** [30] differ by 18% at  $\sqrt{s} = 13$  TeV and 14 TeV, respectively.) Furthermore, different pdfs were used in the computation. Also, **HPAIR** includes all  $s$ -channel Higgs exchange and the box diagrams in the computation of the cross section. The impact of the difference between the cross sections w.r.t. to the application of the experimental limits is negligible, however, as we explicitly verified.

<sup>8</sup>Apart from the combined limit which we do not apply.

<sup>9</sup>We remind the reader that our di-Higgs cross sections are computed at  $\sqrt{s} = 14$  TeV while the limits are obtained at 13 TeV. With future experimental results at 14 TeV, even more points will be excluded. For our rough analysis, however, this is a good enough approach.

### 4.3.1 Distributions of the Mass Spectra

Figure 5 displays the mass distributions of the two neutral non-SM-like Higgs bosons contributing to the cross section for SM-like Higgs pair production in the C2HDM (upper), the N2HDM (middle) and NMSSM (lower) for type I (left) and type II (right) in the former two models.<sup>10</sup> We denote the masses of the heavier one by  $m_\uparrow$  and the one of the lighter Higgs by  $m_\downarrow$ , respectively. In the N2HDM and the NMSSM these Higgs bosons are CP-even, in the C2HDM they have no definite CP quantum number. We found in our scans that the largest freedom in the distributions, after applying all considered constraints, is found in the N2HDM (middle row) where in type I all three neutral Higgs bosons  $H_{1,2,3}$  can be SM-like (red, green, blue points). The overall lightest Higgs mass spectrum is realized for  $H_3 \equiv H_{\text{SM}}$  and becomes increasingly heavier if instead  $H_2$  or  $H_1$  are SM-like, respectively. For the latter two cases large mass gaps can occur between  $m_\uparrow$  and  $m_\downarrow$ . In the NMSSM large mass gaps are also possible. In the C2HDM-I, where all three SM-like cases can be realized, this is not the case any more. In particular for  $H_1 = H_{\text{SM}}$  the masses  $m_\uparrow$  and  $m_\downarrow$  quickly become nearly degenerate with increasing values. This is even more pronounced for the C2HDM-II. Large differences in the mass hierarchies allow for Higgs-to-Higgs cascade decays which is particularly interesting for non-SM-like single Higgs searches or Higgs pair production and is a clear sign of non-minimally extended Higgs sectors in contrast to the R2HDM or MSSM *e.g.* which feature only two CP-even neutral Higgs bosons. We can hence expect such decays in the N2HDM-I, II, and the NMSSM, and to a less extent in the C2HDM-I because of the more compressed mass spectrum. We further found that in the C2HDM-II only the case  $H_1 \equiv H_{\text{SM}}$  is realized in our scan after including the constraints. In the N2HDM-II and the NMSSM,  $H_1$  and  $H_2$  being SM-like is still possible but not  $H_3$ . In the R2HDM, not shown in the plots, in type I, for  $H_1 \equiv H_{\text{SM}}$ , the heavier  $H_2$  mass ranges between 130 GeV and, the upper scan limit of 3 TeV. For  $H_2 \equiv H_{\text{SM}}$ , the lighter  $H_1$  mass varies between 30 and 122.5 GeV.<sup>11</sup> In type II,  $m_{H_2}$  ranges between 800 GeV and the upper scan limit. Also for all other models, the lightest Higgs masses found to be allowed are between around 30 and 122.5 GeV, where the lower bound is due to our scan limit. In the type-II models the overall mass spectrum is pushed to higher values because of the lower limit on the charged Higgs mass.

### 4.3.2 Higgs Couplings

In the SM, the triangle and box diagrams contributing to Higgs pair production interfere destructively. Deviations of the trilinear Higgs self-coupling  $\lambda_{3H_{\text{SM}}}$  and Yukawa coupling to top quarks  $y_{t,H_{\text{SM}}}$  of the SM-like Higgs  $H_{\text{SM}}$  with respect to the SM values  $\lambda_{3H}$  and  $y_{t,H}$ , respectively, will mitigate this destructive interference. In turn, it will allow for larger cross sections in (the non-resonant) SM-like di-Higgs production. Experimental limits on the trilinear Higgs self-coupling derived from Higgs pair production results often assume the top-Yukawa coupling to be SM-like.<sup>12</sup> We therefore want to answer the following questions:

- After applying constraints from single Higgs data, what are the allowed ranges for  $\lambda_{3H_{\text{SM}}}$  and  $y_{t,H_{\text{SM}}}$  in our models? What is the impact of di-Higgs constraints?
- How do di-Higgs cross sections behave as a function of  $\lambda_{3H_{\text{SM}}}$  and  $y_{t,H_{\text{SM}}}$ ?

<sup>10</sup>For a previous phenomenological investigation of the models, *cf.* [147]. Due to less strict constraints at that time, the mass spectra were less constrained.

<sup>11</sup>Note that we applied a gap of  $\pm 2.5$  GeV around 125.09 GeV.

<sup>12</sup>Results where this assumption has been dropped are given in [51, 199–202].

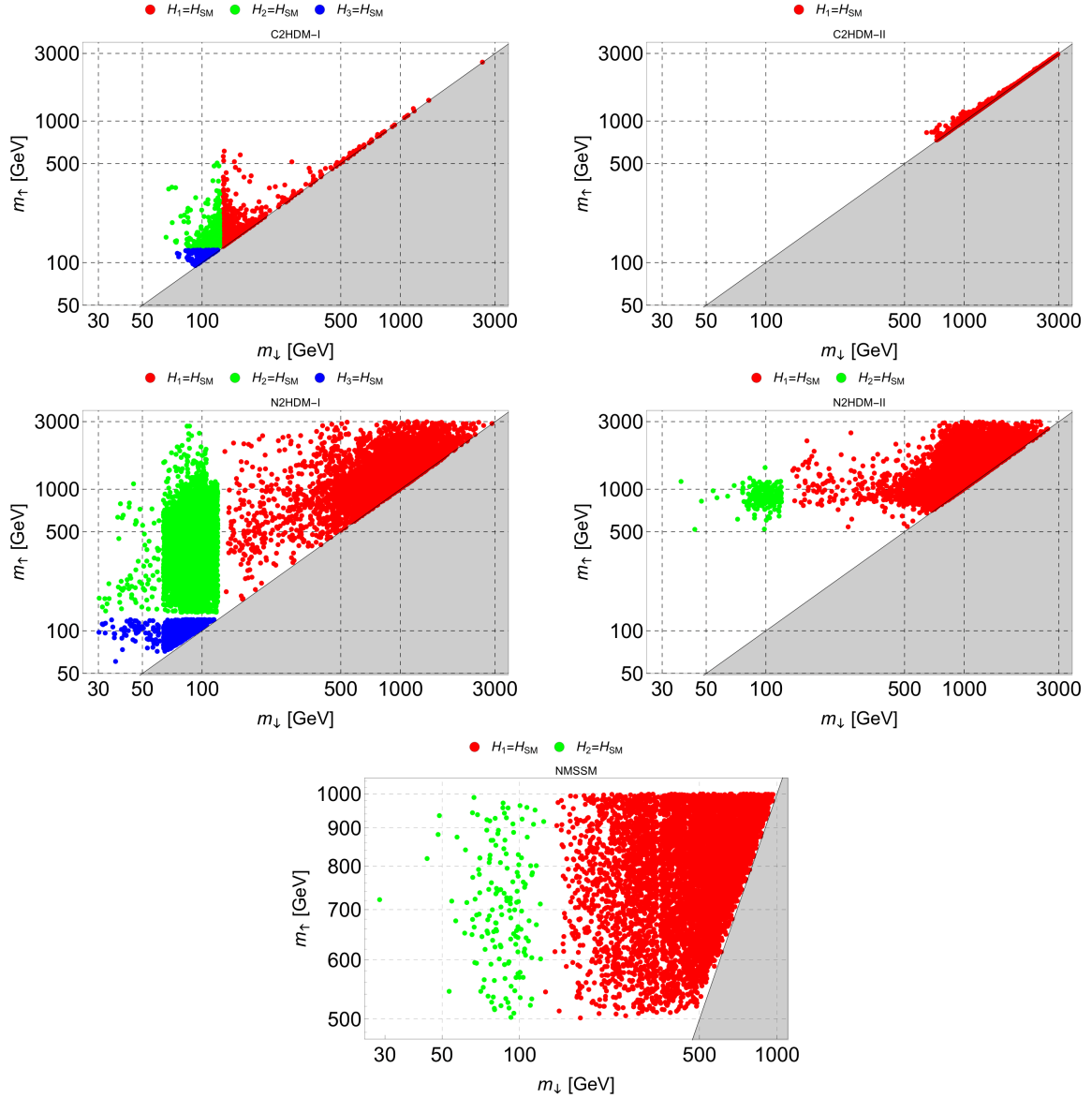


Figure 5: Mass distributions of the non-SM-like neutral Higgs bosons in the C2HDM-I and II (upper left and right), the N2HDM-I and II (middle left and right), and the NMSSM (lower) for the parameter points respecting all applied constraints. The colour of the points denotes which Higgs boson is SM-like. In the shaded region  $m_\uparrow \leq m_\downarrow$ .

- What is the relation of the  $\lambda_{3H_{SM}}$  and  $y_{t,H_{SM}}$  limits to the effective coupling parameters in SM effective field theory (SMEFT)?

#### 4.3.3 Allowed Coupling Ranges and Impact of Di-Higgs Constraints

Figure 6 depicts for the R2HDM-I (left) and the N2HDM-I (right), with  $H_1 \equiv H_{SM}$ , the absolute top-Yukawa versus the trilinear self-coupling values of the SM-like Higgs normalized each to the corresponding SM-values. Black points are allowed parameter points after applying all but the single Higgs constraints, blue points additionally include the single Higgs constraints (blue), and

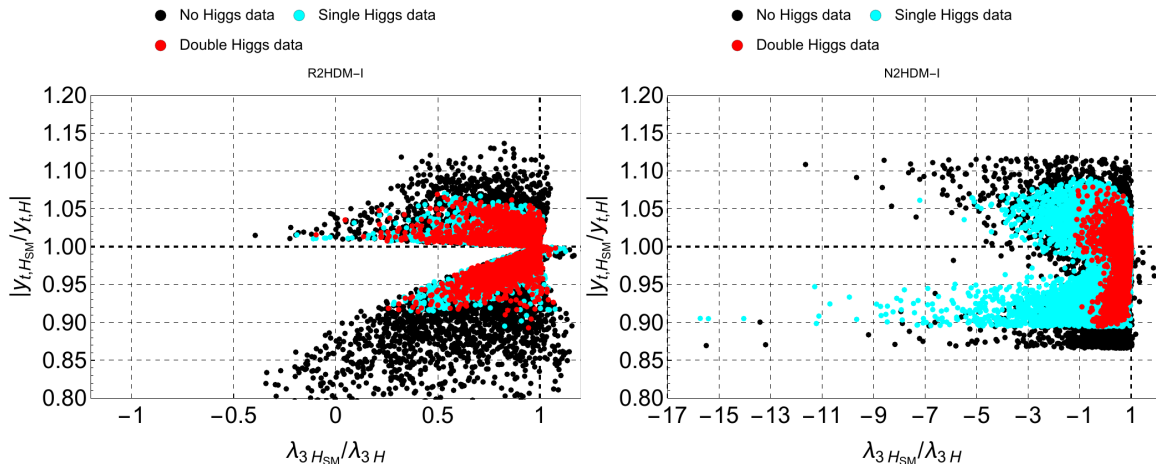


Figure 6: Absolute value of the Higgs top Yukawa coupling  $y_{t,H_{SM}}$  versus the trilinear Higgs self-coupling  $\lambda_{3H_{SM}}$  of the SM-like Higgs boson  $H_{SM}$  given by  $H_1$ ,  $H_1 \equiv H_{SM}$ , normalised each to the SM values  $y_{t,H}$  and  $\lambda_{3H}$  for the R2HDM-I (left) and the N2HDM-I (right) for the parameter points passing all constraints without single and double Higgs constraints (black), including single Higgs constraints (blue) and also including di-Higgs search constraints (red). Dashed lines correspond to the SM-case of each coupling ratio.

red points finally also comply with the di-Higgs constraints. The comparison of the red with the blue points hence shows the impact of the di-Higgs measurements on the coupling values.

As we can see from the left plot, in the R2HDM-I, after applying single Higgs constraints, the Yukawa coupling is restricted to values close to the SM,  $0.87 \leq (y_{t,H_{SM}}^{R2HDM}/y_{t,H}) \leq 1.07$  (blue points). The trilinear Higgs self-coupling is less restricted with values in the range  $-0.2 \leq (\lambda_{3H_{SM}}^{R2HDM}/\lambda_{3H}) \leq 1.15$  (blue points). Note that the restriction of the trilinear Higgs self-coupling at this stage basically stems from the constraints on the Yukawa coupling from the single Higgs data. Di-Higgs constraints (red points) slightly reduce these values, to about  $-0.1 \leq (\lambda_{3H_{SM}}^{R2HDM}/\lambda_{3H}) \leq 1.1$ . Departures from the SM value in the trilinear couplings come along with non-SM-like Yukawa couplings (*cf.* wedge region). Turning to the N2HDM-I (right plot) we see that the usual plus single Higgs constraints reduce the Yukawa coupling to about the same values as in the R2HDM-I (blue points). The trilinear coupling on the other hand can vary in a larger negative range with values between -16 and 1 times the SM value. After including the di-Higgs constraints the trilinear coupling range is reduced to about -1 to 1 times the SM value (red points). This is primarily caused by the unitarity constraint. In addition to the perturbative unitarity check performed by **ScannerS** we applied the following approximate limit on all trilinear Higgs self-couplings  $\lambda_{H_i H_j H_k}$ . We required  $|\lambda_{H_i H_j H_k}/\lambda_{3H}| \leq 30$  for all  $i, j, k$  combinations in the respective model.<sup>13</sup> We found that this additional constraint only affects the N2HDM. In all other models the inclusion of the constraints through **ScannerS** left over only scenarios that already respect this unitarity constraint. Besides the latter, we also found that the di-Higgs searches cut on the allowed trilinear Higgs self-coupling values, though to a lesser extent.

The unitarity constraints are responsible for the wedge regions in the plots. Comparing

<sup>13</sup>The value is derived by assuming a rough perturbative limit on the Higgs mass of  $M_H = 700$  GeV, implying a limit on the trilinear coupling of  $\lambda_{3H}^{perturb} = 3M_H^2/v = 5975$  GeV compared to the value of  $\lambda_{3H} \approx 190$  GeV for the SM-like Higgs mass  $M_H = 125.09$  GeV.

	R2HDM		C2HDM	
	$y_{t,H_{SM}}^{R2HDM}/y_{t,H}$	$\lambda_{3H_{SM}}^{R2HDM}/\lambda_{3H}$	$y_{t,H_{SM}}^{C2HDM}/y_{t,H}$	$\lambda_{3H_{SM}}^{C2HDM}/\lambda_{3H}$
light I	0.893...1.069	-0.096...1.076	0.898...1.035	-0.035...1.227
medium I	n.a.	n.a.	0.889...1.028	0.251...1.172
heavy I	0.946...1.054	0.481...1.026	0.893...1.019	0.671...1.229
light II	0.951...1.040	0.692...0.999	0.956...1.040	0.096...0.999
medium II	n.a.	n.a.	—	—
heavy II	—	—	—	—

	N2HDM		NMSSM	
	$y_{t,H_{SM}}^{N2HDM}/y_{t,H}$	$\lambda_{3H_{SM}}^{N2HDM}/\lambda_{3H}$	$y_{t,H_{SM}}^{NMSSM}/y_{t,H}$	$\lambda_{3H_{SM}}^{NMSSM}/\lambda_{3H}$
light I	0.895...1.079	-1.160...1.004	n.a.	n.a.
medium I	0.874...1.049	-1.247...1.168	n.a.	n.a.
heavy I	0.893...1.030	0.770...1.112	n.a.	n.a.
light II	0.942...1.038	-0.608...0.999	0.826...1.003	0.024...0.747
medium II	0.942...1.029	0.613...0.994	0.916...1.000	-0.502...0.666
heavy II	—	—	—	—

Table 5: Allowed ranges for the top-Yukawa and trilinear Higgs self-coupling of the SM-like Higgs boson after application of all constraints, normalized to the corresponding SM value, for the R2HDM, C2HDM, N2HDM, and NMSSM, respectively, for type 1 (I) and type 2 (II). Light/medium/heavy correspond to  $H_{1/2/3}$  being the SM-like Higgs boson. The medium case is not applicable (n.a.) to the R2HDM, type 1 is not applicable to the NMSSM. In our scans, for type 2 some of the cases were found not to be compatible with the constraints any more (marked by a dash in the table).

the shape of the wedge regions in the R2HDM-I and the N2HDM-I we see that an increased precision in the Yukawa coupling will affect the allowed deviation in the trilinear coupling in the N2HDM-I more than in the R2HDM-I. Overall, we find that the trilinear coupling gets more and more restricted but significant deviations are still possible and that they come along with a non-SM-like Yukawa coupling. The present (observed) limits on the trilinear Higgs self-coupling assuming a SM top-Yukawa coupling are -1.0 to 6.6 times the SM trilinear Higgs self-coupling at 95% CL as derived by ATLAS [51] and -3.3 to 8.5 as given by CMS [52]. These experimental sensitivities to the trilinear Higgs self-coupling of the SM start to constrain the parameter space of our models, namely the N2HDM.<sup>14</sup> This can be inferred from Tab. 5 where we list the allowed ranges for the top-Yukawa and the trilinear Higgs self-couplings in our investigated models after applying all described constraints. For all models, due to the single Higgs constraints, the top-Yukawa coupling is bounded to a range of at most  $\pm 0.1$  around the SM case, with the exception of the NMSSM where it can deviate by up to 17%.<sup>15</sup> The trilinear couplings are less constrained. For the N2HDM-I with  $H_1$  or  $H_2$  being SM-like they are outside the lower ATLAS limit; however, only assuming SM-like Yukawa couplings which is not the case as can be inferred from Fig. 6. Note also that a vanishing trilinear SM-like Higgs self-coupling is also still allowed

<sup>14</sup>This is only true, however, if we assume a SM-like Yukawa coupling which is not appropriate in all models. We will come back to this point later.

<sup>15</sup>Note that we excluded all scenarios where the mass gap between the SM-like and one non-SM-like Higgs boson is less than 2.5 GeV. Would we allow for these scenarios as well then the top-Yukawa coupling could substantially deviate from the SM case, as the Higgs signal is now built up by two Higgs bosons close in mass.

in some of the models.

There is one caveat to be made on the values given in Tab. 5. These limits have been obtained from the scans in the chosen parameter space with application of all constraints. Hence, they depend on the constraints that we apply, and they also depend on our scanning procedure and sampling. More extended scan ranges and scans adapted to specific parameter regions could possibly find more points and extend these allowed coupling values somewhat. With the given coupling values, however, we are on the conservative side. Furthermore, also note that the C2HDM contains per definition the limit of the R2HDM. This is not reflected, however, in the coupling ranges (and will not be in the plots shown below either). The reason is, that the scan in the C2HDM is performed in different input parameters than in the R2HDM and for finite scan ranges necessarily leads to differences. We explicitly checked that larger R2HDM ranges than in the C2HDM indeed coincide with the CP-conserving limit in the C2HDM and that larger C2HDM ranges compared to the R2HDM are due to truly CP-violating points. We chose not to merge the C2HDM sample with the R2HDM as it allows us to investigate CP-violating effects. As a side remark we add that for the values of our scan the SM-like Higgs boson in the C2HDM-I can still have a CP-violating admixture<sup>16</sup> of up to 16%, 20% and 10% for  $H_1$ ,  $H_2$  and  $H_3$  being SM-like, respectively, and of up to 2% in the C2HDM-II with  $H_1 \equiv H_{\text{SM}}$ .

#### 4.4 SM-Like Higgs Pair Production

In this section we discuss the production of two SM-like Higgs bosons  $H_{\text{SM}}$  in our four considered models R2HDM, C2HDM, N2HDM, and NMSSM. We display, for all valid parameter points passing the applied constraints (including those from di-Higgs searches), the cross sections for SM-like Higgs pair production in the R2HDM, C2HDM, and N2HDM in Fig. 7 and for the NMSSM in Fig. 8.<sup>17</sup> The plots are shown as a function of the heavier of the neutral non-SM-like Higgs bosons, denoted by  $m_{\uparrow}$ . Red points depict the results where the SM-like Higgs boson is given by the lightest Higgs boson  $H_1$ , green points are those for  $H_{\text{SM}} \equiv H_2$ , and blue ones correspond to  $H_{\text{SM}} \equiv H_3$ . In the R2HDM, we of course only have red and green points. The overall lower density of the points in the C2HDM compared to the R2HDM is an artifact of the scan, as in the C2HDM one of the neutral masses is not an input parameter but computed from the other two neutral input masses in contrast to the R2HDM so that the same coverage of the parameter space would require a dedicated scan in specific regions, *cf.* also the remark made above on the comparison of the coupling ranges of the R2HDM and C2HDM. Qualitatively, a larger scan would not change the overall picture, however.

From the plots we can infer from the steep rise of the cross section values, once  $m_{\uparrow} \geq 2m_{H_{\text{SM}}}$ , the resonant enhancement of the cross sections. In the case of the R2HDM this is due to resonant  $H_2$  production and for the C2HDM, N2HDM or NMSSM this can be resonant  $H_2$  and/or  $H_3$  production. For the latter models, in the case of  $H_{\text{SM}} \equiv H_3$ , and for the R2HDM in the case of  $H_{\text{SM}} \equiv H_2$  we can only have non-resonant di-Higgs production. We can also see that the cross section values can be suppressed compared to the SM case which is given by the horizontal line in the plots. The R2HDM and C2HDM cross sections approach the SM-like cross section for large mass values (red points) whereas this is not the case for the N2HDM with  $H_1 \equiv H_{\text{SM}}$ . In

<sup>16</sup>It is defined by the rotation matrix element squared  $|R_{i3}|^2$ , the index  $i$  denotes the SM-like Higgs boson in the mass basis, the index 3 the CP-violating degree of freedom in the interaction basis.

<sup>17</sup>The values of the signal rates for the various final states after the  $H_{\text{SM}}$  decays can be obtained by multiplying the cross section by the SM branching ratio into the final state of interest. To a very good approximation the values of the branching ratios of the SM Higgs boson can be applied here as the present LHC results push any SM extension strongly towards the SM limit.

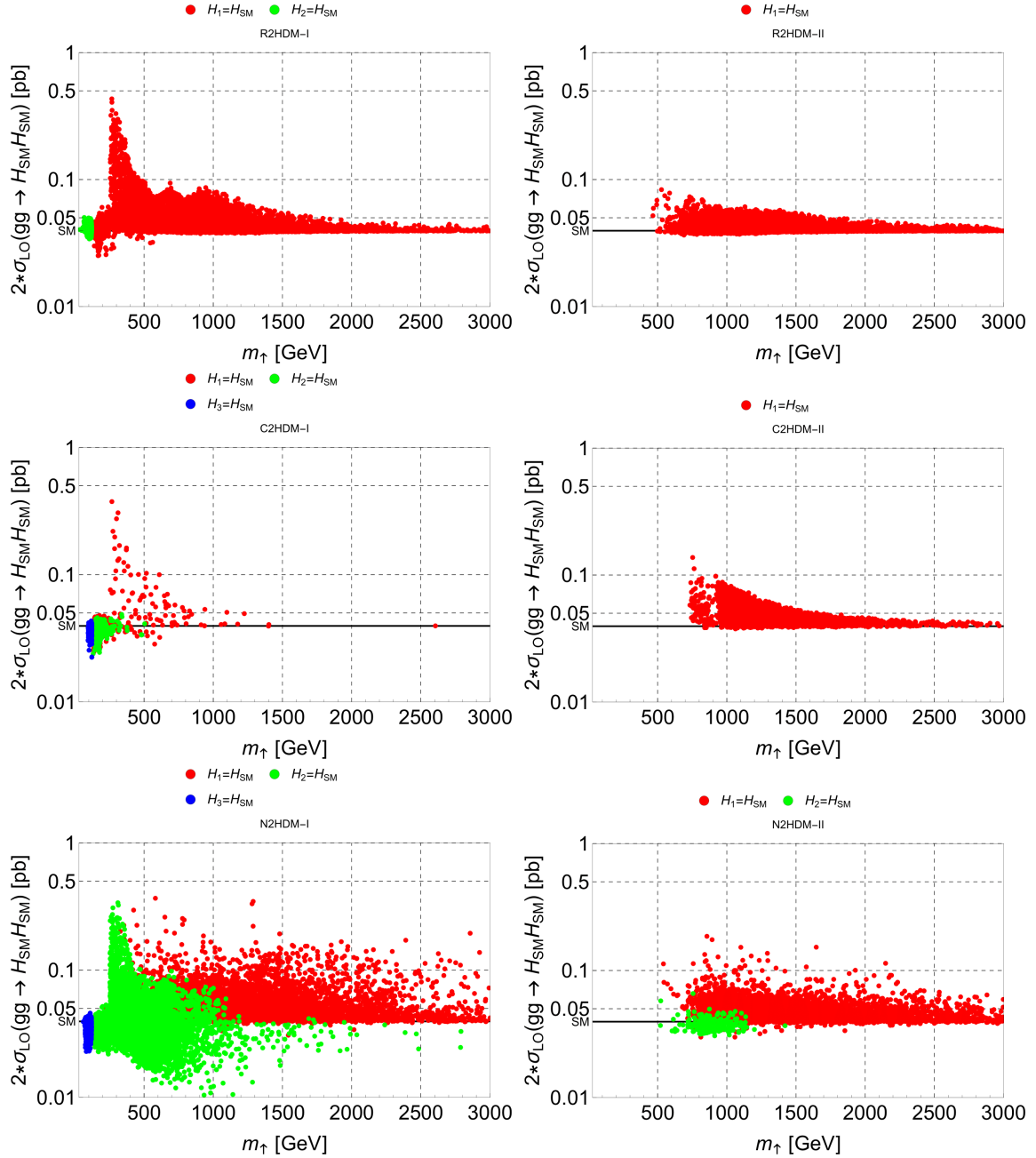


Figure 7: Scatter plots for SM-like Higgs pair production including a factor of 2 for estimating the NLO QCD corrections, for all points passing the constraints, as a function of the mass of the heavier of the non-SM-like Higgs bosons  $m_+$  for the R2HDM (upper), the C2HDM (middle), and the N2HDM (lower line), for type 1 (left column) and type 2 (right column). Red points for scenarios with  $H_1 \equiv H_{\text{SM}}$ , green ones for those where  $H_2 \equiv H_{\text{SM}}$ , and blue points for those where  $H_3 \equiv H_{\text{SM}}$ . Horizontal line: SM result.

the R2HDM, we approach the decoupling limit when  $m_{H_2}$  becomes large. For large  $H_2$  mass the production cross section decreases, and furthermore with increasing  $m_{H_2}$  the trilinear coupling  $\lambda_{H_2 H_1 H_1}$  that is relevant for resonant  $H_1 H_1$  production goes to zero as it is proportional to  $\cos(\beta - \alpha)$  which approaches zero in the decoupling limit. In the N2HDM, for  $H_1 \equiv H_{\text{SM}}$ , we

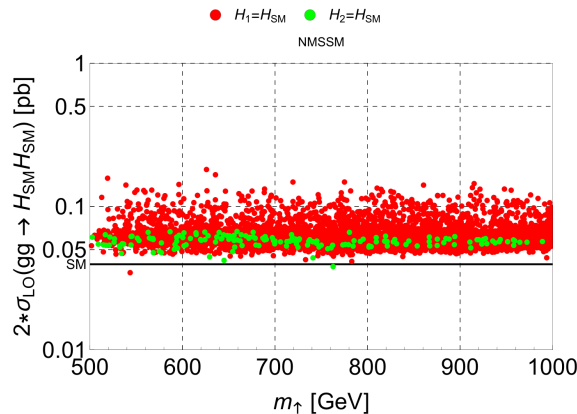


Figure 8: Same as Fig. 7, but for the NMSSM.

	$H_1$	$H_2$	$H_3$		$H_1$	$H_2$
R2HDM-I	59	49		R2HDM-I	92	–
R2HDM-II	–	–		R2HDM-II	59	–
C2HDM-I	46	44	42	C2HDM-I	98	42
C2HDM-II	–	–	–	C2HDM-II	75	–
N2HDM-I	50	52	44	N2HDM-I	151	96
N2HDM-II	–	–	–	N2HDM-II	112	48
NMSSM	–	–	–	NMSSM	73	65

Table 6: Maximum NLO QCD gluon fusion cross section values in fb for the case where  $H_{\text{SM}} \equiv H_1$ ,  $H_2$ , and  $H_3$ , respectively, in the R2HDM-I/II, C2HDM-I/II, N2HDM-I and NMSSM. Left: scenarios with  $m_{H_i \neq H_{\text{SM}}} < 2m_{H_{\text{SM}}}$ ; right: scenarios with suppressed resonance contributions (*cf.* text).

can have resonant enhancement both from  $H_2$  and  $H_3$  production so that although  $m_{H_3} = m_{\uparrow}$  grows in Fig. 7 (middle) large cross sections are still possible due to resonant  $H_2$  production. For  $H_2 \equiv H_{\text{SM}}$  (green), on the other hand, we also see the decoupling behavior. Note that for the C2HDM-I we observe the decoupling behaviour for  $H_1 \equiv H_{\text{SM}}$  in contrast to the N2HDM. In the C2HDM  $m_{\downarrow}$  and  $m_{\uparrow}$  become nearly degenerate for large non-SM-like masses so that both the  $H_2$  and the  $H_3$  resonant contributions are small. Also, for lower masses  $m_{\uparrow}$  the masses of  $H_{\downarrow}$  and  $H_{\uparrow}$  do not differ much so that for  $H_2 \equiv H_{\text{SM}}$  (green points) the resonant enhancement is not efficient in increasing the cross section.

In Tab. 6 (left), we compare the maximum cross section values in the different models for all parameter scenarios where  $m_{H_i \neq H_{\text{SM}}} < 2m_{H_{\text{SM}}}$ , in case the SM-like Higgs boson is not given by the heaviest neutral one. For these scenarios resonance enhancement is kinematically forbidden. We have included the NLO QCD correction in the large top-mass limit. In the R2HDM-II and C2HDM-II for  $H_{\text{SM}} \equiv H_1$ , in the N2HDM-II and NMSSM for  $H_{\text{SM}} \equiv H_{1,2}$  we did not find any points where  $m_{H_i \neq H_{\text{SM}}} < 2m_{H_{\text{SM}}}$ , because of the constraints. Furthermore, in the C2HDM-II the application of the experimental constraints excludes scenarios with  $H_{\text{SM}} \equiv H_2$  or  $H_3$ , and in the N2HDM-II and the NMSSM for  $H_{\text{SM}} \equiv H_3$ . In the table, we put dashes for all these cases. We observe that the non-resonant cross sections for all models (where they are available) are above the SM value which is given by  $\sigma_{\text{SM}} = 38 \text{ fb}$ .<sup>18</sup> The largest value is obtained for the R2HDM-I with  $H_1 \equiv H_{\text{SM}}$ . The enhancements are due to a combination of Yukawa and self-coupling values deviating from the SM. Altogether the cross sections deviate by not more than a factor 1.5 from the SM value in the defined non-resonant regions.

<sup>18</sup>This value has been obtained with HPAIR in the heavy top-quark limit which we apply in the scans. In this limit the  $K$ -factor, *i.e.* the ratio between NLO and LO cross section, amounts to 1.93.

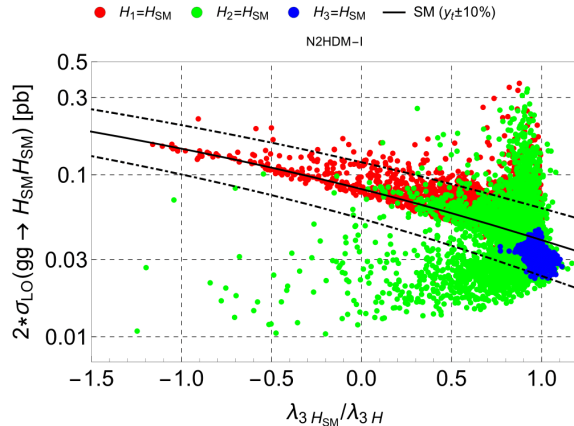


Figure 9: N2HDM-I: SM-like Higgs pair production including a factor 2 to roughly account for the NLO QCD corrections, for  $H_{1,2,3} \equiv H_{\text{SM}}$  (red, green, blue), as a function of the trilinear SM-like Higgs self-coupling  $\lambda_{3H_{\text{SM}}}$  normalized to the SM value  $\lambda_{3H}$ . The full line shows SM di-Higgs production as a function of  $\lambda_{3H_{\text{SM}}}/\lambda_{3H}$ . The dot-dashed lines show the additional change of this cross section for a variation of  $y_{t,H_{\text{SM}}}/y_{t,H} = 1 \pm 0.1$ .

It can also be that, although kinematically possible, the di-Higgs production cross section is not much enhanced compared to the SM value through resonance production. This is the case for suppressed Yukawa and/or trilinear coupling values of the  $s$ -channel exchanged heavy Higgs boson or because it is very heavy or its total width is large. Also destructive interferences can lead to a suppression. Therefore there is no clear correlation between the computed resonantly enhanced cross sections and the Higgs mass values of the resonantly produced Higgs boson as can also be inferred from Figs. 7 and 8. Only the obtained maximum values show the correlation with the mass value, namely that these maximum possible values decrease with increasing mass of the non-SM-like heavy Higgs as it is expected in models with a decoupling limit. In the suppressed case, from an experimental point of view, these scenarios would be interpreted as non-resonant di-Higgs production. As discussed above, the transition between resonant and non-resonant cases is not trivial. In accordance with our choice of separation given above, we also give the maximum cross section values for those scenarios where the resonance contribution makes up for less than 10% of the total di-Higgs cross section.<sup>19</sup> The NLO QCD values are summarised in Tab. 6 (right) for all models with  $H_{\text{SM}} = H_{1,2}$  (only  $H_1$  for the R2HDM).<sup>20</sup> As expected, they exceed the values given in Tab. 6 (left) but by at most a factor 3.

If not suppressed, the cross sections can be much more enhanced compared to the SM case in the resonance case. This can nicely be inferred from Fig. 9 which depicts the cross section values for SM-like Higgs pair production in the N2HDM-I as a function of the SM-like trilinear Higgs self-coupling ratio for all possible  $H_{\text{SM}}$  scenarios. The full line in the plot shows the SM di-Higgs production cross section as a function of the trilinear Higgs self-coupling variation, the dot-dashed lines additionally depict the change if we allow for a  $\pm 10\%$  variation of the top Yukawa coupling as is still compatible with the data. The comparison with these lines allows us to estimate the resonant enhancement effects beyond the cross section change due to modified trilinear Higgs self- and top-Yukawa-couplings. Close to the SM case  $\lambda_{3H_{\text{SM}}}/\lambda_{3H} = 1$  and  $y_{t,H_{\text{SM}}}/y_{t,H} = 1$ , we observe enhancements of up to 10 (9) times the SM expectation for  $H_1(H_2) \equiv H_{\text{SM}}$ . The enhancement stems from resonant heavy Higgs production which can be

<sup>19</sup>The values are obtained from the plateau region, *cf.* the horizontal branches in Figs. 4.

<sup>20</sup>For  $H_3 \equiv H_{\text{SM}}$  ( $H_2$  in the R2HDM) resonant production is not possible per definition.

	$H_1$	$H_2$
R2HDM-I	444	n.a.
R2HDM-II	81	n.a.
C2HDM-I	387	47
C2HDM-II	130	–
N2HDM-I	376	344
N2HDM-II	188	63
NMSSM	183	65

Table 7: Maximum NLO QCD gluon fusion cross section values for resonant SM-like Higgs pair production in fb for the case where  $H_{\text{SM}} \equiv H_1$ , and  $H_2$ , respectively, in the various considered models. In the R2HDM the case  $H_{\text{SM}} = H_2$  is not applicable (n.a.) as we cannot have resonant  $H_2 H_2$  production.

$H_2$  and/or  $H_3$  (only  $H_3$ ) for  $H_1 \equiv H_{\text{SM}}$  ( $H_2 \equiv H_{\text{SM}}$ ). For  $H_3 \equiv H_{\text{SM}}$ , no such enhancement is possible and the (small) deviations from the SM case (in the vicinity of  $\lambda_{3H_{\text{SM}}}^{\text{N2HDM}}/\lambda_{3H} = 1$ ) are due to the small deviations of the involved couplings from the SM values or due to interference effects with nearby Higgs bosons. In Tab. 7, we summarize the maximum cross section values in each model for the different SM-like Higgs configurations and for the parameter sets where resonant production is kinematically possible. The values in the tables are to be compared to the corresponding NLO QCD SM value (in the heavy top-limit) of 38 fb. The largest cross section with about 444 fb is obtained in the R2HDM-I, followed by the C2HDM-I with a value of 387 fb and the N2HDM-I with 376 fb, all for  $H_1 \equiv H_{\text{SM}}$ . The resonant BSM cross sections largely exceed the SM value by up to a factor 12. The clear hierarchy in the cross sections gives us a handle to at least partially distinguish the models by investigating solely Higgs pair production. Clearly cross section values above 400 fb would exclude all investigated models but the R2HDM-I with the lightest neutral Higgs boson being the SM-like one. A value above 100 fb on the other hand would exclude the R2HDM-II with  $H_1 \equiv H_{\text{SM}}$ , the C2HDM-I with  $H_2 \equiv H_{\text{SM}}$ , the N2HDM-II with  $H_2 \equiv H_{\text{SM}}$  and the NMSSM with  $H_2 \equiv H_{\text{SM}}$ . The numbers have to be taken with some care, however, as a more complete scan could find additional values. They should rather be taken as a rough guideline. Note furthermore, that in the NMSSM with  $H_2 \equiv H_{\text{SM}}$  the resonant production makes up only a small contribution of the full cross section meaning that it is the same point as the one quoted in Tab. 6 (right). The enhancement of the cross section is rather due to coupling deviations of the SM-like trilinear Higgs coupling, while the  $H_2$  top-Yukawa coupling is close to the SM value, and from an experimental point of view this would look like non-resonant di-Higgs production.

For completion, we include in Appendix A separately the information on resonant and non-resonant cross section values corresponding to Figs. 7 and 8. In the transition region, where resonant and non-resonant cross sections are similar in size, they should be taken, however, with a grain of salt.

## 5 Benchmarks for SM-Like Higgs Pair Production

In the following, we give the input parameters and basic features of all scenarios listed in Tab. 7. The various models and mass hierarchies have different interesting features: large di-Higgs cross sections, large rates for di-Higgs associated production with gauge bosons but also large triple Higgs production rates from Higgs-to-Higgs cascade decays that are only possible

in non-minimal Higgs sectors. Additionally, in the C2HDM, we have the possibility to test CP violation through the measurement of Higgs-to-Higgs or Higgs-to-gauge plus Higgs boson decays. These features will be specified for the various benchmarks. We will also give the dominant decay channels of the non-SM-like Higgs bosons. Due to space limitations, we cannot give all decay channels. They can be obtained, however, from the publicly available programs `HDECAY` [184–186], `C2HDM.HDECAY` [84], `N2HDECAY` [85, 86], and `NMSSMCALC` [172] by using the input values that we give for each benchmark point. The benchmark points comply with the present and past Higgs searches as explicitly checked by applying the code `HiggsBounds` where we made sure to take into account the latest search limits. Note in this context that light Higgs bosons still escape detection due to suppressed couplings. Moreover, for some light mass regions there are no experimental analyses available yet. This emphasizes once again the necessity to investigate the low BSM Higgs mass region to constrain extended Higgs sectors. Also the heavy Higgs bosons given in the following benchmarks are escaping all present exclusion limits with rates lying below the current experimental sensitivity.

All Higgs pair cross sections have been obtained with our codes based on `HPAIR` [179], that has been extended to include the various models, at NLO QCD in the heavy loop particle limit. The single Higgs cross sections are calculated at NNLO with the program `SusHi v1.6.1` [181–183]. The single and double Higgs production cross sections are given for  $\sqrt{s} = 14$  TeV. Further information on all benchmarks can be provided on request. Please write an email to the authors of the paper in this case.

### 5.1 Resonant SM-like $H_1 H_1$ Production in the R2HDM-I

This benchmark scenario provides maximum SM-like  $H_1 H_1$  production through resonant enhancement in the R2HDM-I, and is defined by the input parameters given in Tab. 8 (upper). Further information is provided in Tab. 8 (lower) where we give the NLO QCD  $H_1 H_1$  cross section value computed with `HPAIR` at  $\sqrt{s} = 14$  TeV along with the total widths of the Higgs bosons. We also give the values of the  $K$ -factor, *i.e.* the ratio between NLO and LO cross section, of the SM-like Yukawa and trilinear Higgs self-couplings normalized to their SM values and we list the single Higgs cross sections at NNLO QCD obtained from `SusHi` at the same c.m. energy.<sup>21</sup> Besides a large SM-like Higgs pair production cross section, the benchmark sce-

$m_{H_1}$ [GeV]	$m_{H_2}$ [GeV]	$m_A$ [GeV]	$m_{H^\pm}$ [GeV]	$\alpha$	$\tan \beta$	$m_{12}^2$ [GeV <sup>2</sup> ]
125.09	267	512	516	-0.259	4.276	15020
$\sigma_{H_1 H_1}^{\text{NLO}}$ [fb]	$K$ -factor	$\Gamma_{H_1}^{\text{tot}}$ [GeV]	$\Gamma_{H_2}^{\text{tot}}$ [GeV]	$\Gamma_A^{\text{tot}}$ [GeV]	$\Gamma_{H^\pm}^{\text{tot}}$ [GeV]	
444	2.06	$4.029 \times 10^{-3}$	0.011	14.57	16.07	
$\lambda_{3H_1}/\lambda_{3H}$	$y_{t,H_1}/y_{t,H}$	$\sigma_{H_1}^{\text{NNLO}}$ [pb]	$\sigma_{H_2}^{\text{NNLO}}$ [pb]	$\sigma_A^{\text{NNLO}}$ [pb]		
0.993	0.993	48.56	0.916	0.489		

Table 8: **BP1** Upper: R2HDM-1 input parameters. Lower: NLO QCD  $H_1 H_1$  pair production cross section in gluon fusion in the heavy loop particle limit,  $K$ -factor, the total widths of the Higgs bosons, the SM-like ( $H_1$ ) Yukawa and trilinear Higgs couplings normalized to their SM values and the single Higgs production cross sections at NNLO QCD for  $H_{1,2}$  and  $A$ .

nario features a large rate for SM-like Higgs pair production in association with a  $Z$  boson. The

<sup>21</sup>All single Higgs production cross sections quoted in this section are computed at NNLO QCD for  $\sqrt{s} = 14$  TeV.

dominant branching ratios of  $H_2$ ,  $A$ , and  $H^\pm$  are given by

$$\begin{aligned} \text{BR}(H_2 \rightarrow H_1 H_1) &= 0.544, & \text{BR}(H_2 \rightarrow WW) &= 0.280, & \text{BR}(H_2 \rightarrow ZZ) &= 0.121, \\ \text{BR}(A \rightarrow ZH_2) &= 0.912, & \text{BR}(A \rightarrow t\bar{t}) &= 0.086, \\ \text{BR}(H^\pm \rightarrow W^\pm H_2) &= 0.922, & \text{BR}(H^+ \rightarrow t\bar{b}) &= 0.076. \end{aligned} \quad (5.20)$$

With the values given we see that indeed  $H_2$  resonant production is responsible for the enhancement of the cross section as

$$\sigma_{H_2}^{\text{NNLO}} \times \text{BR}(H_2 \rightarrow H_1 H_1) = 498 \text{ fb}. \quad (5.21)$$

The fact that the HPAIR result for  $H_1 H_1$  production is somewhat lower is due to the finite width of  $H_2$  that is taken into account in the HPAIR calculation when we integrate across the  $H_2$  resonance in the  $s$ -channel. We find that for associated  $H_1 H_1$  production with a  $Z$  boson we have

$$\sigma_A^{\text{NNLO}} \times \text{BR}(A \rightarrow ZH_2) \times \text{BR}(H_2 \rightarrow H_1 H_1) = 0.489 \text{ pb} \times 0.912 \times 0.544 = 247 \text{ fb}. \quad (5.22)$$

This leads to a  $Z + (4b)$  final state with a signal rate of 84 fb so that this discovery channel for  $A$  exceeds  $A$  production in the  $t\bar{t}$  final state which amounts to 43 fb.

## 5.2 Resonant SM-like $H_1 H_1$ Production in the R2HDM-II

This is the benchmark scenario for maximum SM-like  $H_1 H_1$  production through resonant enhancement in the R2HDM-II, with the input parameters given in Tab. 9 (upper) and Higgs pair and single Higgs production information in Tab. 9 (lower). As we are in the type 2 model, the overall Higgs spectrum is heavier than BP1. Here we also have, apart from a large SM-like Higgs

$m_{H_1}$ [GeV]	$m_{H_2}$ [GeV]	$m_A$ [GeV]	$m_{H^\pm}$ [GeV]	$\alpha$	$\tan \beta$	$m_{12}^2$ [GeV <sup>2</sup> ]
125.09	528	798	809	-0.695	1.268	130388

$\sigma_{H_1 H_1}^{\text{NLO}}$ [fb]	$K$ -factor	$\Gamma_{H_1}^{\text{tot}}$ [GeV]	$\Gamma_{H_2}^{\text{tot}}$ [GeV]	$\Gamma_A^{\text{tot}}$ [GeV]	$\Gamma_{H^\pm}^{\text{tot}}$ [GeV]
81	1.94	$4.239 \times 10^{-3}$	10.15	47.82	51.56

$\lambda_{3H_1}/\lambda_{3H}$	$y_{t,H_1}/y_{t,H}$	$\sigma_{H_1}^{\text{NNLO}}$ [pb]	$\sigma_{H_2}^{\text{NNLO}}$ [pb]	$\sigma_A^{\text{NNLO}}$ [pb]	
0.974	0.978	47.02	2.84	0.47	

Table 9: **BP2** Upper: R2HDM-II input parameters. Lower: Additional double and single Higgs production related information.

pair production cross section, SM-like Higgs pair production in association with a  $Z$  boson, though at a much lower rate. The dominant  $H_2$ ,  $A$ , and  $H^\pm$  branching ratios are given by

$$\begin{aligned} \text{BR}(H_2 \rightarrow H_1 H_1) &= 0.012, & \text{BR}(H_2 \rightarrow t\bar{t}) &= 0.979, \\ \text{BR}(A \rightarrow ZH_2) &= 0.514, & \text{BR}(A \rightarrow t\bar{t}) &= 0.482, \\ \text{BR}(H^\pm \rightarrow W^\pm H_2) &= 0.560, & \text{BR}(H^+ \rightarrow t\bar{b}) &= 0.437. \end{aligned} \quad (5.23)$$

From the values given we calculate the di-Higgs  $H_1 H_1$  cross section from resonant  $H_2$  production,

$$\sigma_{H_2}^{\text{NNLO}} \times \text{BR}(H_2 \rightarrow H_1 H_1) = 34 \text{ fb}. \quad (5.24)$$

Comparing this with the  $H_1 H_1$  Higgs pair production cross section we see that resonant  $H_2$  production is responsible for the enhanced cross section (as can be seen when taking into account

also the SM-like contribution of 38 fb included in HPAIR).<sup>22</sup> Also the deviations of the  $H_1$  trilinear and Yukawa couplings from the SM values cause a slight enhancement. For  $H_1 H_1$  associated production with a  $Z$  boson we find

$$\sigma_{\text{prod}}(A) \times \text{BR}(A \rightarrow ZH_2) \times \text{BR}(H_2 \rightarrow H_1 H_1) = 0.47 \text{ pb} \times 0.514 \times 0.012 = 2.9 \text{ fb} , \quad (5.25)$$

leading to a  $Z + (4b)$  rate of 1.04 fb.

### 5.3 Resonant SM-like $H_1 H_1$ Production in the C2HDM-I

In Tab. 10 (upper), the input parameters for the scenario with maximum resonant SM-like Higgs production with  $H_1 \equiv H_{\text{SM}}$  in the C2HDM-I are given. Further Higgs pair and single Higgs production information is summarized in Tab. 10 (lower). Apart from its large SM di-Higgs cross section this scenario is special as it allows for the test of CP violation through Higgs decays when decays are combined [203]. The dominant branching ratios of the non-SM-like Higgs bosons are

$m_{H_1}$ [GeV]	$m_{H_2}$ [GeV]	$m_{H^\pm}$ [GeV]	$\alpha_1$	$\alpha_2$	$\alpha_3$	$\tan \beta$	$\text{Re}(m_{12}^2)$ [GeV <sup>2</sup> ]
125.09	265	236	1.419	0.004	-0.731	5.474	9929

$\sigma_{H_1 H_1}^{\text{NLO}}$ [fb]	$K$ -factor	$\Gamma_{H_1}^{\text{tot}}$ [GeV]	$\Gamma_{H_2}^{\text{tot}}$ [GeV]	$\Gamma_{H_3}^{\text{tot}}$ [GeV]	$\Gamma_{H^\pm}^{\text{tot}}$ [GeV]
387	2.06	$4.106 \times 10^{-3}$	$3.625 \times 10^{-3}$	$4.880 \times 10^{-3}$	0.127

$\lambda_{3H_1}/\lambda_{3H}$	$y_{t,H_1}^c/y_{t,H}$	$\sigma_{H_1}^{\text{NNLO}}$ [pb]	$\sigma_{H_2}^{\text{NNLO}}$ [pb]	$\sigma_{H_3}^{\text{NNLO}}$ [pb]	
0.995	1.005	49.75	0.76	0.84	

Table 10: **BP3** Upper: C2HDM-I input parameters. The third Higgs boson mass calculated from the input parameters is given by  $m_{H_3} = 267$  GeV. Lower: Additional double and single Higgs production related information. The value for  $y_{t,H_1}^c$  is the CP-even part of the Yukawa coupling. The CP-odd part for the SM-like Higgs is tiny.

$$\begin{aligned}
\text{BR}(H_2 \rightarrow H_1 H_1) &= 0.252 , & \text{BR}(H_2 \rightarrow WW) &= 0.335 , \\
\text{BR}(H_2 \rightarrow ZZ) &= 0.144 , & \text{BR}(H_2 \rightarrow ZH_1) &= 0.161 , \\
\text{BR}(H_3 \rightarrow H_1 H_1) &= 0.280 , & \text{BR}(H_3 \rightarrow WW) &= 0.376 , \\
\text{BR}(H_3 \rightarrow ZZ) &= 0.162 , & \text{BR}(H_3 \rightarrow ZH_1) &= 0.090 , \\
\text{BR}(H^\pm \rightarrow tb) &= 0.995 .
\end{aligned} \quad (5.26)$$

With the single Higgs production cross sections given in Tab. 10 (lower) the large cross section is due to resonant enhancement from both  $H_2$  and  $H_3$ ,

$$\begin{aligned}
\sigma_{H_2}^{\text{NNLO}} \times \text{BR}(H_2 \rightarrow H_1 H_1) &= 191 \text{ fb} \\
\sigma_{H_3}^{\text{NNLO}} \times \text{BR}(H_3 \rightarrow H_1 H_1) &= 235 \text{ fb} ,
\end{aligned} \quad (5.27)$$

and we arrive at the following Higgs-to-Higgs, Higgs-to-gauge bosons and Higgs-to-gauge+Higgs rates

$$\begin{aligned}
\sigma(H_2) \times \text{BR}(H_2 \rightarrow H_1 H_1) &= 191 \text{ fb} , & \sigma(H_2) \times \text{BR}(H_2 \rightarrow WW) &= 254 \text{ fb} , \\
\sigma(H_2) \times \text{BR}(H_2 \rightarrow ZZ) &= 109 \text{ fb} , & \sigma(H_2) \times \text{BR}(H_2 \rightarrow ZH_1) &= 122 \text{ fb} , \\
\sigma(H_3) \times \text{BR}(H_3 \rightarrow H_1 H_1) &= 235 \text{ fb} , & \sigma(H_3) \times \text{BR}(H_3 \rightarrow WW) &= 315 \text{ fb} , \\
\sigma(H_3) \times \text{BR}(H_3 \rightarrow ZZ) &= 136 \text{ fb} , & \sigma(H_3) \times \text{BR}(H_3 \rightarrow ZH_1) &= 76 \text{ fb} .
\end{aligned} \quad (5.28)$$

<sup>22</sup>Note that deviations between the full HPAIR result and the SusHi result are to be expected as HPAIR takes into account all  $s$ -channel (including the total widths of the  $s$ -channel particles) and box contributions and their interferences.

These large rates allow for the test of CP violation through Higgs decays. The decays of  $H_{2/3}$  each into  $WW/ZZ$  and the SM-like Higgs boson pair  $H_1H_1$  assuming  $H_1$  is CP-even<sup>23</sup> attribute the CP quantum number +1 to  $H_{2/3}$ . On the other hand, the decays into  $ZH_1$  of  $H_{2/3}$  identify them to be CP-odd. The simultaneous measurement of all these decays with substantial rates would clearly identify  $H_{2/3}$  to be states with mixed CP quantum numbers. Note that  $\text{BR}(H_1 \rightarrow b\bar{b}) = 0.592$ .

#### 5.4 Resonant SM-like $H_2H_2$ Production in the C2HDM-I

Information on this benchmark point is gathered in Tab. 11. It features an overall light Higgs mass spectrum. In contrast to the previous C2HDM scenario, the corresponding rates are too small to allow for the test of CP violation through Higgs decays. This is also the case for the other C2HDM scenario presented in the following. The dominant branching ratios of the

$m_{H_1}$ [GeV]	$m_{H_2}$ [GeV]	$m_{H^\pm}$ [GeV]	$\alpha_1$	$\alpha_2$	$\alpha_3$	$\tan \beta$	$\text{Re}(m_{12}^2)$ [GeV <sup>2</sup> ]
74	125.09	347	-0.308	-1.328	-0.434	10.69	9758

$\sigma_{H_2H_2}^{\text{NLO}}$ [fb]	$K$ -factor	$\Gamma_{H_1}^{\text{tot}}$ [GeV]	$\Gamma_{H_2}^{\text{tot}}$ [GeV]	$\Gamma_{H_3}^{\text{tot}}$ [GeV]	$\Gamma_{H^\pm}^{\text{tot}}$ [GeV]
47	1.95	$2.662 \times 10^{-5}$	$3.990 \times 10^{-3}$	9.22	10.33

$\lambda_{3H_2}/\lambda_{3H}$	$y_{t,H_2}^e/y_{t,H}$	$\sigma_{H_1}^{\text{NNLO}}$ [pb]	$\sigma_{H_2}^{\text{NNLO}}$ [pb]	$\sigma_{H_3}^{\text{NNLO}}$ [pb]	
1.127	0.993	3.37	48.56	0.22	

Table 11: **BP4** Upper: C2HDM-I input parameters. The third Higgs boson mass calculated from the input parameters is given by  $m_{H_3} = 338$  GeV. Lower: Additional double and single Higgs production related information. The value for  $y_{t,H_2}^e$  is the CP-even part of the Yukawa coupling. The CP-odd part for the SM-like Higgs is tiny.

non-SM-like Higgs bosons are given by

$$\begin{aligned} \text{BR}(H_1 \rightarrow b\bar{b}) &= 0.797, & \text{BR}(H_3 \rightarrow ZH_1) &= 0.865, & \text{BR}(H_3 \rightarrow H_2H_2) &= 0.047, \\ \text{BR}(H_3 \rightarrow WW) &= 0.048, & \text{BR}(H^\pm \rightarrow W^\pm H_1) &= 0.954. \end{aligned}$$

In this scenario, the enhancement of the cross section is due to resonant  $H_3$  production. We have

$$\sigma_{H_3}^{\text{NNLO}} \times \text{BR}(H_3 \rightarrow H_2H_2) = 10.34 \text{ fb}. \quad (5.29)$$

#### 5.5 Resonant SM-like $H_1H_1$ Production in the C2HDM-II

For the C2HDM-II the maximum resonant production of a SM-like Higgs pair with  $H_{\text{SM}} \equiv H_1$  is given by **BP5** with the input parameters defined in Tab. 12 (upper) and additional information related to double and single Higgs production in Tab. 12 (lower). Overall, the Higgs spectrum is rather heavy as expected in type-2 models. The dominant branching ratios of the non-SM-like

<sup>23</sup>Note that although it is by now clear that the SM-like Higgs cannot be a pure CP-odd state, we are far from excluding large CP-odd components in its Yukawa couplings. In fact, there are so far only direct measurements of the  $t\bar{t}H_{\text{SM}}$  and  $\tau^+\tau^-H_{\text{SM}}$  couplings. Both ATLAS and CMS [204, 205] were able to exclude the purely CP-odd hypothesis in the process  $pp \rightarrow t\bar{t}(H_{\text{SM}} \rightarrow \gamma\gamma)$  with 3.9 standard deviations and to establish a 95% CL observed (expected) exclusion upper limit for the mixing angle of  $43^\circ$  ( $63^\circ$ ). Recently CMS [206] has performed the first measurement of the CP mixing angle of the tau lepton Yukawa coupling, using 13 TeV data, and an integrated luminosity of  $137 \text{ fb}^{-1}$ . The CP mixing angle was found to be  $4^\circ \pm 17^\circ$ , allowing to set an observed (expected) exclusion upper limit for the mixing angle of  $36^\circ$  ( $55^\circ$ ). This angle is defined as  $\arctan(b/a)$ , if the generic Yukawa coupling is written as  $a + ib\gamma_5$ .

$m_{H_1}$ [GeV]	$m_{H_2}$ [GeV]	$m_{H^\pm}$ [GeV]	$\alpha_1$	$\alpha_2$	$\alpha_3$	$\tan \beta$	$\text{Re}(m_{12}^2)$ [GeV <sup>2</sup> ]
125.09	743	820	0.717	0.096	1.151	0.924	206750

$\sigma_{H_1 H_1}^{\text{NLO}}$ [fb]	$K$ -factor	$\Gamma_{H_1}^{\text{tot}}$ [GeV]	$\Gamma_{H_2}^{\text{tot}}$ [GeV]	$\Gamma_{H_3}^{\text{tot}}$ [GeV]	$\Gamma_{H^\pm}^{\text{tot}}$ [GeV]
130	1.88	$4.179 \times 10^{-3}$	40.26	41.54	44.66
$\lambda_{3H_1}/\lambda_{3H}$	$y_{t,H_1}^e/y_{t,H}$	$\sigma_{H_1}^{\text{NNLO}}$ [pb]	$\sigma_{H_2}^{\text{NNLO}}$ [pb]	$\sigma_{H_3}^{\text{NNLO}}$ [pb]	
0.494	0.964	46.92	1.20	1.03	

Table 12: **BP5** Upper: C2HDM-II input parameters. The third Higgs boson mass calculated from the input parameters is given by  $m_{H_3} = 753$  GeV. Lower: Additional double and single Higgs production related information. The value for  $y_{t,H_1}^e$  is the CP-even part of the Yukawa coupling. The CP-odd part for the SM-like Higgs is very small.

Higgs bosons are given by

$$\begin{aligned} \text{BR}(H_2 \rightarrow t\bar{t}) &= 0.928, \quad \text{BR}(H_3 \rightarrow t\bar{t}) = 0.939, \\ \text{BR}(H^\pm \rightarrow tb) &= 0.961. \end{aligned} \quad (5.30)$$

The dominant contribution to resonant production stems from  $H_2$ . More specifically, we have

$$\sigma(H_2) \times \text{BR}(H_2 \rightarrow H_1 H_1) = 1.20 \text{ pb} \times 0.031 = 37 \text{ fb} \quad (5.31)$$

$$\sigma(H_3) \times \text{BR}(H_3 \rightarrow H_1 H_1) = 1.03 \text{ pb} \times 0.022 = 23 \text{ fb}. \quad (5.32)$$

The sum of the two resonant contributions makes up for about half of the total cross section. The remaining part is given by non-resonant production which is enhanced compared to the SM case because the trilinear coupling between three SM-like Higgs bosons deviates from the SM case so that the destructive interference between box and triangle diagrams is not effective.

## 5.6 Resonant SM-like $H_1 H_1$ Production in the N2HDM-I

The input parameters for the scenario BP6 with maximum resonant SM-like Higgs production with  $H^{\text{SM}} \equiv H_1$  in the N2HDM-I are given in Tab. 13 (upper) with additional information related to double and single Higgs production in Tab. 13 (lower). For this N2HDM point it is basically the resonant contribution of both  $H_2$  that leads to the enhanced  $H_1 H_1$  production with  $H_2$  being rather light, namely  $m_{H_2} = 269$  GeV. Additionally we have a large rate for Higgs pair production in association with a  $Z$  boson, and we can produce three SM-like Higgs bosons at a rate that might be accessible at a high-luminosity collider. The dominant branching ratios of the non-SM-like Higgs bosons into observable final states are

$$\begin{aligned} \text{BR}(H_2 \rightarrow H_1 H_1) &= 0.946, \quad \text{BR}(H_2 \rightarrow WW) = 0.035, \quad \text{BR}(H_2 \rightarrow ZZ) = 0.015, \\ \text{BR}(H_3 \rightarrow H_2 H_2) &= 0.314, \quad \text{BR}(H_3 \rightarrow W^+ H^-) = 0.299, \quad \text{BR}(H_3 \rightarrow ZA) = 0.117, \\ \text{BR}(A \rightarrow t\bar{t}) &= 0.533, \quad \text{BR}(A \rightarrow ZH_2) = 0.396, \quad \text{BR}(H^\pm \rightarrow tb) = 0.560. \end{aligned} \quad (5.33)$$

The resonant contribution stems here basically from  $H_2$  resonant production where we have

$$\sigma(H_2) \times \text{BR}(H_2 \rightarrow H_1 H_1) = 397 \text{ fb} \quad (5.34)$$

The resonant contribution from  $H_3$  amounts only to 0.63 fb. We find that the  $H_1 H_1$  production value computed with HPAIR is lower than the value given in Eq. (5.34). The comparatively lower

$m_{H_1}$ [GeV]	$m_{H_2}$ [GeV]	$m_{H_3}$ [GeV]	$m_A$ [GeV]	$m_{H^\pm}$ [GeV]	$\tan \beta$
125.09	269	582	390	380	4.190
$\alpha_1$	$\alpha_2$	$\alpha_3$	$v_s$ [GeV]	$\text{Re}(m_{12}^2)$ [GeV <sup>2</sup> ]	
1.432	-0.109	0.535	1250	28112	

$\sigma_{H_1 H_1}^{\text{NLO}}$ [fb]	$K$ -factor	$\Gamma_{H_1}^{\text{tot}}$ [GeV]	$\Gamma_{H_2}^{\text{tot}}$ [GeV]	$\Gamma_{H_3}^{\text{tot}}$ [GeV]	$\Gamma_A^{\text{tot}}$ [GeV]	$\Gamma_{H^\pm}^{\text{tot}}$ [GeV]
376	2.05	$4.130 \times 10^{-3}$	0.0752	15.279	1.483	1.477
$\lambda_{3H_1}/\lambda_{3H}$	$y_{t,H_1}/y_{t,H}$	$\sigma_{H_1}^{\text{NNLO}}$ [pb]	$\sigma_{H_2}^{\text{NNLO}}$ [pb]	$\sigma_{H_3}^{\text{NNLO}}$ [pb]	$\sigma_A^{\text{NNLO}}$	
0.876	1.012	50.47	0.42	0.002	2.16	

Table 13: **BP6** Upper: N2HDM-I input parameters. Lower: Additional double and single Higgs production related information.

value of the **HPAIR** result is caused by the finite width of  $H_2$  as we explicitly checked.

We note that in this scenario SM-like plus additional Higgs boson pair production can amount to

$$\sigma(H_1 H_2) = 5.17 \text{ fb} , \quad (5.35)$$

which leads to a triple SM-like  $H_1$  rate of 4.89 fb and a  $6b$ -quark final state at 1.04 fb as  $\text{BR}(H_1 \rightarrow b\bar{b})=0.597$ . Higgs pair production in association with a  $Z$  boson can be large,

$$\sigma_{\text{prod}}(A) \times \text{BR}(A \rightarrow Z H_2) \times \text{BR}(H_2 \rightarrow H_1 H_1) = 2.16 \text{ pb} \times 0.396 \times 0.946 = 809 \text{ fb} , \quad (5.36)$$

leading to a  $Z + (4b)$  rate of 288 fb.

## 5.7 Resonant SM-like $H_2 H_2$ Production in the N2HDM-I

Here we have the scenario **BP7** where  $H_2 \equiv H_{\text{SM}}$ . The point is interesting not only because of its large  $H_2 H_2$  cross section but also because it allows for significant production of a Higgs pair with a  $Z$  boson in the final state and it leads to a large pair production rate for the SM-like Higgs together with a non-SM-like lighter one. All  $Z H_1 H_2$ ,  $Z H_1 H_1$  and  $H_1 H_2$  production channels have significant rates in the  $4b$  (plus  $Z$ ) final states. The input parameters are listed in Tab. 14 (upper) together with double and single Higgs production related information in Tab. 14 (lower). The CP-even Higgs bosons are rather light.

$m_{H_1}$ [GeV]	$m_{H_2}$ [GeV]	$m_{H_3}$ [GeV]	$m_A$ [GeV]	$m_{H^\pm}$ [GeV]	$\tan \beta$
75	125.09	311	646	659	1.619
$\alpha_1$	$\alpha_2$	$\alpha_3$	$v_s$ [GeV]	$\text{Re}(m_{12}^2)$ [GeV <sup>2</sup> ]	
-0.936	-1.020	-0.341	1432	20022	

$\sigma_{H_2 H_2}^{\text{NLO}}$ [fb]	$K$ -factor	$\Gamma_{H_1}^{\text{tot}}$ [GeV]	$\Gamma_{H_2}^{\text{tot}}$ [GeV]	$\Gamma_{H_3}^{\text{tot}}$ [GeV]	$\Gamma_A^{\text{tot}}$ [GeV]	$\Gamma_{H^\pm}^{\text{tot}}$ [GeV]
344	2.04	$4.666 \times 10^{-4}$	$3.605 \times 10^{-3}$	0.137	57.43	62.72
$\lambda_{3H_2}/\lambda_{3H}$	$y_{t,H_2}/y_{t,H}$	$\sigma_{H_1}^{\text{NNLO}}$ [pb]	$\sigma_{H_2}^{\text{NNLO}}$ [pb]	$\sigma_{H_3}^{\text{NNLO}}$ [pb]	$\sigma_A^{\text{NNLO}}$	
0.921	0.928	29.98	42.39	3.08	0.95	

Table 14: **BP7** Upper: N2HDM-I input parameters. Lower: Additional double and single Higgs production related information.

The dominant branching ratios of the non-SM-like Higgs bosons are

$$\begin{aligned}
\text{BR}(H_1 \rightarrow b\bar{b}) &= 0.838, \text{BR}(H_3 \rightarrow H_1 H_2) = 0.831, \text{BR}(H_3 \rightarrow H_2 H_2) = 0.123, \\
\text{BR}(A \rightarrow Z H_1) &= 0.327, \text{BR}(A \rightarrow Z H_3) = 0.464, \text{BR}(A \rightarrow t\bar{t}) = 0.199, \\
\text{BR}(H^\pm \rightarrow tb) &= 0.179, \text{BR}(H^\pm \rightarrow W^\pm H_1) = 0.324, \text{BR}(H^\pm \rightarrow W^\pm H_3) = 0.487.
\end{aligned} \tag{5.37}$$

This leads to substantial production rates for Higgs pair plus gauge boson final states, namely

$$\begin{aligned}
\sigma_{\text{prod}}(A) \times \text{BR}(A \rightarrow Z H_3) \times \text{BR}(H_3 \rightarrow H_1 H_2) &= 0.95 \text{ pb} \times 0.464 \times 0.831 = 366 \text{ fb}, \\
\sigma_{\text{prod}}(A) \times \text{BR}(A \rightarrow Z H_3) \times \text{BR}(H_3 \rightarrow H_2 H_2) &= 0.95 \text{ pb} \times 0.464 \times 0.123 = 54 \text{ fb}.
\end{aligned} \tag{5.38}$$

With *e.g.*  $\text{BR}(H_2 \rightarrow b\bar{b}) = 0.575$  and  $\text{BR}(H_1 \rightarrow b\bar{b}) = 0.838$ , this leads to  $Z + 4b$  final states with rates of 176 fb in  $Z H_1 H_2$  production and 18 fb in  $Z H_2 H_2$  production. Since the branching ratio of  $H_3$  into  $H_1 H_2$  is rather large and also the  $H_3$  production cross section is significant with  $\sigma(H_3) = 3.08 \text{ pb}$ , we can expect  $H_1 H_2$  production to be large due to resonant enhancement. And indeed we find at NLO QCD a large cross section of

$$\sigma(H_1 H_2) = 2.15 \text{ pb}, \tag{5.39}$$

leading to 1.04 pb in the  $4b$  final state.

## 5.8 Resonant SM-like $H_1 H_1$ Production in the N2HDM-II

For this scenario, the information is given in Tab. 15. The dominant branching ratios of the

$m_{H_1}$ [GeV]	$m_{H_2}$ [GeV]	$m_{H_3}$ [GeV]	$m_A$ [GeV]	$m_{H^\pm}$ [GeV]	$\tan \beta$
125.09	302	856	959	946	1.650
$\alpha_1$	$\alpha_2$	$\alpha_3$	$v_s$ [GeV]	$\text{Re}(m_{12}^2)$ [GeV <sup>2</sup> ]	
1.077	-0.258	-1.444	4548	277693	

$\sigma_{H_1 H_1}^{\text{NLO}}$ [fb]	$K$ -factor	$\Gamma_{H_1}^{\text{tot}}$ [GeV]	$\Gamma_{H_2}^{\text{tot}}$ [GeV]	$\Gamma_{H_3}^{\text{tot}}$ [GeV]	$\Gamma_A^{\text{tot}}$ [GeV]	$\Gamma_{H^\pm}^{\text{tot}}$ [GeV]
188	2.02	$3.426 \times 10^{-3}$	1.076	12.97	18.84	23.36
$\lambda_{3H_1}/\lambda_{3H}$	$y_{t,H_1}/y_{t,H}$	$\sigma_{H_1}^{\text{NNLO}}$ [pb]	$\sigma_{H_2}^{\text{NNLO}}$ [pb]	$\sigma_{H_3}^{\text{NNLO}}$ [pb]	$\sigma_A^{\text{NNLO}}$ [pb]	
0.719077	0.996	49.11	0.40	0.12	0.09	

Table 15: **BP8** Upper: N2HDM-II input parameters. Lower: Additional double and single Higgs production related information.

non-SM-like Higgs bosons are

$$\begin{aligned}
\text{BR}(H_2 \rightarrow H_1 H_1) &= 0.478, \text{BR}(H_2 \rightarrow WW) = 0.361, \\
\text{BR}(H_2 \rightarrow ZZ) &= 0.160, \\
\text{BR}(H_3 \rightarrow t\bar{t}) &= 0.907, \\
\text{BR}(A \rightarrow Z H_2) &= 0.133, \text{BR}(A \rightarrow t\bar{t}) = 0.818, \\
\text{BR}(H^\pm \rightarrow W^\pm H_2) &= 0.134, \text{BR}(H^\pm \rightarrow tb) = 0.822.
\end{aligned} \tag{5.40}$$

With  $\text{BR}(H_3 \rightarrow H_1 H_1) = 0.0458$ , we have the resonant  $H_1 H_1$  production rates

$$\sigma(H_2) \times \text{BR}(H_2 \rightarrow H_1 H_1) = 191 \text{ fb}, \tag{5.41}$$

$$\sigma(H_3) \times \text{BR}(H_3 \rightarrow H_1 H_1) = 5.50 \text{ fb}. \tag{5.42}$$

The di-Higgs cross section enhancement hence basically stems from the  $H_2$  exchange in the triangle diagram. Higgs pair production in association with a  $Z$  boson has a rather low rate of

$$\sigma_{\text{prod}}(A) \times \text{BR}(A \rightarrow ZH_2) \times \text{BR}(H_2 \rightarrow H_1H_1) = 90 \text{ fb} \times 0.133 \times 0.478 = 5.72 \text{ fb} , \quad (5.43)$$

leading to a  $Z + (4b)$  rate of 1.72 fb.

## 5.9 Resonant SM-like $H_2H_2$ Production in the N2HDM-II

In Tab. 16, we summarize information on this scenario. For the non-SM-like Higgs bosons, the

$m_{H_1}$ [GeV]	$m_{H_2}$ [GeV]	$m_{H_3}$ [GeV]	$m_A$ [GeV]	$m_{H^\pm}$ [GeV]	$\tan \beta$
117	125.09	756	792	836	1.040
$\alpha_1$	$\alpha_2$	$\alpha_3$	$v_s$ [GeV]	$\text{Re}(m_{12}^2)$ [GeV <sup>2</sup> ]	
0.392	1.484	-1.193	865	252856	

$\sigma_{H_2H_2}^{\text{NLO}}$ [fb]	$K$ -factor	$\Gamma_{H_1}^{\text{tot}}$ [GeV]	$\Gamma_{H_2}^{\text{tot}}$ [GeV]	$\Gamma_{H_3}^{\text{tot}}$ [GeV]	$\Gamma_A^{\text{tot}}$ [GeV]	$\Gamma_{H^\pm}^{\text{tot}}$ [GeV]
63	1.91	$3.644 \times 10^{-5}$	$4.204 \times 10^{-3}$	30.14	34.49	35.03
$\lambda_{3H_2}/\lambda_{3H}$	$y_{t,H_2}/y_{t,H}$	$\sigma_{H_1}^{\text{NNLO}}$ [pb]	$\sigma_{H_2}^{\text{NNLO}}$ [pb]	$\sigma_{H_3}^{\text{NNLO}}$ [pb]	$\sigma_A^{\text{NNLO}}$ [pb]	
0.917	0.964	0.11	45.61	0.73	0.72	

Table 16: **BP9** Upper: N2HDM-II input parameters. Lower: Additional double and single Higgs production related information.

dominant branching ratios into detectable final states are

$$\begin{aligned} \text{BR}(H_1 \rightarrow b\bar{b}) &= 0.826 , & \text{BR}(H_3 \rightarrow t\bar{t}) &= 0.968 , \\ \text{BR}(A \rightarrow t\bar{t}) &= 0.987 , & \text{BR}(H^\pm \rightarrow tb) &= 0.986 . \end{aligned} \quad (5.44)$$

The resonant contribution to the cross section amounts to

$$\sigma_{H_3}^{\text{NNLO}} \times \text{BR}(H_3 \rightarrow H_2H_2) = 720 \times 0.0167 \text{ fb} = 12.02 \text{ fb} , \quad (5.45)$$

so that the larger SM-like  $H_2H_2$  production compared to the SM value is partly caused by resonant enhancement from  $H_3$  production.

## 5.10 Resonant SM-like $H_1H_1$ Production in the NMSSM

This NMSSM benchmark point features, besides a large  $H_1H_1$  production cross section, large rates for  $ZH_1H_1$  and triple  $H_1$  production. As stated above, in the NMSSM, the Higgs boson masses are computed from the input parameters of the model and higher-order corrections are important to shift the SM-like Higgs mass to the observed 125 GeV. We have computed these masses using the new version of **NMSSMCALC** which includes the two-loop Higgs mass corrections at  $\mathcal{O}((\alpha_\lambda + \alpha_\kappa + \alpha_t)^2 + \alpha_t \alpha_s)$  [176]. In Tab. 17, we list all input parameters for this benchmark point<sup>24</sup>

<sup>24</sup>In accordance with the SUSY Les Houches Accord (SLHA) [207, 208] the soft SUSY breaking masses and trilinear couplings are understood as  $\overline{\text{DR}}$  parameters at the scale  $M_{\text{SUSY}} = \sqrt{m_{\tilde{Q}_3} m_{\tilde{t}_R}}$  which is also the renormalisation scale used in the computation of the higher-order corrections to the Higgs masses. The soft SUSY breaking parameters of the first two generations are not listed as their influence is negligible. The remaining SM input parameters are given in Ref. [176]. The Higgs mass corrections are computed with on-shell renormalisation in the top/stop sector and on-shell renormalised charged Higgs mass, *cf.* [176] for details. For completeness, we also list the corresponding value of  $A_\lambda$ .

that are required by **NMSSMCALC** to compute the Higgs spectrum. Higgs masses, mixing angles and the total widths of the Higgs bosons, are given in Tab. 18. The table contains additional information related to double and single Higgs production. The given CP-even mixing elements  $h_{ij}$  ( $i, j = 1, 2, 3$ ) comply with the SLHA [207, 208], while the elements  $a_{ij}$  relate to the SLHA definition  $a_{ij}^{\text{SLHA}}$  through

$$\begin{aligned} a_{11}^{\text{SLHA}} &= \frac{a_{11}}{\sin \beta}, & a_{21}^{\text{SLHA}} &= \frac{a_{21}}{\sin \beta}, \\ a_{12}^{\text{SLHA}} &= a_{13}, & a_{22}^{\text{SLHA}} &= a_{23}. \end{aligned} \quad (5.46)$$

The dominant branching ratios of the non-SM-like Higgs bosons are given by

$\lambda$	$\kappa$	$A_\lambda$ [GeV]	$A_\kappa$ [GeV]	$\mu_{\text{eff}}$ [GeV]	$\tan \beta$
0.650	0.645	359.27	-432.19	224.95	2.622
$m_{H^\pm}$ [GeV]	$M_1$ [GeV]	$M_2$ [GeV]	$M_3$ [TeV]	$A_t$ [GeV]	$A_b$ [GeV]
610.64	810	642	2	-46	-1790
$m_{\tilde{Q}_3}$ [GeV]	$m_{\tilde{t}_R}$ [GeV]	$m_{\tilde{b}_R}$ [GeV]	$A_\tau$ [GeV]	$m_{\tilde{L}_3}$ [GeV]	$m_{\tilde{\tau}_R}$ [GeV]
1304	3000	3000	-93	3000	3000

Table 17: **BP10** NMSSM input parameters required by **NMSSMCALC** for the computation of the NMSSM spectrum. Lower: Additional double and single Higgs production related information.

$m_{H_1}$ [GeV]	$m_{H_2}$ [GeV]	$m_{H_3}$ [GeV]	$m_{A_1}$ [GeV]	$m_{A_2}$ [GeV]	$m_{H^\pm}$
122.39	300	626	543	616	611
$\Gamma_{H_1}^{\text{tot}}$ [GeV]	$\Gamma_{H_2}^{\text{tot}}$ [GeV]	$\Gamma_{H_3}^{\text{tot}}$ [GeV]	$\Gamma_{A_1}^{\text{tot}}$ [GeV]	$\Gamma_{A_2}^{\text{tot}}$ [GeV]	$\Gamma_{H^\pm}^{\text{tot}}$ [GeV]
$3.947 \times 10^{-3}$	0.127	4.81	5.52	5.82	5.61
$h_{11}$	$h_{12}$	$h_{13}$	$h_{21}$	$h_{22}$	$h_{23}$
0.372	0.924	0.092	0.170	-0.165	0.971
$h_{31}$	$h_{32}$	$h_{33}$	$a_{11}$	$a_{21}$	$a_{13}$
0.912	-0.346	-0.219	0.133	0.925	0.990
$a_{23}$	$\lambda_{3H_1}/\lambda_{3H}$	$y_{t,H_1}/y_{t,H}$			
-0.143	0.594	0.988			
$\sigma_{H_1 H_1}^{\text{NLO}}$ [fb]	$\sigma_{H_1}^{\text{NNLO}}$ [pb]	$\sigma_{H_2}^{\text{NNLO}}$ [pb]	$\sigma_{H_3}^{\text{NNLO}}$ [pb]	$\sigma_{A_1}^{\text{NNLO}}$ [pb]	$\sigma_{A_2}^{\text{NNLO}}$ [pb]
183	49.93	0.38	0.26	0.017	0.42
$K$ -factor					
2.01					

Table 18: **BP10** Additional information related to double and single Higgs production.

$$\begin{aligned} \text{BR}(H_2 \rightarrow WW) &= 0.404, & \text{BR}(H_2 \rightarrow ZZ) &= 0.179, & \text{BR}(H_2 \rightarrow H_1 H_1) &= 0.404, \\ \text{BR}(H_3 \rightarrow t\bar{t}) &= 0.626, & \text{BR}(H_3 \rightarrow H_1 H_2) &= 0.298, & \text{BR}(A_1 \rightarrow \tilde{\chi}_1^+ \tilde{\chi}_1^-) &= 0.506, \\ \text{BR}(A_1 \rightarrow \tilde{\chi}_1^0 \tilde{\chi}_1^0) &= 0.300, & \text{BR}(H^+ \rightarrow t\bar{b}) &= 0.731, & \text{BR}(A_2 \rightarrow t\bar{t}) &= 0.714, \\ \text{BR}(A_2 \rightarrow ZH_2) &= 0.235, \end{aligned}$$

where  $\tilde{\chi}^{\pm,0}$  denote the charginos and neutralinos, respectively. We can infer that the dominant contribution to  $H_1 H_1$  production stems from the  $H_2$  triangle resonance diagram as

$$\sigma_{H_2}^{\text{NNLO}} \times \text{BR}(H_2 \rightarrow H_1 H_1) = 154 \text{ fb}. \quad (5.47)$$

Interesting signatures are the  $H_1$  pair production in association with a  $Z$  boson and triple  $H_1$  production from Higgs cascades

$$\begin{aligned}\sigma_{\text{prod}}(A_2) \times \text{BR}(A_2 \rightarrow ZH_2) \times \text{BR}(H_2 \rightarrow H_1H_1) &= 420 \text{ fb} \times 0.235 \times 0.404 = 39.87 \text{ fb} , \\ \sigma_{\text{prod}}(H_3) \times \text{BR}(H_3 \rightarrow H_1H_2) \times \text{BR}(H_2 \rightarrow H_1H_1) &= 260 \text{ fb} \times 0.298 \times 0.404 = 31.30 \text{ fb} .\end{aligned}\tag{5.48}$$

With a branching ratio of  $\text{BR}(H_1 \rightarrow b\bar{b}) = 0.652$ , this results in a  $Zb\bar{b}b\bar{b}$  final state with a rate of 16.95 fb for  $ZH_1H_1$  production and in  $6b$ -quark final state with a rate of 8.68 fb for triple  $H_1$  production.

### 5.11 Resonant SM-like $H_2H_2$ Production in the NMSSM

Although for this point resonant production is kinematically possible, it is very suppressed. The (small) enhancement compared to the SM is caused by the deviation of the trilinear coupling from the SM value. The relevant information on this scenario is given in Tabs. 19 and 20.

$\lambda$	$\kappa$	$A_\lambda$ [GeV]	$A_\kappa$ [GeV]	$\mu_{\text{eff}}$ [GeV]	$\tan \beta$
0.0749	0.0646	425.77	-705.59	215.06	3.007
$m_{H^\pm}$ [GeV]	$M_1$ [GeV]	$M_2$ [GeV]	$M_3$ [TeV]	$A_t$ [GeV]	$A_b$ [GeV]
660.53	728	430	2	3226.33	584.37
$m_{\tilde{Q}_3}$ [GeV]	$m_{\tilde{t}_R}$ [GeV]	$m_{\tilde{b}_R}$ [GeV]	$A_\tau$ [GeV]	$m_{\tilde{L}_3}$ [GeV]	$m_{\tilde{\tau}_R}$ [GeV]
1196.41	1440.66	3000	1796	3000	3000

Table 19: **BP11**: NMSSM input parameters required by **NMSSMCALC** for the computation of the NMSSM spectrum.

$m_{H_1}$ [GeV]	$m_{H_2}$ [GeV]	$m_{H_3}$ [GeV]	$m_{A_1}$ [GeV]	$m_{A_2}$ [GeV]	$m_{H^\pm}$
81	125.05	659	626	656	661
$\Gamma_{H_1}^{\text{tot}}$ [GeV]	$\Gamma_{H_2}^{\text{tot}}$ [GeV]	$\Gamma_{H_3}^{\text{tot}}$ [GeV]	$\Gamma_{A_1}^{\text{tot}}$ [GeV]	$\Gamma_{A_2}^{\text{tot}}$ [GeV]	$\Gamma_{H^\pm}^{\text{tot}}$ [GeV]
$2.888 \times 10^{-5}$	$4.281 \times 10^{-3}$	4.17	0.088	5.23	4.40
$h_{11}$	$h_{12}$	$h_{13}$	$h_{21}$	$h_{22}$	$h_{23}$
0.039	0.055	0.998	0.331	0.941	-0.065
$h_{31}$	$h_{32}$	$h_{33}$	$a_{11}$	$a_{21}$	$a_{13}$
0.943	-0.333	-0.018	-0.012	0.949	0.999
$a_{23}$	$\lambda_{3H_2}/\lambda_{3H}$	$y_{t,H_2}/y_{t,H}$			
0.013	0.333	0.992			
$\sigma_{H_2H_2}^{\text{NLO}}$ [fb]	$\sigma_{H_1}^{\text{NNLO}}$ [pb]	$\sigma_{H_2}^{\text{NNLO}}$ [pb]	$\sigma_{H_3}^{\text{NNLO}}$ [pb]	$\sigma_{A_1}^{\text{NNLO}}$ [pb]	$\sigma_{A_2}^{\text{NNLO}}$ [pb]
65	0.32	42.76	0.16	$5.10^{-5}$	0.25
$K$ -factor					
1.95					

Table 20: **BP11**: Additional information related to double and single Higgs production.

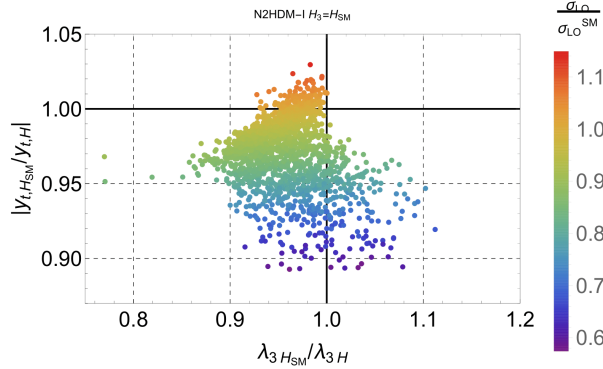


Figure 10: N2HDM-I with  $H_3 \equiv H_{\text{SM}}$ : Cross section values normalized to the SM value (color code) as function of the top-Yukawa and trilinear Higgs self-couplings of  $H_3$  normalized to the respective SM values. A factor of two is applied to the LO cross section to roughly account for the QCD corrections.

The dominant branching ratios of the non-SM-like Higgs bosons are given by

$$\begin{aligned} \text{BR}(H_1 \rightarrow b\bar{b}) &= 0.89, & \text{BR}(H_3 \rightarrow t\bar{t}) &= 0.709, & \text{BR}(A_1 \rightarrow \tilde{\chi}_1^+ \tilde{\chi}_1^-) &= 0.47, \\ \text{BR}(A_2 \rightarrow t\bar{t}) &= 0.66, & \text{BR}(A_2 \rightarrow \tilde{\chi}_1^+ \tilde{\chi}_1^-) &= 0.32, & \text{BR}(A_2 \rightarrow \tilde{\chi}_1^0 \tilde{\chi}_1^0) &= 0.152, \\ \text{BR}(A_2 \rightarrow \tilde{\chi}_2^0 \tilde{\chi}_2^0) &= 0.202, & \text{BR}(H^+ \rightarrow t\bar{b}) &= 0.778. \end{aligned}$$

Since the branching ratio  $\text{BR}(H_3 \rightarrow H_2 H_2) = 6.5 \times 10^{-5}$  is tiny, it is not resonance  $H_3$  production that enhances the cross section but rather the SM-like trilinear coupling deviation from the SM as stated above.

## 6 Constraining Model Parameters

With the SM-like Higgs pair production cross section in the non-resonant case being three orders of magnitude smaller than single Higgs production, deriving constraints on the parameter spaces of the models from di-Higgs production may not be very efficient. This picture changes of course in case of resonance enhancements. To get a rough picture of what can be learnt from di-Higgs production, we present a few selected heat plots for the SM-like Higgs pair production cross sections as a function of relevant model parameters.

In the non-resonant case, it is the top Yukawa and trilinear Higgs self-couplings of the SM-like Higgs boson that determine the size of the SM-like Higgs pair production cross section. In Fig. 10, we show as colour code the size of the cross section for SM-like Higgs pair production normalized to the SM value in the N2HDM-I for the case where  $H_3 \equiv H_{\text{SM}}$ , as a function of its top-Yukawa and trilinear Higgs self-coupling normalized to their SM values, respectively. By choosing  $H_3 \equiv H_{\text{SM}}$ , we make sure that the contributions from lighter  $s$ -channel Higgs boson exchanges to the cross section are subdominant and that it is the SM-like couplings that determine its size. As can be inferred from the plot, the size of the cross section is mostly insensitive to the value of the trilinear Higgs self-coupling in the limited range that is still allowed for it, while it shows a strong dependence on the top-Yukawa coupling. Taking off the resonance contribution for the case where  $H_1 \equiv H_{\text{SM}}$  and where the allowed range for the trilinear Higgs self-coupling is larger we find a significant dependence of the cross section on the trilinear coupling.

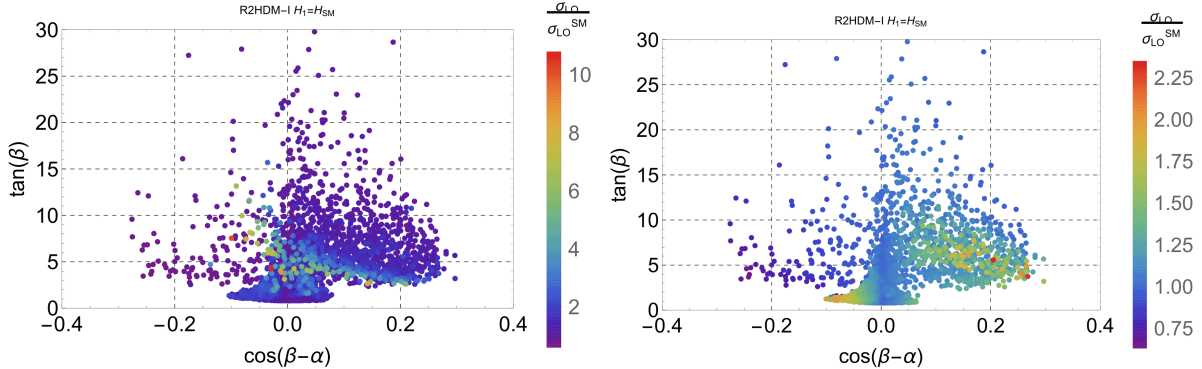


Figure 11: R2HDM-I with  $H_1 \equiv H_{\text{SM}}$ : NLO (through a factor of 2) QCD cross section values normalized to the SM value (color code) as function of  $\tan\beta$  and  $\cos(\beta - \alpha)$ . Left: complete cross section, right: only points with  $\sigma_{H_2}^{\text{NNLO}}(H_2) \times \text{BR}(H_2 \rightarrow H_1 H_1) \leq 0.1 \sigma^{\text{NLO}}(H_1 H_1)$

Let us investigate if di-Higgs production can possibly contribute to constraining the parameter space of the model. For this, we resort to the simpler R2HDM whose tree-level Higgs couplings are described by only two mixing angles. In Fig. 11, we depict in the  $\tan\beta$ - $\cos(\beta - \alpha)$  plane, through the colour code, the NLO QCD-corrected (by including a factor 2) di-Higgs cross section normalized to the SM value for the R2HDM-I, where the lighter Higgs  $H_1 \equiv H_{\text{SM}}$ . On the left, the complete cross section is plotted. On the right plot, we consider only points where the resonant contribution from  $H_2 \rightarrow H_1 H_1$  makes up for less than 10% of the total cross section. More specifically, we only include points where  $\sigma_{H_2}^{\text{NNLO}} \times \text{BR}(H_2 \rightarrow H_1 H_1) \leq 0.1 \times \sigma^{\text{NLO}}(H_1 H_1)$ . From an experimental point of view this would correspond to non-resonant  $H_1 H_1$  production (according to our definition). From the right plot, we could infer that cross section values deviating from the SM value allow us to constrain  $\cos(\beta - \alpha)$ . The true picture is more complex though, as shown by the left plot: the possible resonance enhancements in BSM di-Higgs production also allow for larger cross sections very close to the SM Higgs alignment limit  $\cos(\beta - \alpha) = 0$ . Indeed we found by comparing the constraints on  $\cos(\beta - \alpha)$  before and after applying the di-Higgs constraints that the impact of di-Higgs constraints is vanishingly small.

With increasing complexity of the Higgs sectors, the superposition of the various Higgs contributions to the cross sections make it more and more complicated to derive conclusive statements on the various trilinear and Yukawa couplings and require the combination of different cross sections to extract all involved couplings (*cf.* [11] for a discussion in the MSSM).

## 7 Effective Field Theory versus Specific Models

In this paper so far, we discussed mainly Higgs pair production in specific models. In this section, we switch gears towards a different approach to describe new physics effects. This is given by the effective field theory (EFT) framework where BSM physics is expected to appear at some high new physics scale  $\Lambda$ . In the linear approach called SMEFT [209–212] new physics is formulated as a power series in the dimensionful parameter  $1/\Lambda$ . The non-linearly realized EFT, on the other hand, can be viewed as organised by chiral dimension [213–226]. If we choose to describe Higgs pair production in the EFT approach this means that effects from additional

non-SM-like light Higgs bosons cannot be described.<sup>25</sup> A discussion of the higher-dimensional operators relevant for Higgs pair production can be found in [230–234]. The QCD corrections in the infinite top mass limit,  $m_t \rightarrow \infty$  have been provided at NLO QCD in [97] and also extended to the CP-violating case in [106]. At NNLO QCD they have been calculated in [235]. The authors of [236] presented the NLO QCD corrections including the full top quark mass effects in a non-linearly realized EFT. An interface with POWHEG [237–239] has been provided in [125].

For the models that we considered, only the new physics operators that modify the trilinear Higgs self-coupling and the Yukawa coupling are relevant. The induced effective couplings of one or two Higgs bosons to two gluons only appear in the NMSSM, where integrating out heavy stops and sbottoms in the Higgs-to-gluon loop couplings would induce such couplings. We neglect that effect in the present discussion for simplicity, by setting the associated couplings ( $c_g$  and  $c_{gg}$  in the notation of the non-linear Lagrangian of Ref. [97]) to zero. In the R2HDM, C2HDM and N2HDM, these couplings do not appear as long as we do not include additional heavy coloured particles beyond the SM. Furthermore, we do not consider effects from the chromomagnetic operator as they are of different order in the chiral expansion.<sup>26</sup> Finally, integrating out a possible heavy Higgs boson exchange in the  $s$ -channel leads to an effective two-Higgs-two-fermion coupling. Denoting by  $c_3$  the trilinear coupling modification and by  $c_t$  the top-Yukawa coupling modification with respect to the SM and by  $c_{tt}$  the effective two-Higgs-two-fermion coupling coefficient, *i.e.* adapting the notation of [97], our considered correction  $\Delta\mathcal{L}_{\text{non-lin}}$  to the SM Lagrangian reads,

$$\Delta\mathcal{L}_{\text{non-lin}} \supset -m_t t\bar{t} \left( c_t \frac{h}{v} + c_{tt} \frac{h^2}{2v^2} \right) - c_3 \frac{1}{6} \left( \frac{3M_h^2}{v} \right) h^3, \quad (7.49)$$

where  $h$  denotes the physical Higgs boson. Since the single and double-Higgs coefficients  $c_t$  and  $c_{tt}$  to the top-quark pair are taken to be independent, we adapt the non-linear effective Lagrangian approach here. In SMEFT, they are correlated (as well as  $c_g$  and  $c_{gg}$ ). In Fig. 12, we show the generic diagrams that contribute to our EFT approach to Higgs pair production and indicate the EFT coupling modifiers. In the notation of [29] and [97], we have the following

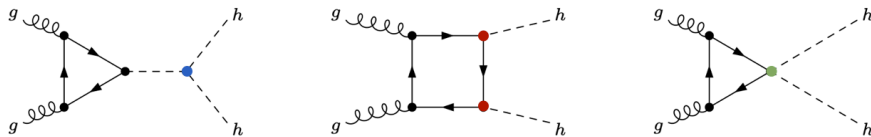


Figure 12: Diagrams contributing to Higgs pair production in the EFT approach (with  $c_g = c_{gg} = 0$  and neglecting the chromomagnetic operator). The blue, red and green blobs denote the modified Higgs trilinear, Higgs top-Yukawa and the new two-Higgs-two-top-quark couplings, respectively.

<sup>25</sup>For an extension of the EFT approach to include an extended particle content, an EFT for the 2HDM, *cf.* [227]. Also for composite Higgs models a concrete model with two Higgs doublets has been proposed, *cf.* [228, 229].

<sup>26</sup>For a discussion on the chromomagnetic operator, see [236].

matching relations of our specific models to the EFT Lagrangian,

$$\begin{aligned}
\text{Higgs-top Yukawa coupling} & : & g_t^{H_{\text{SM}}}(\alpha_i, \beta) & \rightarrow c_t \\
\text{trilinear Higgs coupling} & : & \frac{g_3^{H_{\text{SM}}H_{\text{SM}}H_{\text{SM}}}(p_i)}{3M_{H_{\text{SM}}}^2/v} & \rightarrow c_3 \\
\text{two-Higgs-two-top quark coupling} & : & \sum_{k=1}^{k_{\text{max}}} \left( \frac{-v}{m_{H_k}^2} \right) g_3^{H_k H_{\text{SM}} H_{\text{SM}}}(p_i) g_t^{H_k}(\alpha_i, \beta) & \rightarrow c_{tt}
\end{aligned} \tag{7.50}$$

Here  $g_t^\phi(\alpha_i, \beta)$  denotes the dimensionless function of the mixing angles  $\alpha_i$  and  $\beta$  that specifies for each model under consideration the modification of the Yukawa coupling of a Higgs boson  $\phi$  of the model with respect to the SM Yukawa coupling. The function  $g_3^{H_{\text{SM}}H_{\text{SM}}H_{\text{SM}}}(p_i)$  denotes the dimensionful trilinear coupling of three SM-like Higgs bosons  $H_{\text{SM}}$  in our BSM model that in the SM case would approach  $3M_{H_{\text{SM}}}^2/v$ . We denote by  $p_i$  the various parameters on which the trilinear coupling depends in the respective model. The third matching relation to  $c_{tt}$  is obtained by assuming a possible heavy Higgs  $H_k$   $s$ -channel exchange (*cf.* the first diagram in Fig. 1 for  $H_k \neq H_{\text{SM}}$ ) where the mass of the exchanged Higgs boson, denoted by  $m_{H_k}$ , is very large. By  $g_3^{H_k H_{\text{SM}} H_{\text{SM}}}$  we denote the corresponding  $H_k$  trilinear coupling to two SM-like Higgs bosons. Note that, in non-minimal models, we would have two such contributions. Hence  $k_{\text{max}} = 1$  in the R2HDM and 2 in the C2HDM, N2HDM and NMSSM.<sup>27</sup> Table 5 gives us an overview of the  $c_t$  and  $c_3$  values that are allowed by the bulk of the parameter points.

We have chosen a few benchmark points from our samples in order to investigate the validity of the EFT approach. In Tab. 21, we present the benchmark point **SMEFTBP1** for the R2HDM-II with the heavy scalar Higgs  $M_{H_2}$  mass above 1 TeV so that the EFT approach should be justified. The corresponding SMEFT coupling coefficients are

$$\text{SMEFTBP1: } c_3 = 0.782, \quad c_t = 0.951, \quad c_{tt} = -0.122. \tag{7.51}$$

In Tab. 22 we give, for the listed  $m_{H_2}$ ,  $c_{tt}$ , the corresponding R2HDM cross section values and

$m_{H_1}$ [GeV]	$m_{H_2}$ [GeV]	$m_A$ [GeV]	$m_{H^\pm}$ [GeV]	$\alpha$	$\tan \beta$	$m_{12}^2$ [GeV <sup>2</sup> ]
125.09	1131	1082	1067	-0.924	0.820	552749

Table 21: **SMEFTBP1**: R2HDM-II input parameters.

$m_{H_2}$ [GeV]	$\Gamma_{H_2}$ [GeV]	$c_{tt}$	$g_3^{H_2 H_1 H_1}$ [GeV]	$\sigma_{\text{R2HDM}}^{\text{w/res}}$ [fb]	$\sigma_{\text{SMEFT}}^{c_{tt} \neq 0}$ [fb]	ratio
1131	78.80	-0.1222	-504.52	30.5	26.1	86%
1200	89.74	-0.1031	-479.29	27.7	24.8	90%
1500	470.2	$-4.853 \cdot 10^{-2}$	-352.42	21.8	21.4	98%

Table 22: **SMEFTBP1**: Value of  $m_{H_2}$  and corresponding  $\Gamma_{H_2}$ ,  $c_{tt}$  and  $g_3^{H_2 H_1 H_1}$  values together with the R2HDM-II and the SMEFT results for LO  $H_2 H_2$  production including the resonance contribution.

the results in the SMEFT approach, as well as the ratios of these two cross sections. Note that  $g_3^{H_2 H_1 H_1}$  also changes when we change  $m_{H_2}$ , whereas  $g_t^{H_2} = -1.126$  remains the same. Thus, we list  $g_3^{H_2 H_1 H_1}$  in Tab. 22. We also give the value of the total width  $\Gamma_{H_2}$  which changes as well.

<sup>27</sup>We only take into account in the cross section linear EFT contributions and no squared ones. For details on the LO partonic cross section, we refer to Eqs. (2.5)-(2.13) of Ref. [97].

$m_{H_1}$ [GeV]	$m_{H_2}$ [GeV]	$m_{H_3}$ [GeV]	$m_A$ [GeV]	$m_{H^\pm}$ [GeV]	$\tan \beta$
125.09	269	582	390	380	4.190
$\alpha_1$	$\alpha_2$	$\alpha_3$	$v_s$ [GeV]	$\text{Re}(m_{12}^2)$ [GeV <sup>2</sup> ]	
1.432	-0.109	0.535	1250	28112	

Table 23: SMEFTBP2=BP6: N2HDM-I input parameters

Note that in this subsection all gluon fusion cross sections are given at LO. From the second line, we read off that in our scenario the SMEFT approach approximates the cross section in the full model by only 86% for a Higgs mass  $m_{H_2}$  of the order of 1 TeV. When we turn off the  $H_2$  resonance and compare the results with the one in the SMEFT approach where we accordingly set  $c_{tt} = 0$  we get

$$\sigma_{\text{R2HDM}}^{\text{w/o res}} = 18.6 \text{ fb} \quad \text{and} \quad \sigma_{\text{SMEFT}}^{c_{tt}=0} = 18.6 \text{ fb} . \quad (7.52)$$

Both cross sections agree as expected in contrast to the case with the resonance included. Since in the di-Higgs cross section we integrate  $\sqrt{s}$  in the  $s$ -channel exchange across the resonance, the SMEFT approach is not a good approximation. We want to investigate the minimum mass values from which the SMEFT rate is close to the full R2HDM result. For this, we gradually increase  $m_{H_2}$  and calculate for the corresponding  $c_{tt}$  and trilinear Higgs coupling values the SMEFT cross section and also the full R2HDM cross section.<sup>28</sup> The values are given in the third and fourth line in Tab. 22. We clearly see that with increasing  $m_{H_2}$ , and hence decreasing contribution of the resonance to the cross section, the SMEFT and the full R2HDM results approach each other. Starting from about  $m_{H_2} = 1200$  GeV the deviation is less than 10%, continuously decreasing with increasing  $m_{H_2}$ .

We perform the same investigation but now for the N2HDM-I with  $H_1 = H_{\text{SM}}$  where we have two resonance contributions. As benchmark point SMEFTBP2 we take the N2HDM benchmark point BP6 given in Tab. 13. For convenience, we repeat the input parameters in Tab. 23. The SMEFT coupling coefficients read

$$\text{SMEFTBP2: } c_3 = 0.877, \quad c_t = 1.012, \quad c_{tt} = 4.127 \times 10^{-2} . \quad (7.53)$$

And we have for this scenario

$$g_t^{H_2} = 0.179 \quad \text{and} \quad g_t^{H_3} = 2.337 \times 10^{-2} . \quad (7.54)$$

The cross section values for the N2HDM and the SMEFT calculation are given in the second line of Tab. 24. We vary  $m_{H_2}$  together with the corresponding total width  $\Gamma_{H_2}$ , accordingly. The mass  $m_{H_3}$  is kept at its original value. Its total width is given by  $\Gamma_{H_3} = 15.28$  GeV. We also list the corresponding  $c_{tt}$  value for  $H_2$  only, named  $c_{tt}^{H_2}$ , as well as the sum  $c_{tt}$  of the  $H_2$  and  $H_3$  contributions, *i.e.*  $c_{tt} = c_{tt}^{H_2} + c_{tt}^{H_3}$  with  $c_{tt}^{H_3} = -2.832 \times 10^{-3}$ . We furthermore give the corresponding trilinear coupling  $g_3^{H_2 H_1 H_1}$ . For  $g_3^{H_3 H_1 H_1}$  which does not change as we keep  $m_{H_3}$  at its original value, we have  $g_3^{H_3 H_1 H_1} = 167$  GeV. With a rather light  $H_2$  mass and a medium-valued  $H_3$  mass we expect significant resonance contributions. This was already confirmed by the investigation of this parameter point in Subsec. 5.6 where we found that the resonance contribution is given by the  $s$ -channel  $H_2$  exchange whereas the  $H_3$  resonance contribution

<sup>28</sup>The resulting scenarios do not then necessarily fulfil all applied constraints any more. We still take them for illustrative purposes.

$m_{H_2}$	$\Gamma_{H_2}$	$c_{tt}^{H_2}$	$c_{tt}$	$g_3^{H_2 H_1 H_1}$	$\sigma_{\text{N2HDM}}^{\text{w/res}} [\text{fb}]$	$\sigma_{\text{SMEFT}}^{c_{tt} \neq 0} [\text{fb}]$	ratio
269	0.075	$4.410 \times 10^{-2}$	$4.127 \times 10^{-2}$	-72.42	183.70	20.56	11%
300	0.083	$3.170 \times 10^{-2}$	$2.877 \times 10^{-2}$	-64.80	162.80	21.28	13%
400	0.177	$9.544 \times 10^{-3}$	$6.721 \times 10^{-3}$	-34.68	43.33	22.60	52%
420	0.229	$6.895 \times 10^{-3}$	$4.063 \times 10^{-3}$	-27.62	31.70	22.76	72%
440	0.284	$4.600 \times 10^{-3}$	$1.767 \times 10^{-3}$	-20.22	26.26	22.90	87%
450	0.315	$3.564 \times 10^{-3}$	$7.323 \times 10^{-4}$	-16.39	24.84	22.96	92%
500	2.567	$-7.132 \times 10^{-4}$	$-3.545 \times 10^{-3}$	4.05	23.56	23.22	99%

Table 24: **SMEFTBP2**: Values of  $m_{H_2}$  in GeV,  $\Gamma_{H_2}$  in GeV,  $c_{tt}^{H_2}$ ,  $c_{tt}$ , and  $g_3^{H_2 H_1 H_1}$  in GeV together with the N2HDM-I and the SMEFT result for  $H_1 H_1$  production at LO including the resonance contribution.

is negligible which can be explained by the tiny  $H_3$  top-Yukawa coupling. Due to the large resonance contribution of the rather light  $H_2$  the result in the SMEFT approach is completely off. When we turn off the  $H_2$  and  $H_3$  resonances (where  $H_3$  has only a tiny effect) and compare the result with the one in the SMEFT approach where we accordingly set  $c_{tt} = 0$  we obtain

$$\sigma_{\text{N2HDM}}^{\text{w/o res}} = 23.05 \text{ fb} \quad \text{and} \quad \sigma_{\text{SMEFT}}^{c_{tt}=0} = 23.01 \text{ fb} . \quad (7.55)$$

The cross sections in the two approaches agree as expected. Starting from our original N2HDM-I scenario we then gradually increase the  $m_{H_2}$  mass which hence changes  $c_{tt}^{H_2}$  and thereby  $c_{tt}$  in order to investigate when the SMEFT result starts to reproduce the full result. The corresponding values are given in Tab. 24 from the third line onwards. The SMEFT and the N2HDM results start to deviate by less than 10% for  $H_2$  masses above about 440 GeV. This agreement also depends on the total width  $\Gamma_{H_2}$  of the  $s$ -channel resonance. Keeping *e.g.* the total width at the value  $\Gamma_{H_2} = 0.075$  GeV (corresponding to the mass  $m_{H_2} = 269$  GeV) the agreement between full and EFT approach within 10% would be reached around  $M_{H_2} = 465$  GeV.<sup>29</sup> We hence find in this scenario with two possible heavy resonances that the Higgs mass limit, from which the SMEFT approach starts to approximate the full result, ranges at lower values.

The investigation of these two benchmarks with additional Higgs bosons has shown that first, the results calculated in the full theory and in the EFT approach can differ severely. Second, the agreement between the full theory and the EFT approach depends on the masses of the additionally present Higgs bosons and their total widths. The total width plays an important role when we integrate across the resonance in the  $s$ -channel within **HPAIR**. A priori, one cannot predict to which extent the full theory and the EFT approach agree, as this depends on the parameters of the full model.

## 8 Mixed Higgs Pair Final States - $H_{\text{SM}} + \Phi$

In all presented models it is possible to produce Higgs pair final states that consist of a SM-like Higgs boson  $H_{\text{SM}}$  plus a non-SM-like one  $\Phi$ . In the R2HDM, N2HDM and the NMSSM the non-SM-like Higgs boson can be a scalar or a pseudoscalar. In the C2HDM it would be a CP-mixed state. There is a plethora of final states with substantial production rates possible depending on the major decay modes of the non-SM-like Higgs boson. They range from pure

<sup>29</sup>In our investigation of different benchmark scenarios we also found cases where the total width has a much more dramatic effect, moving agreement *e.g.* from a resonance mass of 410 GeV to 2.1 TeV if the width is kept at its original value.

multi-fermion, multi-photon, mixed fermion-photon to multi-Higgs boson, multi-gauge boson, mixed Higgs-plus-gauge boson or mixed fermion-plus-Higgs or gauge boson final states. In the NMSSM, we can additionally have supersymmetric particles in the final state which we will not discuss in this paper. In the following, we present some selected benchmark points. All of them have the common feature that their rates exceed 10 fb at NLO. We have many more final state signatures beyond the presented ones that we can provide on request.

### 8.1 The $(b\bar{b})(b\bar{b})$ Final State

The largest  $4b$  final state from mixed Higgs pair production is found in the N2HDM-I. We present a benchmark point for

$$\text{N2HDM-I: } \sigma(pp \rightarrow H_1 H_2 (\equiv H_{\text{SM}}) \rightarrow (b\bar{b})(b\bar{b})) = 2.11 \text{ pb} . \quad (8.56)$$

The related branching ratios are  $\text{BR}(H_1 \rightarrow b\bar{b}) = 0.857$  and  $\text{BR}(H_2 \rightarrow b\bar{b}) = 0.559$ . In Tab. 25 (upper), we give the input parameters for this point and in Tab. 25 (lower) the  $H_1 H_2$  Higgs pair cross section value at NLO QCD, the total widths of the particles and other interesting final states rates. The SM Higgs pair ( $H_2 H_2$ ) cross section in this case is very SM-like with 18 fb at LO, and  $H_1 H_1$  production reaches 778 fb at LO and is hence rather large.

$m_{H_1}$ [GeV]	$m_{H_2}$ [GeV]	$m_{H_3}$ [GeV]	$m_A$ [GeV]	$m_{H^\pm}$ [GeV]	$\tan \beta$
54	125.09	229	664	676	1.442
$\alpha_1$	$\alpha_2$	$\alpha_3$	$v_s$ [GeV]	$m_{12}^2$ [GeV <sup>2</sup> ]	
-0.989	1.010	0.381	1420	5760	

$\sigma_{H_1 H_2 (\equiv H_{\text{SM}})}^{\text{NLO}}$ [pb]	$\Gamma_{H_1}^{\text{tot}}$ [GeV]	$\Gamma_{H_2}^{\text{tot}}$ [GeV]	$\Gamma_{H_3}^{\text{tot}}$ [GeV]	$\Gamma_A^{\text{tot}}$ [GeV]	$\Gamma_{H^\pm}^{\text{tot}}$ [GeV]
4.403	$3.062 \times 10^{-4}$	$3.947 \times 10^{-3}$	0.248	80.67	85.89
$(b\bar{b})(\tau\bar{\tau})$ [fb]	$(\tau\bar{\tau})(b\bar{b})$ [fb]	$(b\bar{b})(\gamma\gamma)$ [fb]	$(\gamma\gamma)(b\bar{b})$ [fb]	$(b\bar{b})(WW)$ [fb]	$(WW)(b\bar{b})$ [fb]
227	190	8	0.03	790	0.01

Table 25: **BP12** Upper: N2HDM-I input parameters. Lower: Further information on this point.

The same channel in the N2HDM-II reaches 18 fb. We present in Tab. 26 for the  $4b$  final state the maximum NLO QCD values in the heavy loop particle limit together with the respective  $K$ -factors, for these channels and other mixed Higgs pair combinations in the models under investigation. In the case of resonantly enhanced di-Higgs cross sections, we give the mass of the “resonant” Higgs boson and the corresponding resonant production cross section. It is obtained by calculating the production cross section of the “resonant” particle with **SusHi** at NNLO QCD and subsequently multiplying it with the branching ratio into the investigated Higgs pair final state.

### 8.2 The $(b\bar{b})(WW)$ Final State

If the SM-like Higgs boson decays into  $WW$  then the rates are easily obtained from those of the previous subsection in the  $4b$  final state by multiplying them with  $\text{BR}(H_{\text{SM}} \rightarrow WW)/\text{BR}(H_{\text{SM}} \rightarrow b\bar{b}) \approx 1/3$ . However, we can also have the case that the non-SM-like Higgs boson decays into  $WW$ , which are the benchmark points that we list here. The maximum rate (at NLO) is obtained for

$$\text{N2HDM-I: } \sigma(pp \rightarrow H_1 H_2 (\equiv H_{\text{SM}}) \rightarrow (WW)(b\bar{b})) = 590 \text{ fb} . \quad (8.57)$$

Model	Mixed Higgs State	$m_{\text{res.}}$ [GeV]	res. rate [fb]	$m_\Phi$ [GeV]	Rate [fb]	$K$ -factor
R2HDM-I	$AH_1(\equiv H_{\text{SM}})$	—	—	82	46	2.02
	$H_1H_2(\equiv H_{\text{SM}})$	—	—	68	35	1.97
C2HDM-I	$H_2H_1(\equiv H_{\text{SM}})$	266	9	128	19	2.02
	$H_1H_2(\equiv H_{\text{SM}})$	—	—	122	14	2.01
	$H_1H_3(\equiv H_{\text{SM}})$	—	—	99	11	1.96
N2HDM-I	$H_2H_1(\equiv H_{\text{SM}})$	360	109	146	105	2.01
	$AH_1(\equiv H_{\text{SM}})$	—	—	75	830	2.06
	$H_1H_2(\equiv H_{\text{SM}})$	229	2260	54	2110	2.09
	$AH_2(\equiv H_{\text{SM}})$	—	—	101	277	2.04
	$H_1H_3(\equiv H_{\text{SM}})$	—	—	73	44	1.97
	$H_2H_3(\equiv H_{\text{SM}})$	—	—	83	30	1.97
	$AH_3(\equiv H_{\text{SM}})$	—	—	69	19	2.01
N2HDM-II	$H_1H_2(\equiv H_{\text{SM}})$	640	18	103	18	1.86
NMSSM	$A_1H_1(\equiv H_{\text{SM}})$	553	210	113	201	1.92
	$H_2H_1(\equiv H_{\text{SM}})$	535	42	167	43	1.91
	$A_1H_2(\equiv H_{\text{SM}})$	511	42	87	40	1.94
	$H_1H_2(\equiv H_{\text{SM}})$	714	58	80	59	1.90

Table 26: Maximum rates at NLO QCD in the  $4b$  final state for different mixed Higgs pair final states in the investigated models; the corresponding  $K$ -factor is given in the last column. In case of resonantly enhanced production, we give in the third and fourth column, respectively, the mass of the resonant Higgs boson and the resonant cross section as defined in the text. The fifth column contains the mass of the non-SM-like final state Higgs boson. More details on these points can be provided on request.

The related branching ratios are given by  $\text{BR}(H_1 \rightarrow WW) = 0.402$  and  $\text{BR}(H_2 \rightarrow bb) = 0.598$ . The input parameters of the corresponding benchmark point and additional relevant information together with the rates in other final states are given in Tabs. 27 (upper) and (lower). The maximum rates at NLO QCD for all investigated models in the various final state Higgs pair combinations, where the non-SM-like Higgs decays into  $WW$ , are summarized in Tab. 28 (provided they exceed 10 fb at NLO). The approximate rates for the  $4W$  final state are obtained from those given in the table by multiplying them with a factor  $1/3$ .

$m_{H_1}$ [GeV]	$m_{H_2}$ [GeV]	$m_{H_3}$ [GeV]	$m_A$ [GeV]	$m_{H^\pm}$ [GeV]	$\tan \beta$
113	125.09	304	581	581	1.804
$\alpha_1$	$\alpha_2$	$\alpha_3$	$v_s$ [GeV]	$m_{12}^2$ [GeV <sup>2</sup> ]	
0.173	1.276	-0.651	414	999	

$\sigma_{H_1H_2(\equiv H_{\text{SM}})}^{\text{NLO}}$ [pb]	$\Gamma_{H_1}^{\text{tot}}$ [GeV]	$\Gamma_{H_2}^{\text{tot}}$ [GeV]	$\Gamma_{H_3}^{\text{tot}}$ [GeV]	$\Gamma_A^{\text{tot}}$ [GeV]	$\Gamma_{H^\pm}^{\text{tot}}$ [GeV]
2.453	$1.691 \times 10^{-5}$	$4.103 \times 10^{-3}$	0.477	30.41	32.10
$(b\bar{b})(\tau\bar{\tau})$ [fb]	$(\tau\bar{\tau})(b\bar{b})$ [fb]	$(b\bar{b})(\gamma\gamma)$ [fb]	$(\gamma\gamma)(b\bar{b})$ [fb]	$(b\bar{b})(WW)$ [fb]	$(WW)(b\bar{b})$ [fb]
67	66	2	23	210	590

Table 27: **BP13** Upper: N2HDM-I input parameters. Lower: Further information on this point.

Model	Mixed Higgs State	$m_{\text{res.}}$ [GeV]	res. rate [fb]	$m_\Phi$ [GeV]	Rate [fb]	$K$ -factor
N2HDM-I	$H_2H_1(\equiv H_{\text{SM}})$	406	497	179	498	1.98
	$H_1H_2(\equiv H_{\text{SM}})$	304	615	113	590	2.04
NMSSM	$H_2H_1(\equiv H_{\text{SM}})$	531	45	205	47	1.92

Table 28: Maximum rates at NLO QCD in the  $(b\bar{b})(WW)$  final state for different mixed Higgs pair final states in the investigated models with the non-SM-like Higgs decaying into  $WW$ ; the corresponding  $K$ -factor is given in the last column. In case of resonantly enhanced production, we give in the third and fourth column, respectively, the mass of the resonant Higgs boson and the resonant cross section as defined in the text. The fifth column contains the mass of the non-SM-like final state Higgs boson. More details on these points can be provided on request.

### 8.3 The $(b\bar{b})(t\bar{t})$ Final State

As the SM-Higgs decay into  $t\bar{t}$  is kinematically forbidden, it is always the non-SM-like Higgs that decays into  $t\bar{t}$ . We find the maximum rate for

$$\text{N2HDM-I: } \sigma(pp \rightarrow H_2H_1(\equiv H_{\text{SM}}) \rightarrow (t\bar{t})(b\bar{b})) = 88 \text{ fb} . \quad (8.58)$$

The related branching ratios are given by  $\text{BR}(H_1 \rightarrow b\bar{b}) = 0.595$  and  $\text{BR}(H_2 \rightarrow t\bar{t}) = 0.902$ . Information on this benchmark point, together with the rates into other final states, is given in Tabs. 29 (upper) and (lower). The maximum rates at NLO QCD into  $(b\bar{b})(t\bar{t})$  for all investigated models in the various final state Higgs pair combinations are listed in Tab. 30 for the cases that exceed 10 fb at NLO.

$m_{H_1}$ [GeV]	$m_{H_2}$ [GeV]	$m_{H_3}$ [GeV]	$m_A$ [GeV]	$m_{H^\pm}$ [GeV]	$\tan \beta$
125.09	443.65	633.69	445.65	584.34	1.570
$\alpha_1$	$\alpha_2$	$\alpha_3$	$v_s$ [GeV]	$\text{Re}(m_{12}^2)$ [GeV <sup>2</sup> ]	
1.027	-0.046	-0.832	9361	52724	

$\sigma_{H_1(\equiv H_{\text{SM}})H_2}$ [fb]	$\Gamma_{H_1}^{\text{tot}}$ [GeV]	$\Gamma_{H_2}^{\text{tot}}$ [GeV]	$\Gamma_{H_3}^{\text{tot}}$ [GeV]	$\Gamma_A^{\text{tot}}$ [GeV]	$\Gamma_{H^\pm}^{\text{tot}}$ [GeV]
164	$4.155 \times 10^{-3}$	1.303	16.05	7.603	14.32
$(b\bar{b})(\tau\bar{\tau})$ [fb]	$(\tau\bar{\tau})(b\bar{b})$ [fb]	$(b\bar{b})(\gamma\gamma)$ [fb]	$(\gamma\gamma)(b\bar{b})$ [fb]	$(b\bar{b})(WW)$ [fb]	$(WW)(b\bar{b})$ [fb]
0.01	0.01	0.001	0	4	0.02

Table 29: **BP14** Upper: N2HDM-I input parameters. Lower: Further information on this point.

Model	Mixed Higgs State	$m_{\text{res.}}$ [GeV]	res. rate [fb]	$m_\Phi$ [GeV]	Rate [fb]	$K$ -factor
R2HDM-I	$AH_1(\equiv H_{\text{SM}})$	—	—	346	11	1.94
N2HDM-I	$H_2H_1(\equiv H_{\text{SM}})$	634	81	444	88	1.86
	$AH_1(\equiv H_{\text{SM}})$	—	—	363	15	1.90
N2HDM-II	$H_2H_1(\equiv H_{\text{SM}})$	813	23	511	34	1.79
NMSSM	$A_1H_1(\equiv H_{\text{SM}})$	—	—	53	82	1.88
	$H_2H_1(\equiv H_{\text{SM}})$	535	19	371	19	1.91

Table 30: Maximum rates at NLO QCD in the  $(b\bar{b})(t\bar{t})$  final state at NLO for different mixed Higgs pair final states in the investigated models with the non-SM-like Higgs decaying into  $t\bar{t}$ ; the corresponding  $K$ -factor is given in the last column. In case of resonantly enhanced production, we give in the third and fourth column, respectively, the mass of the resonant Higgs boson and the resonant cross section as defined in the text. The fifth column contains the mass of the non-SM-like final state Higgs boson. More details on these points can be provided on request.

## 8.4 Multi-Higgs Final States

In non-minimal Higgs models like the C2HDM, N2HDM, and NMSSM we can have multi-Higgs final states from cascade Higgs-to-Higgs decays. In the production of a SM-like plus non-SM-like Higgs final state,  $H_{\text{SM}}\Phi$ , we found that both the Higgs-to-Higgs decay of the SM-like Higgs or the non-SM-like one can lead to substantial final state rates. The largest NLO rates that we found above 10 fb, in the multi-Higgs final state, are summarised in Tab. 31. In the C2HDM, we did not find NLO rates above 10 fb. We maintain the ordering of particles with regards to their decay chains, so that it becomes clear which Higgs boson decays into which Higgs pair. We give the rates in the  $(6b)$  final state as they lead to the largest cross sections for all shown scenarios. In the following, we highlight a few benchmark scenarios from the table.

Model	Mixed Higgs State	$m_{\Phi_1}$ [GeV]	$m_{\Phi_2}$ [GeV]	Rate [fb]	$K$ -factor
N2HDM-I	$H_2H_3(\equiv H_{\text{SM}}) \rightarrow H_1H_1(b\bar{b}) \rightarrow (b\bar{b})(b\bar{b})(b\bar{b})$	98	41	15	1.95
	$H_2H_1(\equiv H_{\text{SM}}) \rightarrow H_1H_1(b\bar{b}) \rightarrow (b\bar{b})(b\bar{b})(b\bar{b})$	282	-	40	1.96
	$H_2H_1(\equiv H_{\text{SM}}) \rightarrow AA(b\bar{b}) \rightarrow (b\bar{b})(b\bar{b})(b\bar{b})$	157	73	33	2.05
	$H_1H_2(\equiv H_{\text{SM}}) \rightarrow (b\bar{b})H_1H_1 \rightarrow (b\bar{b})(b\bar{b})(b\bar{b})$	54	-	111	2.09
	$H_3H_2(\equiv H_{\text{SM}}) \rightarrow H_1H_1(b\bar{b}) \rightarrow (b\bar{b})(b\bar{b})(b\bar{b})$	212	83	8	1.93
N2HDM-II	$H_2H_1(\equiv H_{\text{SM}}) \rightarrow H_1H_1(b\bar{b}) \rightarrow (b\bar{b})(b\bar{b})(b\bar{b})$	271	-	3	1.87
NMSSM	$H_2H_1(\equiv H_{\text{SM}}) \rightarrow H_1H_1(b\bar{b}) \rightarrow (b\bar{b})(b\bar{b})(b\bar{b})$	319	-	11	1.90
	$H_2H_1(\equiv H_{\text{SM}}) \rightarrow A_1A_1(b\bar{b}) \rightarrow (b\bar{b})(b\bar{b})(b\bar{b})$	253	116	26	1.92

Model	Mixed Higgs State	$m_{\text{res.}}$ [GeV]	res. rate [fb]
N2HDM-I	$H_2H_3(\equiv H_{\text{SM}}) \rightarrow H_1H_1(b\bar{b}) \rightarrow (b\bar{b})(b\bar{b})(b\bar{b})$	—	—
	$H_2H_1(\equiv H_{\text{SM}}) \rightarrow H_1H_1(b\bar{b}) \rightarrow (b\bar{b})(b\bar{b})(b\bar{b})$	441	39
	$H_2H_1(\equiv H_{\text{SM}}) \rightarrow AA(b\bar{b}) \rightarrow (b\bar{b})(b\bar{b})(b\bar{b})$	294	37
	$H_1H_2(\equiv H_{\text{SM}}) \rightarrow (b\bar{b})H_1H_1 \rightarrow (b\bar{b})(b\bar{b})(b\bar{b})$	229	119
	$H_3H_2(\equiv H_{\text{SM}}) \rightarrow H_1H_1(b\bar{b}) \rightarrow (b\bar{b})(b\bar{b})(b\bar{b})$	—	—
N2HDM-II	$H_2H_1(\equiv H_{\text{SM}}) \rightarrow H_1H_1(b\bar{b}) \rightarrow (b\bar{b})(b\bar{b})(b\bar{b})$	615	2
NMSSM	$H_2H_1(\equiv H_{\text{SM}}) \rightarrow H_1H_1(b\bar{b}) \rightarrow (b\bar{b})(b\bar{b})(b\bar{b})$	560	11
	$H_2H_1(\equiv H_{\text{SM}}) \rightarrow A_1A_1(b\bar{b}) \rightarrow (b\bar{b})(b\bar{b})(b\bar{b})$	518	26

Table 31: Upper: Maximum rates for multi-Higgs final states given at NLO QCD. The  $K$ -factor is given in the last column. In the third and fourth column we also give the mass values  $m_{\Phi_1}$  and  $m_{\Phi_2}$  of the non-SM-like Higgs bosons involved in the process, in the order of their appearance. Lower: In case of resonantly enhanced production the mass of the resonantly produced Higgs boson is given together with the NNLO QCD production rate. More details on these points can be provided on request.

### 8.4.1 Non-SM-like Higgs Search: Di-Higgs beats Single Higgs

In the following we present N2HDM-I and NMSSM scenarios with three SM-like Higgs bosons in the final states with  $H_1$  being SM-like and with NLO rates above 10 fb. These benchmark points are special in the sense that the production of the non-SM-like Higgs boson  $H_2$  from di-Higgs states beats, or is at least comparable, to its direct production.<sup>30</sup> This appears in cases where the non-SM-like Higgs is singlet-like and/or is more down- than up-type like. The latter suppresses direct production from gluon fusion. The former suppresses all couplings to SM-like particles. In these cases the heavy non-SM-like Higgs boson might rather be discovered in the

<sup>30</sup>For another example where New Physics might first be accessible in Higgs pair production in a composite Higgs model, see [100].

di-Higgs channel than in direct single Higgs production.

The input parameters for the N2HDM-I point are given in Tab. 32. With the values for the

$m_{H_1}$ [GeV]	$m_{H_2}$ [GeV]	$m_{H_3}$ [GeV]	$m_A$ [GeV]	$m_{H^\pm}$ [GeV]	$\tan \beta$
125.09	281.54	441.25	386.98	421.81	1.990
$\alpha_1$	$\alpha_2$	$\alpha_3$	$v_s$ [GeV]	$\text{Re}(m_{12}^2)$ [GeV <sup>2</sup> ]	
1.153	0.159	0.989	9639	29769	

Table 32: **BP15** N2HDM-I input parameters

NLO  $H_1 H_2$  cross section and the branching ratios  $\text{BR}(H_2 \rightarrow H_1 H_1)$  and  $\text{BR}(H_1 \rightarrow b\bar{b})$  we get the following rate in the  $6b$  final state,

$$\sigma_{H_1 H_2}^{\text{NLO}} \times \text{BR}(H_2 \rightarrow H_1 H_1) \times \text{BR}(H_1 \rightarrow b\bar{b})^3 = 509 \cdot 0.37 \cdot 0.60^3 \text{ fb} = 40 \text{ fb} . \quad (8.59)$$

We can compare this with direct  $H_2$  production (we use the NNLO value calculated with **SusHi**) in either the  $4b$  final state from the  $H_2 \rightarrow H_1 H_1$  decay,

$$\sigma^{\text{NNLO}}(H_2) \times \text{BR}(H_2 \rightarrow H_1 H_1) \times \text{BR}(H_1 \rightarrow b\bar{b})^2 = 161 \cdot 0.37 \cdot 0.60^2 \text{ fb} = 21 \text{ fb} , \quad (8.60)$$

or direct  $H_2$  production in the other dominant decay channel given by the  $WW$  final state,

$$\sigma^{\text{NNLO}}(H_2) \times \text{BR}(H_2 \rightarrow WW) = 161 \cdot 0.44 \text{ fb} = 71 \text{ fb} . \quad (8.61)$$

Note that the  $H_2$  branching ratio into  $(b\bar{b})$  is tiny. The second lightest Higgs boson  $H_2$  has a significant down-type and large singlet admixture but only a small up-type admixture so that its production in gluon fusion is not very large<sup>31</sup> and also its decay branching ratios into a lighter Higgs pair are comparable to the largest decay rates into SM particles. In this case, the non-SM-like Higgs boson  $H_2$  has better chances of being discovered in di-Higgs when compared to single Higgs channels. Note, that the  $W$  bosons still need to decay into fermionic final states where additionally the neutrinos are not detectable so that the  $H_2$  mass cannot be reconstructed.

The input parameters for the first NMSSM scenario that we discuss here are given in Tab. 33. We also specify in Tab. 34 the parameters required for the computation of the Higgs pair production cross sections through **HPAIR**.

$\lambda$	$\kappa$	$A_\lambda$ [GeV]	$A_\kappa$ [GeV]	$\mu_{\text{eff}}$ [GeV]	$\tan \beta$
0.593	0.390	296	5.70	200	2.815
$m_{H^\pm}$ [GeV]	$M_1$ [GeV]	$M_2$ [GeV]	$M_3$ [TeV]	$A_t$ [GeV]	$A_b$ [GeV]
505	989.204	510.544	2	-2064	-1246
$m_{\tilde{Q}_3}$ [GeV]	$m_{\tilde{t}_R}$ [GeV]	$m_{\tilde{b}_R}$ [GeV]	$A_\tau$ [GeV]	$m_{\tilde{L}_3}$ [GeV]	$m_{\tilde{\tau}_R}$ [GeV]
1377	1207	3000	-1575.91	3000	3000

Table 33: **BP16** NMSSM input parameters required by **NMSSMCALC** for the computation of the NMSSM spectrum.

Since  $H_2$  is rather singlet-like, its production cross section through gluon fusion is small and also its decay branching ratios into SM-final states. The gluon fusion production cross section amounts to

$$\sigma^{\text{NNLO}}(H_2) = 13.54 \text{ fb} . \quad (8.62)$$

<sup>31</sup>The production in association with  $b$  quarks is very small for the small  $\tan \beta$  value of this scenario.

$m_{H_1}$ [GeV]	$m_{H_2}$ [GeV]	$m_{H_3}$ [GeV]	$m_{A_1}$ [GeV]	$m_{A_2}$ [GeV]
127.78	253	518	116	508
$\Gamma_{H_1}^{\text{tot}}$ [GeV]	$\Gamma_{H_2}^{\text{tot}}$ [GeV]	$\Gamma_{H_3}^{\text{tot}}$ [GeV]	$\Gamma_{A_1}^{\text{tot}}$ [GeV]	$\Gamma_{A_2}^{\text{tot}}$ [GeV]
$4.264 \cdot 10^{-3}$	0.466	3.145	$9.910 \cdot 10^{-7}$	4.750
$h_{11}$	$h_{12}$	$h_{13}$	$h_{21}$	$h_{22}$
0.325	0.939	-0.112	0.234	0.034
$h_{23}$	$h_{31}$	$h_{32}$	$h_{33}$	$a_{11}$
0.971	0.916	-0.321	-0.209	-0.0063
$a_{21}$	$a_{13}$	$a_{23}$		
-0.0022	0.999	0.0067		

Table 34: **BP16** These input parameters and those given in the first line of Tab. 33 are required by **HPAIR** for the computation of the Higgs pair production cross sections. The total width of the charged Higgs boson is not required but given here for completeness  $\Gamma_{H^\pm}^{\text{tot}} = 3.94$  GeV.

Its dominant branching ratio is given by the decay into  $A_1 A_1$ , reaching

$$\text{BR}(H_2 \rightarrow A_1 A_1) = 0.887 . \quad (8.63)$$

We hence get for direct  $H_2$  production in the  $A_1 A_1$  final state the rate

$$\sigma^{\text{NNLO}}(H_2) \times \text{BR}(H_2 \rightarrow A_1 A_1) = 12.01 \text{ fb} . \quad (8.64)$$

On the other hand, we have for di-Higgs production of  $H_1 H_2$  at NLO QCD where  $H_1$  is the SM-like Higgs state,

$$\sigma^{\text{NLO}}(H_1 H_2) = 111 \text{ fb} . \quad (8.65)$$

With

$$\text{BR}(H_1 \rightarrow b\bar{b}) = 0.539, \quad (8.66)$$

and the  $H_2$  branching ratio into  $A_1 A_1$  given above we hence have

$$\sigma^{\text{NLO}}(H_1 H_2) \times \text{BR}(H_1 \rightarrow b\bar{b}) \times \text{BR}(H_2 \rightarrow A_1 A_1) = 53 \text{ fb} . \quad (8.67)$$

With

$$\text{BR}(A_1 \rightarrow b\bar{b}) = 0.704 \quad (8.68)$$

we then obtain in double Higgs production in the  $6b$  final state the rate

$$\sigma^{\text{NLO}}(H_1 H_2)_{6b} = 53 \times 0.704^2 \text{ fb} = 26 \text{ fb} . \quad (8.69)$$

On the other hand, we have in single Higgs production for the  $4b$  final state

$$\begin{aligned} \sigma^{\text{NNLO}}(H_2)_{4b} &= \sigma^{\text{NNLO}}(H_2) \times \text{BR}(H_2 \rightarrow A_1 A_1) \times \text{BR}(A_1 \rightarrow b\bar{b})^2 \\ &= 13.54 \times 0.887 \times 0.704^2 \text{ fb} = 5.95 \text{ fb} . \end{aligned} \quad (8.70)$$

Note that direct  $H_2$  production with subsequent decay into  $W^+ W^-$  only reaches a rate of 1 fb. We clearly see that di-Higgs beats single Higgs production and the non-SM-like singlet-dominated state  $H_2$  might be first discovered in di-Higgs production instead directly in single

$\lambda$	$\kappa$	$A_\lambda$ [GeV]	$A_\kappa$ [GeV]	$\mu_{\text{eff}}$ [GeV]	$\tan \beta$
0.545	0.598	168	-739	258	2.255
$m_{H^\pm}$ [GeV]	$M_1$ [GeV]	$M_2$ [GeV]	$M_3$ [TeV]	$A_t$ [GeV]	$A_b$ [GeV]
548	437.872	498.548	2	-1028	1083
$m_{\tilde{Q}_3}$ [GeV]	$m_{\tilde{t}_R}$ [GeV]	$m_{\tilde{b}_R}$ [GeV]	$A_\tau$ [GeV]	$m_{\tilde{L}_3}$ [GeV]	$m_{\tilde{\tau}_R}$ [GeV]
1729	1886	3000	-1679.21	3000	3000

Table 35: **BP17** NMSSM input parameters required by **NMSSMCALC** for the computation of the NMSSM spectrum.

$m_{H_1}$ [GeV]	$m_{H_2}$ [GeV]	$m_{H_3}$ [GeV]	$m_{A_1}$ [GeV]	$m_{A_2}$ [GeV]
123.20	319	560	545	783
$\Gamma_{H_1}^{\text{tot}}$ [GeV]	$\Gamma_{H_2}^{\text{tot}}$ [GeV]	$\Gamma_{H_3}^{\text{tot}}$ [GeV]	$\Gamma_{A_1}^{\text{tot}}$ [GeV]	$\Gamma_{A_2}^{\text{tot}}$ [GeV]
$3.985 \times 10^{-3}$	0.010	4.207	6.399	6.913
$h_{11}$	$h_{12}$	$h_{13}$	$h_{21}$	$h_{22}$
0.419	0.909	0.015	0.187	-0.102
$h_{23}$	$h_{31}$	$h_{32}$	$h_{33}$	$a_{11}$
0.977	0.889	-0.407	-0.212	0.908
$a_{21}$	$a_{13}$	$a_{23}$		
-0.104	0.114	0.994		

Table 36: **BP17** These input parameters and those given in the first line of Tab. 33 are required by **HPAIR** for the computation of the Higgs pair production cross sections. The total width of the charged Higgs boson is not required but given here for completeness  $\Gamma_{H^\pm}^{\text{tot}} = 5.503$  GeV.

$H_2$  production through gluon fusion.

For the second NMSSM benchmark scenario that we present here the input parameters for **NMSSMCALC** and **HPAIR** are summarized in Tabs. 35 and 36. The singlet-like  $H_2$  dominantly decays into an SM-like pair  $H_1 H_1$ , and in the  $H_1 H_1$  final state we obtain the rate

$$\sigma^{\text{NNLO}}(H_2) \times \text{BR}(H_2 \rightarrow H_1 H_1) = 134.95 \cdot 0.566 \text{ fb} = 76.38 \text{ fb} . \quad (8.71)$$

With  $\text{BR}(H_1 \rightarrow b\bar{b}) = 0.636$  this results in the  $4b$  rate

$$\sigma^{\text{NNLO}}(H_2) \times \text{BR}(H_2 \rightarrow H_1 H_1) \times \text{BR}^2(H_1 \rightarrow b\bar{b}) = 31.00 \text{ fb} . \quad (8.72)$$

On the other hand, with  $\text{BR}(H_2 \rightarrow b\bar{b}) = 0.103$ , we have the  $2b$  final state rate

$$\sigma^{\text{NNLO}}(H_2) \times \text{BR}(H_2 \rightarrow b\bar{b}) = 134.95 \cdot 0.104 \text{ fb} = 14.03 \text{ fb} . \quad (8.73)$$

The rate for direct  $H_2$  production in the  $4b$  final state via its decay into  $H_1 H_1$  beats the one of direct  $H_2$  production in the  $2b$  final state by more than a factor 2. Note finally that the  $6b$  rate for  $H_2$  production, through  $H_1 H_2$  production and further  $H_2$  decay into Higgs pairs, amounts to

$$\sigma^{\text{NLO}}(H_1 H_2) \times \text{BR}(H_2 \rightarrow H_1 H_1) \times \text{BR}^3(H_1 \rightarrow b\bar{b}) = 75 \cdot 0.566 \cdot 0.636^3 \text{ fb} = 11 \text{ fb} , \quad (8.74)$$

which is not much below the  $2b$  final state rate.

## 9 Non-SM-Like Higgs Pair Final States

For non-SM-like Higgs pair production, we can have a large plethora of all possible Higgs pair combinations inducing final states with multiple Higgs bosons, two or three Higgs bosons in association with one or two gauge bosons, or also with a top-quark pair, resulting finally in multi-fermion, multi-photon or multi-fermion plus multi-photon final states. We present a few selected interesting signatures from non-SM-like Higgs pair production in Tab. 37. More signatures and benchmark points can be provided on request. As we can infer from the table, we can have high rates in non-SM-like Higgs pair production, *e.g.* up to 9 pb in the  $4b$  final state from non-SM-like  $H_1 H_1$  production in the N2HDM-I with  $H_2 \equiv H_{\text{SM}}$ .

**Cascade Decays with Multiple Higgs Final States** As already stated, in non-minimal Higgs extensions, we can have Higgs-to-Higgs cascade decays that can lead to multiple Higgs final states. The largest rate at NLO QCD that we found, for a final state with more than three Higgs bosons, is given in the N2HDM-I, where we have

$$\sigma(pp \rightarrow H_2 H_2 \rightarrow H_1 H_1 H_1 H_1 \rightarrow 4(b\bar{b})) = 1.4 \text{ fb} . \quad (9.75)$$

The SM-like Higgs is  $H_1$  and the  $K$ -factor for the NLO QCD production of  $H_2 H_2$  is 1.82. Also in the NMSSM and C2HDM we can have multiple Higgs production but the rates are below 10 fb after the decays of the Higgs bosons. In the N2HDM, we can even produce up to eight Higgs bosons in the final states but the rates are too small to be measurable.

## 10 Conclusions

In this paper, we have performed a comprehensive analysis of Higgs pair production in some archetypical BSM models, namely the R2HDM, the C2HDM, and the N2HDM as non-SUSY representatives, and the NMSSM as a SUSY model. After applying the relevant theoretical and experimental constraints, in particular limits from non-resonant and resonant di-Higgs searches, we explore the ranges of the parameter spaces of these models that are still allowed. We find that while the SM-like Higgs top-Yukawa couplings are constrained to within about 10% of the SM model value, there is still some freedom on the trilinear Higgs self-coupling. In particular, zero values for the SM-like trilinear Higgs self-coupling are still allowed in all models. Interestingly, the experimental searches start to constrain the trilinear couplings of the N2HDM. In general, in order to derive limits on the couplings both resonant and non-resonant searches will be required. Overall, the delineation of the parameter space from di-Higgs production is difficult as in BSM models we have the Yukawa and trilinear couplings of various Higgs bosons involved and also their total widths play a role in the size of the cross section.

As for the maximum possible sizes of the resonantly enhanced cross sections for SM-like Higgs pair production, we find that they can be quite different across the models studied, so that the cross section value itself might exclude certain models provided it exceeds a specific limit. We presented benchmark scenarios for the maximum cross sections. They not only feature cross sections that can exceed the SM value by up to a factor of 12 but they are also interesting because they can lead to measurable rates of triple Higgs production or the production of a Higgs boson pair in association with a  $Z$  boson. In the C2HDM, we presented a scenario where the simultaneous measurement of Higgs-to-bosons decays would allow for the test of CP violation.

We also investigated to which extent an EFT approach can reproduce the Higgs pair results

Model	SM-like Higgs	Signature	$m_\Phi$ [GeV]	Rate [fb]	$K$ -factor
N2HDM-I	$H_3$	$H_1 H_1 \rightarrow (b\bar{b})(b\bar{b})$	41	14538	2.18
	$H_3$	$H_1 H_1 \rightarrow (4b); (4\gamma)$	41	4545 ; 700	2.24
	$H_1$	$AA \rightarrow (b\bar{b})(b\bar{b})$	75	6117	2.11
	$H_1$	$H_2 H_2 \rightarrow (b\bar{b})(b\bar{b})$	146	73	2.01
	$H_2$	$AA \rightarrow (b\bar{b})(b\bar{b})$	80	2875	2.13
	$H_2$	$AH_1 \rightarrow (b\bar{b})(b\bar{b})$	$m_A : 87$ $m_{H_1} : 91$	921	2.09
	$H_2$	$H_1 H_1 \rightarrow (b\bar{b})(b\bar{b})$	47	8968	2.17
N2HDM-II	$H_2$	$H_1 H_1 \rightarrow (b\bar{b})(b\bar{b})$	44	1146	2.18
C2HDM-I	$H_1$	$H_2 H_2 \rightarrow (b\bar{b})(b\bar{b})$	128	475	2.07
	$H_2$	$H_1 H_1 \rightarrow (b\bar{b})(b\bar{b})$	66	814	2.16
	$H_3$	$H_1 H_1 \rightarrow (b\bar{b})(b\bar{b})$	84	31	2.09
NMSSM	$H_1$	$A_1 A_1 \rightarrow (b\bar{b})(b\bar{b})$	166	359	1.95
	$H_1$	$A_1 A_1 \rightarrow (\gamma\gamma)(\gamma\gamma)$	179	34	1.96
	$H_2$	$H_1 H_1 \rightarrow (b\bar{b})(b\bar{b})$	48	3359	2.18
	$H_2$	$A_1 A_1 \rightarrow (b\bar{b})(b\bar{b})$	54	1100	2.18
	$H_1$	$A_1 A_1 \rightarrow (t\bar{t})(t\bar{t})$	350	20	1.82

Model	Signature	$m_{\text{res.}}$ [GeV]	res. rate [fb]	$m_{\text{res. 2}}$ [GeV]	res. rate 2 [fb]
N2HDM-I	$H_1 H_1 \rightarrow (b\bar{b})(b\bar{b})$	125.09	621	98	17137
	$H_1 H_1 \rightarrow (4b); (4\gamma)$	125.09	126; 19	94	5445;839
	$AA \rightarrow (b\bar{b})(b\bar{b})$	1535	<0.1	323	482
	$H_2 H_2 \rightarrow (b\bar{b})(b\bar{b})$	360	76	—	—
	$AA \rightarrow (b\bar{b})(b\bar{b})$	178	3191	—	—
	$AH_1 \rightarrow (b\bar{b})(b\bar{b})$	—	—	—	—
	$H_1 H_1 \rightarrow (b\bar{b})(b\bar{b})$	588	22	125.09	997
N2HDM-II	$H_1 H_1 \rightarrow (b\bar{b})(b\bar{b})$	520	< 0.1	125.09	1330
C2HDM-I	$H_2 H_2 \rightarrow (b\bar{b})(b\bar{b})$	266	497	—	—
	$H_1 H_1 \rightarrow (b\bar{b})(b\bar{b})$	151	598	—	—
	$H_1 H_1 \rightarrow (b\bar{b})(b\bar{b})$	—	—	—	—
NMSSM	$A_1 A_1 \rightarrow (b\bar{b})(b\bar{b})$	552	31	453	332
	$A_1 A_1 \rightarrow (\gamma\gamma)(\gamma\gamma)$	796	< 0.01	444	34
	$H_1 H_1 \rightarrow (b\bar{b})(b\bar{b})$	882	<0.1	125.59	4173
	$A_1 A_1 \rightarrow (b\bar{b})(b\bar{b})$	676	< 0.1	122.99	1353
	$A_1 A_1 \rightarrow (t\bar{t})(t\bar{t})$	741	7	705	14

Table 37: Upper: Selected rates for non-SM-like Higgs pair final states at NLO QCD. We specify the model, which of the Higgs bosons is the SM-like one, the signature and its rate as well as the  $K$ -factor. In the fourth column we also give the mass value  $m_\Phi$  of the non-SM-like Higgs boson involved in the process. Lower: In case of resonantly enhanced cross sections, the mass of the resonantly produced Higgs boson is given together with the NNLO QCD production rate. Some scenarios contain two heavier Higgs bosons that can contribute to resonant production. All benchmark details can be provided on request.

in specific UV-complete models. Since in gluon fusion into Higgs pairs, we integrate across possible resonances present in extended Higgs sectors due to the additional non-SM-like Higgs bosons, the EFT approach cannot correctly reproduce the results. This is particularly true

if the resonances are rather light. Moreover, we found that the value of the resonance mass from which on the EFT approach starts to approximate the result in the specific UV-complete model by better than 10% depends on the benchmark scenario itself and that the total width of the intermediate resonance plays an important role. This again emphasizes the importance of investigating specific models besides a more general EFT approach in order to get a complete picture of the new physics landscape.

We also presented benchmark points for the production of a SM-like Higgs together with a non-SM-like one, leading to a plethora of different final state signatures. The presented benchmark points represent those with significant rates in certain final state signatures, namely  $(b\bar{b})(b\bar{b})$ ,  $(b\bar{b})(WW)$ , and  $(b\bar{b})(t\bar{t})$ . But also multi-photon final states can have important rates as shown by our results, in particular in non-SM-like Higgs pair final states. We highlighted additionally scenarios that involve further Higgs-to-Higgs decays, of the mixed SM-like plus non-SM-like final state, leading to three-Higgs final states with significant rates. On top of that, three benchmark scenarios were presented where new heavy Higgs bosons might rather be discovered through resonant di-Higgs production than from direct single Higgs production. This is the case for the singlet extended models N2HDM and NMSSM, where the couplings of the searched heavy Higgs boson to SM particles are suppressed due to large singlet admixtures but not its trilinear coupling to other Higgs bosons. Finally, we gave a short overview of the maximum possible rates in the production of two non-SM-like Higgs bosons and also for the production of multiple Higgs bosons.

For all benchmark points, we provided the di-Higgs production cross sections at NLO QCD in the heavy loop particle limit. We found that the  $K$ -factors range between 1.79 and 2.24 depending on the model and the final Higgs pair state.

We collected a large amount of viable parameter points in the R2HDM, C2HDM, N2HDM, and NMSSM with interesting features in the context of Higgs pair production and necessarily had to restrict ourselves on specific scenarios to highlight some prominent features. We emphasize, however, that we can provide benchmarks with specific features on request and invite the readers to contact us.

With this work, we hope to have given a close to complete and comprehensive overview of possible signatures in di-Higgs or even multi-Higgs production in representative BSM models and what can be learnt from them. It can be a starting point for further investigations in many different final state signatures based on the data sample that we have generated. Having a guideline at hand of what can be expected may help us find our way through the vast new physics landscape and get deeper insights in the mechanism behind electroweak symmetry breaking. Ultimately helping us to answer some of our most pressing open questions in the world of elementary particle physics.

## Acknowledgement

We thank the LHC Higgs Working group in general, and in particular we are grateful for numerous fruitful discussions in meetings and workshops of the HH, NMSSM and Extended Higgs sector subgroups. We are also grateful to their conveners E. Brost, M. d’Alfonso, U. Ellwanger, R. Gröber, N. Lu, J. Mazzitelli, T. Robens, N. Rompotis, N. Shah, D. Winterbottom, L. Zivkovic. We acknowledge many helpful discussions with A. Ferrari, M. Klute, J. Müller, M. Spira, J. Wittbrodt, R. Wolf. Thanks go to M. Gabelmann for providing the NMSSM sample. M.M. acknowledges support by the BMBF projects 05H18VKCC1 and 05H21VKCCA. D.A.

acknowledges support the Deutsche Forschungsgemeinschaft (DFG, German Research Foundation) under grant 396021762 - TRR 257. J. El F. would like to thank the Abdus Salam International Centre for Theoretical Physics (ICTP) for hospitality and financial support where part of this work has been done. R.S. and P.F. are supported by CFTC-UL under FCT contracts UIDB/00618/2020, UIDP/00618/2020, and by the projects CERN/FISPAR/0002/2017 and CERN/FIS-PAR/0014/2019. P.F. is supported by the project CERN/FIS-PAR/0004/2019.

## A Resonant and Non-Resonant Production Cross Sections

In this section, we re-present the cross sections of Figs. 7 and 8 by, first, showing all the points that have a resonant contribution and, second, displaying only points that are considered non-resonant by the definition given in Sec. 4.2. Notice that the points displayed for each part are not complementary in the full sample, *i.e.* some point for which we show its resonant contribution might be defined as non-resonant and appear in the non-resonant plots as well. This is because a point being defined as dominantly non-resonant (by our definition) is not exempt from being compared to experimental resonant constraints. On the other hand, it makes no sense to compare points where resonance production is dominant with experimental non-resonant limits, hence only points that we define as non-resonant ones can be compared to non-resonant experimental limits. To be specific, points with resonant contribution means parameter points where at least one of the heavier neutral Higgs bosons<sup>32</sup> has a mass large enough to decay into a pair of two SM-like Higgs bosons. And the resonant production cross sections are obtained by calculating with **SusHi** the NNLO QCD production cross section of the “resonant” Higgs boson and subsequently multiplying it with its branching ratio into the two SM-like Higgs bosons. The points included in the non-resonant plots on the other hand are all those scatter points of Figs. 7 and 8 where resonant production is kinematically not possible, or where the resonant production cross section accounts for less than 10% of the total di-Higgs cross section.

Figure 13 shows the resonant production cross section values for the R2HDM for the points presented in Fig. 7 (upper). The color code denotes the ratio of the total width of the resonant Higgs boson and its mass.

In Fig. 14 we display the resonant production cross sections for the C2HDM for the different cases w.r.t. to which of the  $H_{1,2}$  is the SM-like Higgs boson. Note that in the C2HDM T2 we do not have scenarios compatible with all constraints with resonantly enhanced production in case  $H_2$  is the SM-like Higgs boson. In case  $H_1$  is the SM-like Higgs boson, both  $H_2$  and  $H_3$  can in principle lead to resonant enhancement. We therefore show in separate plots their resonant cross sections as a function of their mass.

The resonant production cross sections for the N2HDM for the different cases w.r.t. to which of the  $H_{1,2}$  is the SM-like Higgs boson are shown in Fig. 15 and those for the NMSSM in Fig. 16.

In Fig. 17 we display the di-Higgs cross sections for points considered non-resonant by our definition, for the R2HDM, C2HDM, and N2HDM type 1 and type 2. We show them as a function of the trilinear Higgs self-coupling of the SM-like Higgs boson in the respective model normalized to the value of the trilinear Higgs self-coupling of the SM,  $\lambda_{3H_{SM}}/\lambda_{3H}$ . In Fig. 18 we show the corresponding NMSSM plot. We also include in the plots as a full line the change of the SM Higgs pair production cross section as a function of  $\lambda_{3H_{SM}}/\lambda_{3H}$ . The dashed lines show

---

<sup>32</sup>Note that in the C2HDM, N2HDM, and NMSSM for the case where the lightest Higgs boson is the SM-like one, we can have two possible resonances.

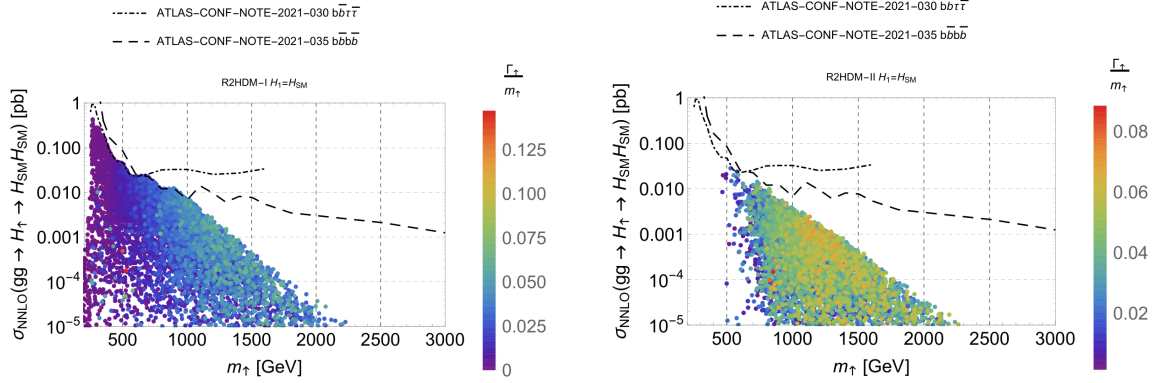


Figure 13: Resonant production cross sections for the R2HDM points of Fig. 7 (upper) for R2HDM-I (left) and R2HDM-II (right) as a function of the resonantly produced heavier Higgs boson  $H_2 \equiv H_{\uparrow}$ . Color code: ratio of the total width of the resonant Higgs boson and its mass.

its change if additionally the top-Yukawa coupling is varied by 10% away from the SM value. From these plots we can infer the importance of interference effects. We see *e.g.* in Fig. 17 (lower left) for the N2HDM-I with  $H_2 \equiv H_{\text{SM}}$  green points that are well below the full and dashed lines. The suppression of the N2HDM cross section cannot be caused by the variation of the trilinear or top-Yukawa coupling away from the SM values (indicated by the full and dashed lines). It is caused by the negative interference between the triangle diagram contributions of  $H_1$  and  $H_2$ , as we explicitly verified.

## B Alignment Limit in the C2HDM

In the following, we derive the limits that are required to achieve the alignment limit in the C2HDM. In terms of the matrix elements of the mixing matrix, defined in Eq. (2.4), the  $H_i$  ( $i = 1, 2, 3$ ) Higgs couplings to massive gauge bosons ( $V = Z, W$ ) and to fermions  $f$  in the C2HDM-I and C2HDM-II, read respectively

$$g_{H_i V V}^{\text{C2HDM-I/II}} = (R_{i1} c_\beta + s_\beta R_{i2}) g_{H V V}^{\text{SM}}, \quad (\text{B.76})$$

$$g_{H_i f f}^{\text{C2HDM-I}} = \left( \frac{R_{i2}}{s_\beta} + i \gamma_5 \frac{R_{i3}}{t_\beta} \right) g_{H f f}^{\text{SM}}, \quad (\text{B.77})$$

$$g_{H_i u u}^{\text{C2HDM-II}} = \left( \frac{R_{i2}}{s_\beta} + i \gamma_5 \frac{R_{i3}}{t_\beta} \right) g_{H u u}^{\text{SM}}, \quad (\text{B.78})$$

$$g_{H_i, dd(l l)}^{\text{C2HDM-II}} = \left( \frac{R_{i1}}{c_\beta} + i \gamma_5 R_{i3} t_\beta \right) g_{H dd(h l l)}^{\text{SM}}, \quad (\text{B.79})$$

where  $u$  denotes up-type quarks,  $d$  down-type quarks,  $l$  leptons and  $g_{H X X}^{\text{SM}}$  are the corresponding SM couplings of the SM Higgs  $H$  to  $XX$ .

We define the conditions to get alignment between the C2HDM and the SM for the SM-like

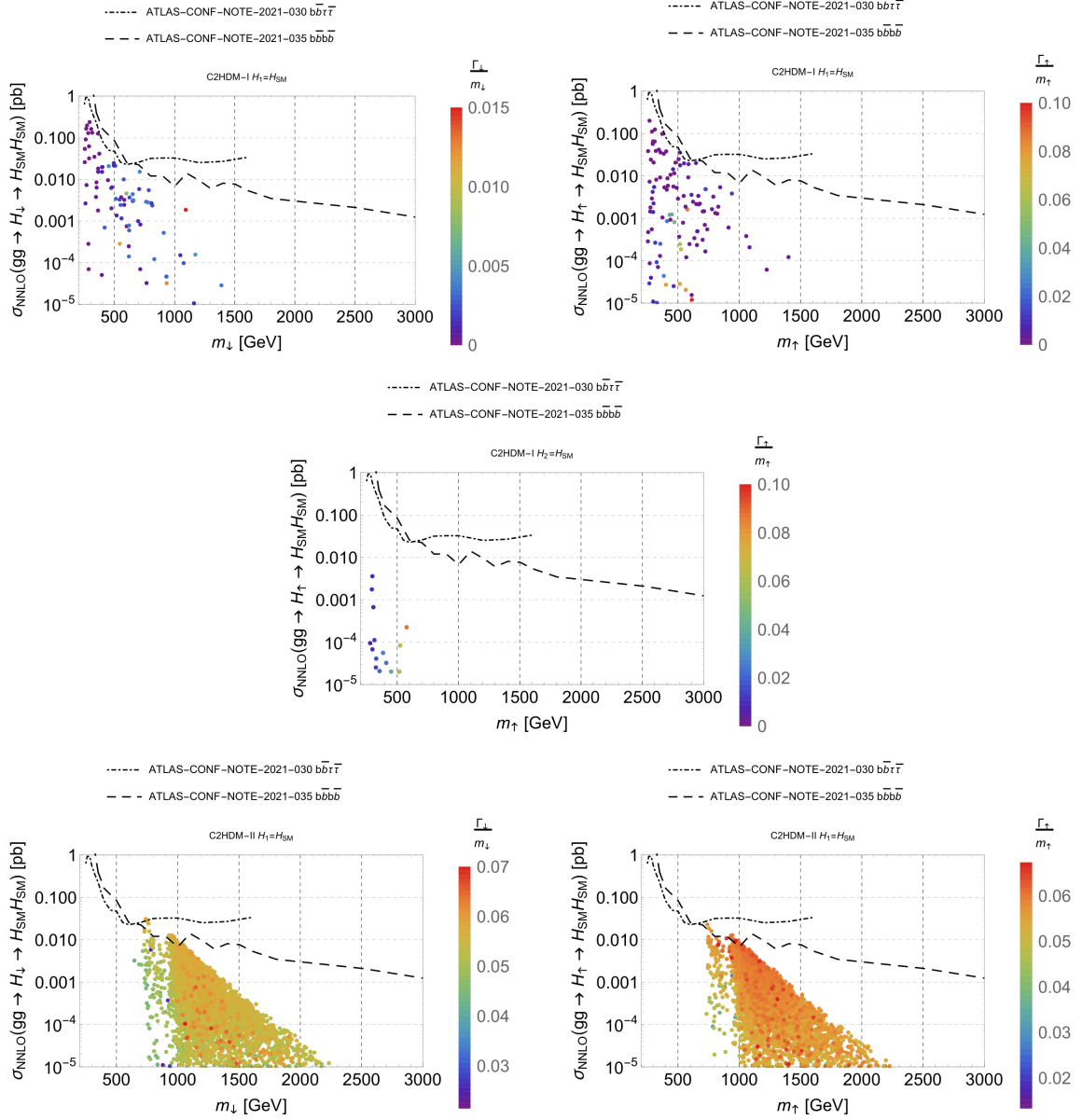


Figure 14: Resonant production cross sections for the C2HDM points of Fig. 7 (middle) for C2HDM-I (upper two rows) and C2HDM-II (lower row) as a function of the resonantly produced heavier Higgs boson  $H_2 \equiv H_\downarrow$  or  $H_3 \equiv H_\uparrow$ . Color code: ratio of the total width of the resonant Higgs boson and its mass.

Higgs given by  $H_i$  as

$$\frac{g_{H_i V V}^{\text{C2HDM}}}{g_{H V V}^{\text{SM}}} = (R_{i1} c_\beta + s_\beta R_{i2}) = 1, \quad (\text{B.80})$$

$$\frac{g_{H_i f f}^{\text{C2HDM}}}{g_{H f f}^{\text{SM}}} = 1 \quad \Rightarrow \quad \frac{R_{i2}}{s_\beta} = \frac{R_{i1}}{c_\beta} = 1 \text{ and } R_{i3} = 0, \quad (\text{B.81})$$

$$\frac{g_{H_i H_i H_i}^{\text{C2HDM}}}{g_{3H}^{\text{SM}}} = 1, \quad (\text{B.82})$$

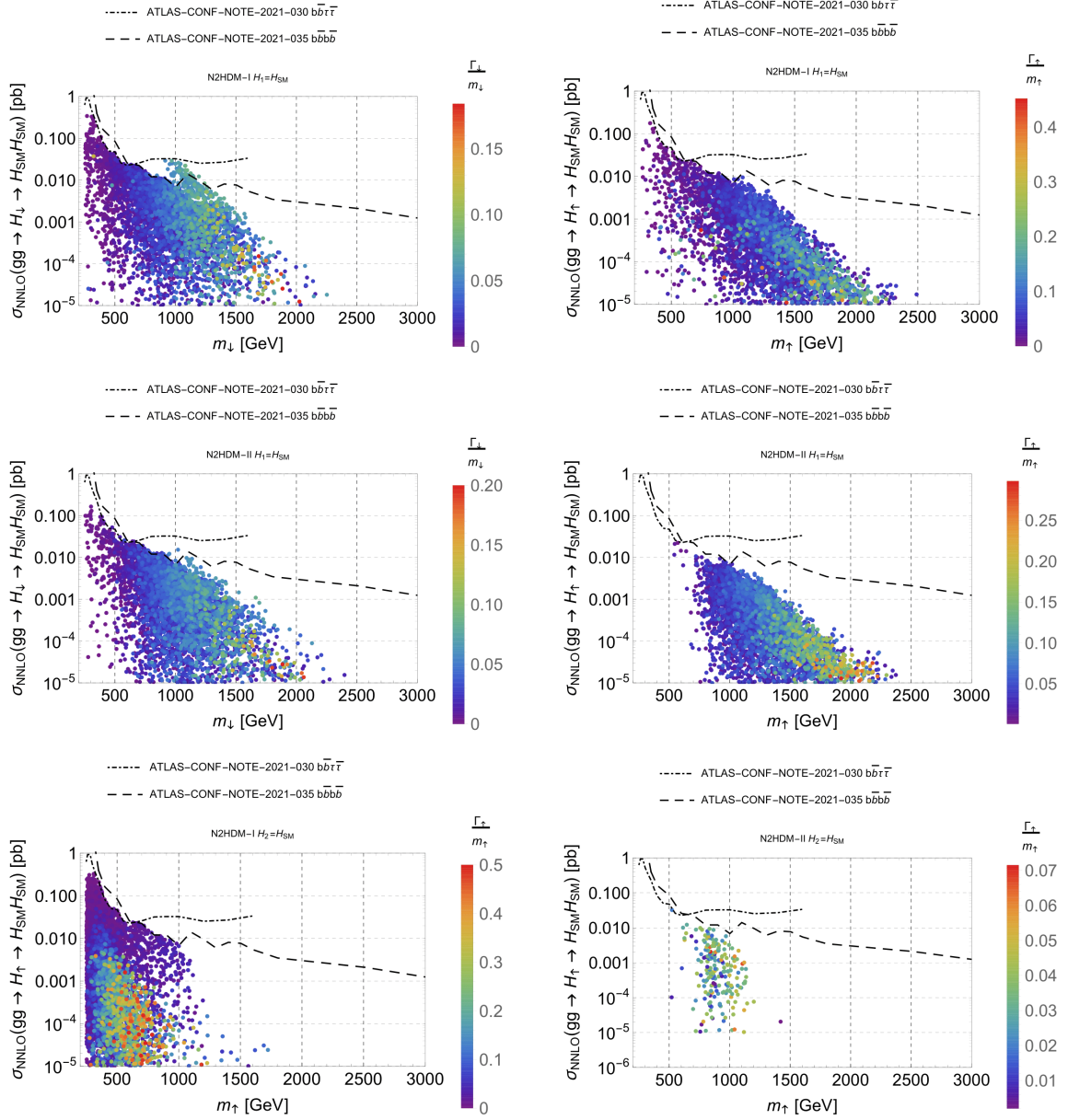


Figure 15: Resonant production cross sections for the N2HDM points of Fig. 7 (lower) for N2HDM-I (upper) and N2HDM-II (middle) with  $H_1 \equiv H_{\text{SM}}$ . Lower row:  $H_2 \equiv H_{\text{SM}}$  in case of type 1 (left) and type 2 (right); all plots as a function of the resonantly produced Higgs boson. Color code: ratio of the total width of the resonant Higgs boson and its mass.

with  $m_{H_i} = m_H$ . The implications of these limits for the various possibilities of  $H_1$ ,  $H_2$ , or  $H_3$  being SM-like for the mixing angles are as follows:

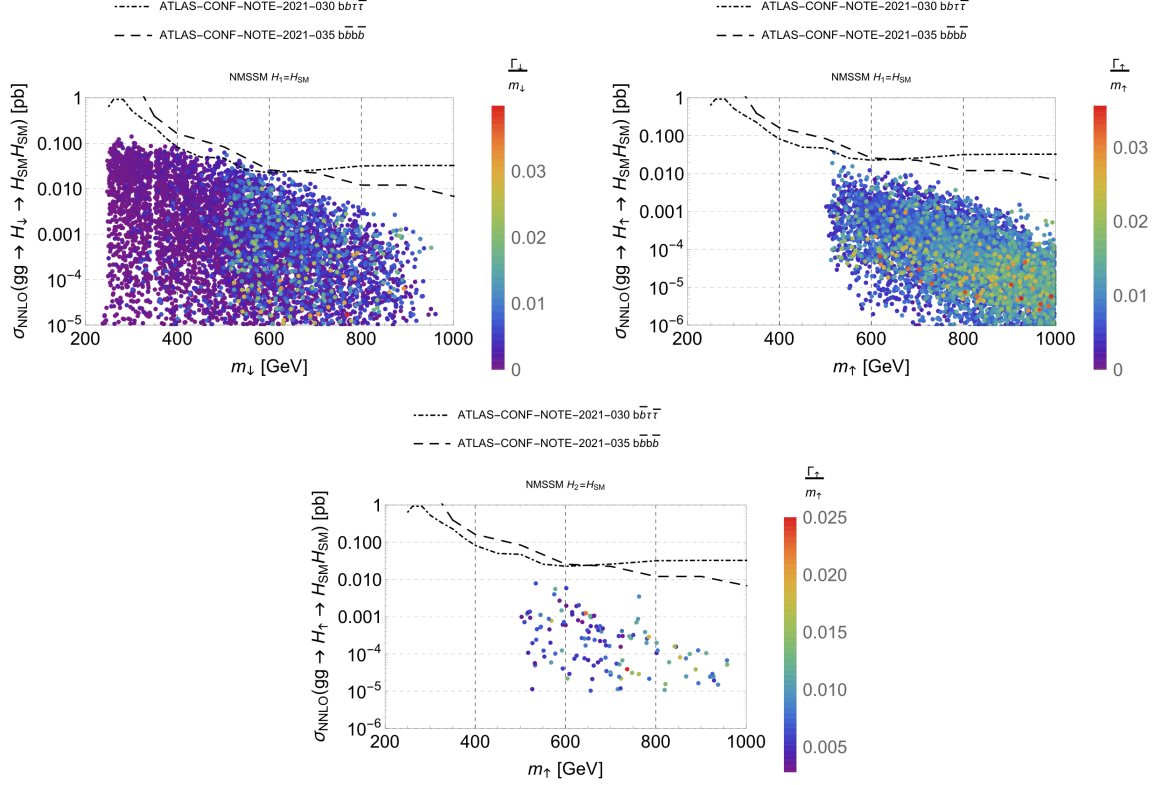


Figure 16: Resonant production cross sections for the NMSSM points of Fig. 8 for  $H_1 \equiv H_{\text{SM}}$  (upper) and  $H_2 \equiv H_{\text{SM}}$  (lower) as a function of the resonantly produced heavier Higgs boson  $H_2 \equiv H_\downarrow$  or  $H_3 \equiv H_\uparrow$ . Color code: ratio of the total width of the resonant Higgs boson and its mass.

**$H_1$  SM-like scenario:** To get the condition for alignment in this case, we have to solve the following equation,

$$\begin{aligned} \frac{g_{H_1 VV}^{\text{C2HDM}}}{g_{HVV}^{\text{SM}}} = 1 & \Rightarrow c_{\alpha_1} c_{\alpha_2} c_\beta + c_{\alpha_2} s_{\alpha_1} s_\beta = 1, \\ & \Rightarrow c_{(\alpha_1 - \beta)} c_{\alpha_2} = 1, \end{aligned} \quad (\text{B.83})$$

from which follows the solution  $S_1$ ,

$$S_1 = \{\alpha_2 = 0 \quad \text{and} \quad \beta = \alpha_1\}. \quad (\text{B.84})$$

Using  $S_1$  it is easy to verify that

$$\frac{R_{12}}{s_\beta} = 1, \quad \frac{R_{11}}{c_\beta} = 1, \quad R_{13} = 0, \quad (\text{B.85})$$

so that also

$$g_{H_1 ff}^{\text{C2HDM}} = g_{Hff}^{\text{SM}} \quad \text{and} \quad g_{H_1 H_1 H_1}^{\text{C2HDM}} = g_{3H}^{\text{SM}}, \quad (\text{B.86})$$

as required in the alignment limit. For the latter, we used the formulae given at the webpage [240].

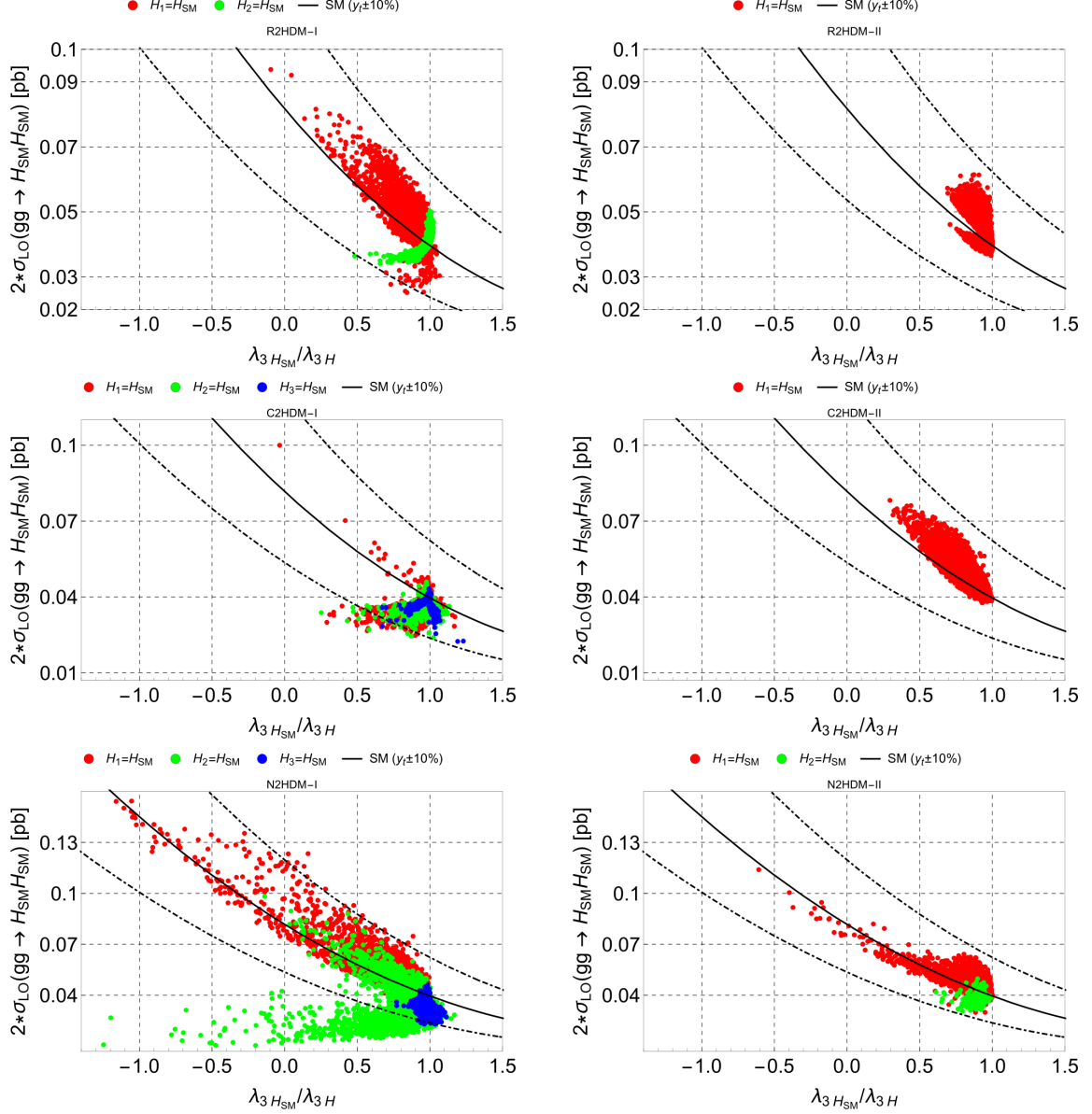


Figure 17: Non-resonant di-Higgs cross sections for the R2HDM (upper), C2HDM (middle) and N2HDM (lower) points of Fig. 8 for type 1 (left) and type 2 (right) as a function of the trilinear Higgs self-coupling of the SM-like Higgs boson of the respective model normalized to the trilinear coupling of the SM Higgs boson. Note the different  $y$ -axis range in the results for the R2HDM and those for the C2HDM and N2HDM. The full line shows the change of the SM Higgs pair cross section as a function of the variation of the trilinear Higgs self-coupling, the dashed lines show the change, when additionally the SM top-Yukawa coupling is varied by  $\pm 10\%$ .

**$H_2$  SM-like scenario:** To get the conditions for alignment in this case, we analogously set

$$\begin{aligned}
 \frac{g_{H_2 VV}^{\text{C2HDM}}}{g_{H V V}^{\text{SM}}} = 1 & \Rightarrow -(c_{\alpha_1} s_{\alpha_2} s_{\alpha_3} + s_{\alpha_1} c_{\alpha_3}) c_{\beta} + (c_{\alpha_1} c_{\alpha_3} - s_{\alpha_1} s_{\alpha_2} s_{\alpha_3}) s_{\beta} = 1 \\
 & \Rightarrow -c_{\beta - \alpha_1} s_{\alpha_2} s_{\alpha_3} + c_{\alpha_3} s_{\beta - \alpha_1} = 1,
 \end{aligned} \tag{B.87}$$

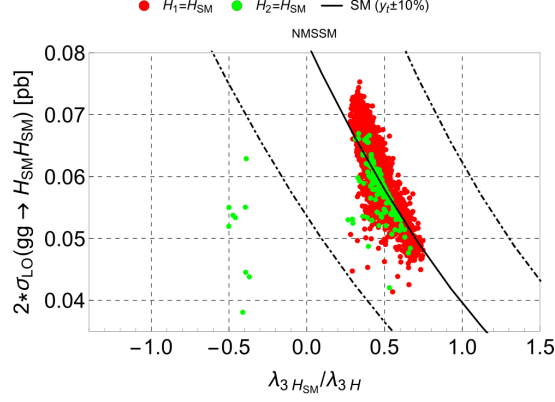


Figure 18: Same as Fig. 17 but for the NMSSM.

from which follows

$$S_2 = \left\{ \{ \alpha_3 = 0 \text{ and } \beta = \pi/2 + \alpha_1 \} \text{ or } \{ \alpha_2 = -\alpha_3 = \pm\pi/2 \text{ and } \beta = \alpha_1 \} \right. \\ \left. \text{ or } \{ \alpha_2 = \alpha_3 = \pm\pi/2 \text{ and } \beta = \alpha_1 + \pi \} \right\}. \quad (\text{B.88})$$

We will call the first, the second and the third solution  $S_{21}$ ,  $S_{22}$  and  $S_{23}$ , respectively. With these conditions, the SM-like Higgs gauge and fermion couplings, as well as the trilinear Higgs self-coupling approach the corresponding SM values.

**$H_3$  SM-like scenario:** For  $H_3$  SM-like we get the condition

$$\frac{g_{H_3 VV}^{\text{C2HDM}}}{g_{H_3 VV}^{\text{SM}}} = 1 \quad \Rightarrow (-c_{\alpha_1} s_{\alpha_2} c_{\alpha_3} + s_{\alpha_1} s_{\alpha_3}) c_{\beta} - (c_{\alpha_1} s_{\alpha_3} + s_{\alpha_1} s_{\alpha_2} c_{\alpha_3}) s_{\beta} = 1 \\ \Rightarrow -c_{\beta-\alpha_1} s_{\alpha_2} c_{\alpha_3} - s_{\alpha_3} s_{\beta-\alpha_1} = 1, \quad (\text{B.89})$$

which is solved by

$$S_3 = \left\{ \{ \alpha_3 = 0, \alpha_2 = \pi/2 \text{ and } \beta = \alpha_1 + \pi \} \text{ or } \{ \alpha_3 = \pm\pi/2 \text{ and } \beta = \alpha_1 \mp \pi/2 \} \right. \\ \left. \text{ or } \{ \alpha_3 = 0, \alpha_2 = -\pi/2 \text{ and } \beta = \alpha_1 \} \right\}. \quad (\text{B.90})$$

In the following, we will call the first, the second and the third solution  $S_{31}$ ,  $S_{32}$  and  $S_{33}$ , respectively. For solution  $S_3$  we obtain the SM values of the  $H_3$  couplings to gauge bosons and fermions as well as for the trilinear Higgs self-coupling.

**Mass dependence in the alignment limit:** In the C2HDM, the mass of the heaviest neutral scalar is a dependent parameter, given by

$$m_{H_3}^2 = \frac{m_{H_1}^2 R_{13}(R_{12}t_{\beta} - R_{11}) + m_{H_2}^2 R_{23}(R_{22}t_{\beta} - R_{21})}{R_{33}(R_{31} - R_{32}t_{\beta})}. \quad (\text{B.91})$$

In the limit where  $H_1$  is the SM-like Higgs boson, after applying the solution  $S_1$  to Eq. (B.91) we find that the terms that depend on  $m_{H_1}$  vanish and we get

$$m_{H_3} = m_{H_2}. \quad (\text{B.92})$$

For the case of  $H_2$  being SM-like and applying the  $S_2$  limits to Eq. (B.91), we find that the first solution  $S_{21}$  gives a similar equality as  $S_1$ , namely

$$m_{H_3} = m_{H_1} , \quad (\text{B.93})$$

but for the second and third solution  $S_{22}$ ,  $S_{23}$ , we first apply the limit  $\beta \rightarrow \alpha_1$  and then  $\alpha_2 \rightarrow \pm\pi/2$ , to obtain

$$m_{H_3}^2|_{\beta \rightarrow \alpha_1, \alpha_2 \rightarrow \pm\pi/2} = \frac{(2m_{H_1}^2 - m_{H_2}^2)c_{2\alpha_1}}{2c_{2(\alpha_1 \pm \alpha_3)}c_{\alpha_3}} + \frac{m_{H_2}^2}{2c_{\alpha_3}} . \quad (\text{B.94})$$

From this limit we can conclude that for  $\alpha_2 \rightarrow \pm\pi/2$  the lightest Higgs boson  $H_1$  is a CP-odd Higgs boson [143] and from Eq. (B.94) that the mass of the third Higgs boson  $H_3$  goes to infinity.

In the scenario where  $H_3$  is SM-like, we have to change the dependent mass from  $m_{H_3}$  to  $m_{H_1}$  or  $m_{H_2}$ . By imposing  $m_{H_1}$  as a dependent parameter, we have

$$m_{H_1}^2 = \frac{m_{H_3}^2 R_{33}(R_{31} - R_{32}t_\beta) - m_{H_2}^2 R_{23}(R_{22}t_\beta - R_{21})}{R_{13}(R_{12}t_\beta - R_{11})} . \quad (\text{B.95})$$

By applying the solution  $S_{31}$  or  $S_{33}$ , we find that  $H_1$  is CP-odd with a mass equal to the mass of the SM-like Higgs boson  $m_H$

$$m_{H_1} = m_{H_3} = m_H . \quad (\text{B.96})$$

For the solution  $S_{32}$ , we get

$$m_{H_1} = m_{H_2} . \quad (\text{B.97})$$

Note that, if we apply the solution  $S_{22}$  or  $S_{23}$  to Eq. (B.95), we obtain

$$m_{H_1} = m_{H_2} = m_H . \quad (\text{B.98})$$

However, applying the solution  $S_{21}$  leads to

$$m_{H_1} = m_{H_3} . \quad (\text{B.99})$$

## C Alignment Limit in the N2HDM

We now turn to the derivation for the alignment limit in the N2HDM. In terms of the matrix elements of the mixing matrix  $R$ , defined as in the C2HDM, *cf.* Eq. (2.4), the  $H_i$  ( $i = 1, 2, 3$ ) Higgs couplings to massive gauge bosons ( $V = Z, W$ ) and to fermions  $f$ , respectively, as well as the trilinear Higgs self-couplings, read in the N2HDM-I and N2HDM-II

$$g_{H_i V V}^{\text{N2HDM-I/II}} = (R_{i1}c_\beta + s_\beta R_{i2}) g_{H V V}^{\text{SM}} , \quad (\text{C.100})$$

$$g_{H_i f f}^{\text{N2HDM-I}} = \frac{R_{i2}}{s_\beta} g_{H f f}^{\text{SM}} , \quad (\text{C.101})$$

$$g_{H_i u u}^{\text{N2HDM-II}} = \frac{R_{i2}}{s_\beta} g_{H u u}^{\text{SM}} , \quad (\text{C.102})$$

$$g_{H_i, dd(ll)}^{\text{N2HDM-II}} = \frac{R_{i1}}{c_\beta} g_{H dd(hll)}^{\text{SM}} , \quad (\text{C.103})$$

$$\begin{aligned} g_{H_i H_i H_i}^{\text{N2HDM-I/II}} &= \frac{3}{v} \left( -\mu^2 \left[ R_{i2}^2 c_\beta \left( \frac{R_{i2} c_\beta}{s_\beta} - R_{i1} \right) + R_{i1}^2 s_\beta \left( \frac{R_{i1} s_\beta}{c_\beta} - R_{i2} \right) \right] \right. \\ &\quad \left. + \frac{m_{H_i}^2}{v_S} \left[ R_{i3}^3 v + R_{i2}^3 \frac{v_S}{s_\beta} + R_{i1}^3 \frac{v_S}{c_\beta} \right] \right) , \end{aligned} \quad (\text{C.104})$$

where  $u$  denotes up-type quarks,  $d$  down-type quarks and  $l$  leptons,  $g_{HXX}^{\text{SM}}$  are the corresponding SM couplings of the SM Higgs  $H$  to  $XX$  and we have introduced

$$\mu^2 = \frac{m_{12}^2}{s_\beta c_\beta} . \quad (\text{C.105})$$

We define the conditions to get alignment between the N2HDM and the SM for the SM-like Higgs given by  $H_i$  as

$$\frac{g_{H_i VV}^{\text{N2HDM}}}{g_{HVV}^{\text{SM}}} = (R_{i1}c_\beta + s_\beta R_{i2}) = 1 , \quad (\text{C.106})$$

$$\frac{g_{H_i ff}^{\text{N2HDM}}}{g_{Hff}^{\text{SM}}} = 1 , \quad (\text{C.107})$$

$$\frac{g_{H_i H_i H_i}^{\text{N2HDM}}}{g_{3H}^{\text{SM}}} = 1 , \quad (\text{C.108})$$

with  $m_{H_i} = m_H$ . The implications of these limits for the various possibilities of  $H_1$ ,  $H_2$ , or  $H_3$  being SM-like for the mixing angles are as follows:

**$H_1$  SM-like scenario:** This is analogous to the C2HDM, where to get the condition of alignment we have to solve the following equation

$$\begin{aligned} \frac{g_{H_1 VV}^{\text{N2HDM}}}{g_{HVV}^{\text{SM}}} = 1 & \Rightarrow c_{\alpha_1} c_{\alpha_2} c_\beta + c_{\alpha_2} s_{\alpha_1} s_\beta = 1 , \\ & \Rightarrow c_{\alpha_1 - \beta} c_{\alpha_2} = 1 , \end{aligned} \quad (\text{C.109})$$

from which we derive

$$S_1 = \{\alpha_2 = 0 \quad \text{and} \quad \beta = \alpha_1\} . \quad (\text{C.110})$$

This leads to

$$\frac{R_{12}}{s_\beta} = 1, \quad \frac{R_{11}}{c_\beta} = 1 \quad \text{and} \quad R_{13} = 0 . \quad (\text{C.111})$$

We also get  $g_{H_i ff}^{\text{N2HDM}} = g_{Hff}^{\text{SM}}$  and  $g_{H_1 H_1 H_1}^{\text{N2HDM}} = g_{3H}^{\text{SM}}$  as required in the alignment limit.

**$H_2$  SM-like scenario:** To get the condition of the alignment in this case we do the same calculation as above,

$$\begin{aligned} \frac{g_{H_2 VV}^{\text{N2HDM}}}{g_{HVV}^{\text{SM}}} = 1 & \Rightarrow -(c_{\alpha_1} s_{\alpha_2} s_{\alpha_3} + s_{\alpha_1} c_{\alpha_3})c_\beta + (c_{\alpha_1} c_{\alpha_3} - s_{\alpha_1} s_{\alpha_2} s_{\alpha_3})s_\beta = 1 \\ & \Rightarrow -c_{\beta - \alpha_1} s_{\alpha_2} s_{\alpha_3} + c_{\alpha_3} s_{\beta - \alpha_1} = 1 , \end{aligned} \quad (\text{C.112})$$

from which follows

$$\begin{aligned} S_2 = \{ & \{\alpha_3 = 0 \text{ and } \beta = \pi/2 + \alpha_1\} \text{ or } \{\alpha_2 = -\alpha_3 = \pm\pi/2 \text{ and } \beta = \alpha_1\} \\ & \text{or } \{\alpha_2 = \alpha_3 = \pm\pi/2 \text{ and } \beta = \alpha_1 + \pi\} \} . \end{aligned} \quad (\text{C.113})$$

With these solutions we can find that all couplings of the SM-like Higgs  $H_2$  to massive gauge bosons and fermions, as well as the trilinear Higgs self-coupling of  $H_2$  approaches the alignment limit.

$H_3$  **SM-like scenario :** For  $H_3$  being SM-like, we require

$$\frac{g_{H_3 VV}^{\text{N2HDM}}}{g_{H VV}^{\text{sm}}} = 1 \quad \Rightarrow (-c_{\alpha_1} s_{\alpha_2} c_{\alpha_3} + s_{\alpha_1} s_{\alpha_3}) c_{\beta} - (c_{\alpha_1} s_{\alpha_3} + s_{\alpha_1} s_{\alpha_2} c_{\alpha_3}) s_{\beta} = 1 \quad (\text{C.114})$$

$$\Rightarrow -c_{\beta-\alpha_1} s_{\alpha_2} c_{\alpha_3} - s_{\alpha_3} s_{\beta-\alpha_1} = 1 \quad (\text{C.115})$$

leading to

$$S_3 = \left\{ \left\{ \alpha_3 = 0, \alpha_2 = \pi/2 \text{ and } \beta = \alpha_1 + \pi \right\} \text{ or } \left\{ \alpha_3 = \pm\pi/2 \text{ and } \beta = \alpha_1 \mp \pi/2 \right\} \right. \\ \left. \text{or } \left\{ \alpha_3 = 0, \alpha_2 = -\pi/2 \text{ and } \beta = \alpha_1 \right\} \right\} . \quad (\text{C.116})$$

In applying these solutions, we explicitly checked that the  $H_3$  couplings approach the alignment values.

## References

- [1] ATLAS Collaboration, G. Aad *et al.*, Phys.Lett. **B716**, 1 (2012), 1207.7214.
- [2] CMS Collaboration, S. Chatrchyan *et al.*, Phys.Lett. **B716**, 30 (2012), 1207.7235.
- [3] CMS, V. Khachatryan *et al.*, Phys. Rev. **D92**, 012004 (2015), 1411.3441.
- [4] CMS, V. Khachatryan *et al.*, Eur. Phys. J. **C75**, 212 (2015), 1412.8662.
- [5] ATLAS, G. Aad *et al.*, Eur. Phys. J. **C75**, 476 (2015), 1506.05669, [Erratum: Eur. Phys. J. **C76**, no.3, 152 (2016)].
- [6] ATLAS, G. Aad *et al.*, Eur. Phys. J. **C76**, 6 (2016), 1507.04548.
- [7] P. W. Higgs, Phys. Rev. Lett. **13**, 508 (1964).
- [8] F. Englert and R. Brout, Phys. Rev. Lett. **13**, 321 (1964).
- [9] G. S. Guralnik, C. R. Hagen, and T. W. B. Kibble, Phys. Rev. Lett. **13**, 585 (1964).
- [10] T. W. B. Kibble, Phys. Rev. **155**, 1554 (1967).
- [11] A. Djouadi, W. Kilian, M. Mühlleitner, and P. M. Zerwas, Eur. Phys. J. **C10**, 27 (1999), hep-ph/9903229.
- [12] A. Djouadi, W. Kilian, M. Mühlleitner, and P. M. Zerwas, Eur. Phys. J. **C10**, 45 (1999), hep-ph/9904287.
- [13] T. Hambye and M. H. G. Tytgat, Phys. Lett. B **659**, 651 (2008), 0707.0633.
- [14] E. Ma, Phys. Rev. D **73**, 077301 (2006), hep-ph/0601225.
- [15] N. G. Deshpande and E. Ma, Phys. Rev. **D18**, 2574 (1978).
- [16] G. Arcadi, A. Djouadi, and M. Raidal, Phys. Rept. **842**, 1 (2020), 1903.03616.
- [17] A. Drozd, B. Grzadkowski, J. F. Gunion, and Y. Jiang, JHEP **11**, 105 (2014), 1408.2106.
- [18] C.-Y. Chen, M. Freid, and M. Sher, Phys. Rev. **D89**, 075009 (2014), 1312.3949.
- [19] Y. Cai and T. Li, Phys. Rev. **D88**, 115004 (2013), 1308.5346.
- [20] P. Ko, Y. Omura, and C. Yu, JHEP **11**, 054 (2014), 1405.2138.
- [21] A. Arhrib, C. Boehm, E. Ma, and T.-C. Yuan, JCAP **04**, 049 (2016), 1512.08796.
- [22] A. Arhrib and M. Maniatis, Phys. Lett. B **796**, 15 (2019), 1807.03554.
- [23] A. D. Sakharov, Pisma Zh. Eksp. Teor. Fiz. **5**, 32 (1967), [Usp. Fiz. Nauk161,61(1991)].
- [24] J. Baglio *et al.*, JHEP **04**, 151 (2013), 1212.5581.
- [25] LHC Higgs Cross Section Working Group, D. de Florian *et al.*, (2016), 1610.07922.
- [26] J. Alison *et al.*, Rev. Phys. **5**, 100045 (2020), 1910.00012.

- [27] E. W. N. Glover and J. J. van der Bij, Nucl. Phys. **B309**, 282 (1988).
- [28] D. A. Dicus, C. Kao, and S. S. D. Willenbrock, Phys. Lett. B **203**, 457 (1988).
- [29] T. Plehn, M. Spira, and P. M. Zerwas, Nucl. Phys. **B479**, 46 (1996), hep-ph/9603205, [Erratum: Nucl. Phys. **B531**, 655 (1998)].
- [30] M. Grazzini *et al.*, JHEP **05**, 059 (2018), 1803.02463.
- [31] S. Dawson, S. Dittmaier, and M. Spira, Phys. Rev. **D58**, 115012 (1998), hep-ph/9805244.
- [32] J. Grigo, J. Hoff, K. Melnikov, and M. Steinhauser, Nucl. Phys. B **875**, 1 (2013), 1305.7340.
- [33] J. Grigo, J. Hoff, and M. Steinhauser, Nucl. Phys. B **900**, 412 (2015), 1508.00909.
- [34] R. Frederix *et al.*, Phys. Lett. B **732**, 142 (2014), 1401.7340.
- [35] F. Maltoni, E. Vryonidou, and M. Zaro, JHEP **11**, 079 (2014), 1408.6542.
- [36] S. Borowka *et al.*, Phys. Rev. Lett. **117**, 012001 (2016), 1604.06447, [Erratum: Phys. Rev. Lett. **117**, no.7, 079901 (2016)].
- [37] S. Borowka *et al.*, JHEP **10**, 107 (2016), 1608.04798.
- [38] J. Baglio *et al.*, Eur. Phys. J. C **79**, 459 (2019), 1811.05692.
- [39] J. Baglio *et al.*, JHEP **04**, 181 (2020), 2003.03227.
- [40] J. Baglio *et al.*, Phys. Rev. D **103**, 056002 (2021), 2008.11626.
- [41] R. Gröber, A. Maier, and T. Rauh, JHEP **03**, 020 (2018), 1709.07799.
- [42] R. Bonciani, G. Degrassi, P. P. Giardino, and R. Gröber, Phys. Rev. Lett. **121**, 162003 (2018), 1806.11564.
- [43] D. de Florian and J. Mazzitelli, Phys. Rev. Lett. **111**, 201801 (2013), 1309.6594.
- [44] J. Grigo, K. Melnikov, and M. Steinhauser, Nucl. Phys. B **888**, 17 (2014), 1408.2422.
- [45] J. Davies, F. Herren, G. Mishima, and M. Steinhauser, (2021), 2110.03697.
- [46] D. Y. Shao, C. S. Li, H. T. Li, and J. Wang, JHEP **07**, 169 (2013), 1301.1245.
- [47] D. de Florian and J. Mazzitelli, JHEP **09**, 053 (2015), 1505.07122.
- [48] P. Banerjee, S. Borowka, P. K. Dhani, T. Gehrmann, and V. Ravindran, JHEP **11**, 130 (2018), 1809.05388.
- [49] L.-B. Chen, H. T. Li, H.-S. Shao, and J. Wang, Phys. Lett. B **803**, 135292 (2020), 1909.06808.
- [50] L.-B. Chen, H. T. Li, H.-S. Shao, and J. Wang, JHEP **03**, 072 (2020), 1912.13001.
- [51] ATLAS Collaboration, ATLAS-CONF-2021-052.
- [52] CMS, A. M. Sirunyan *et al.*, JHEP **03**, 257 (2021), 2011.12373.

- [53] Y. Golfand and E. Likhtman, JETP Lett. **13**, 323 (1971).
- [54] D. Volkov and V. Akulov, Phys.Lett. **B46**, 109 (1973).
- [55] J. Wess and B. Zumino, Nucl. Phys. B **70**, 39 (1974).
- [56] P. Fayet, Nucl. Phys. **B90**, 104 (1975).
- [57] P. Fayet, Phys. Lett. B **69**, 489 (1977).
- [58] P. Fayet and S. Ferrara, Phys. Rept. **32**, 249 (1977).
- [59] H. P. Nilles, M. Srednicki, and D. Wyler, Phys. Lett. **120B**, 346 (1983).
- [60] H. P. Nilles, Phys. Rept. **110**, 1 (1984).
- [61] J. M. Frere, D. R. T. Jones, and S. Raby, Nucl. Phys. **B222**, 11 (1983).
- [62] J. P. Derendinger and C. A. Savoy, Nucl. Phys. **B237**, 307 (1984).
- [63] H. E. Haber and G. L. Kane, Phys.Rept. **117**, 75 (1985).
- [64] M. Sohnius, Phys.Rept. **128**, 39 (1985).
- [65] J. Gunion and H. E. Haber, Nucl.Phys. **B272**, 1 (1986).
- [66] J. Gunion and H. E. Haber, Nucl.Phys. **B278**, 449 (1986).
- [67] R. Barbieri, S. Ferrara, and C. A. Savoy, Phys. Lett. **119B**, 343 (1982).
- [68] M. Dine, W. Fischler, and M. Srednicki, Phys. Lett. **104B**, 199 (1981).
- [69] J. R. Ellis, J. F. Gunion, H. E. Haber, L. Roszkowski, and F. Zwirner, Phys. Rev. **D39**, 844 (1989).
- [70] M. Drees, Int. J. Mod. Phys. **A4**, 3635 (1989).
- [71] U. Ellwanger, M. Rausch de Traubenberg, and C. A. Savoy, Phys. Lett. **B315**, 331 (1993), hep-ph/9307322.
- [72] U. Ellwanger, M. Rausch de Traubenberg, and C. A. Savoy, Z. Phys. **C67**, 665 (1995), hep-ph/9502206.
- [73] U. Ellwanger, M. Rausch de Traubenberg, and C. A. Savoy, Nucl. Phys. **B492**, 21 (1997), hep-ph/9611251.
- [74] T. Elliott, S. F. King, and P. L. White, Phys. Lett. **B351**, 213 (1995), hep-ph/9406303.
- [75] S. F. King and P. L. White, Phys. Rev. **D52**, 4183 (1995), hep-ph/9505326.
- [76] F. Franke and H. Fraas, Int. J. Mod. Phys. **A12**, 479 (1997), hep-ph/9512366.
- [77] M. Maniatis, Int. J. Mod. Phys. **A25**, 3505 (2010), 0906.0777.
- [78] U. Ellwanger, C. Hugonie, and A. M. Teixeira, Phys. Rept. **496**, 1 (2010), 0910.1785.

- [79] P. Slavich *et al.*, Eur. Phys. J. C **81**, 450 (2021), 2012.15629.
- [80] T. D. Lee, Phys. Rev. **D8**, 1226 (1973).
- [81] G. C. Branco and M. N. Rebelo, Phys. Lett. B **160**, 117 (1985).
- [82] I. F. Ginzburg, M. Krawczyk, and P. Osland, Two Higgs doublet models with CP violation, in *Linear colliders. Proceedings, International Workshop on physics and experiments with future electron-positron linear colliders, LCWS 2002, Seogwipo, Jeju Island, Korea, August 26-30, 2002*, pp. 703–706, 2002, hep-ph/0211371, [,703(2002)].
- [83] W. Khater and P. Osland, Nucl. Phys. **B661**, 209 (2003), hep-ph/0302004.
- [84] D. Fontes *et al.*, JHEP **02**, 073 (2018), 1711.09419.
- [85] M. Mühlleitner, M. O. P. Sampaio, R. Santos, and J. Wittbrodt, JHEP **03**, 094 (2017), 1612.01309.
- [86] I. Engeln, M. Mühlleitner, and J. Wittbrodt, Comput. Phys. Commun. **234**, 256 (2019), 1805.00966.
- [87] A. Arhrib, R. Benbrik, C.-H. Chen, R. Guedes, and R. Santos, JHEP **08**, 035 (2009), 0906.0387.
- [88] A. Arhrib, R. Benbrik, J. El Falaki, and A. Jueid, JHEP **12**, 007 (2015), 1507.03630.
- [89] R. S. Gupta, H. Rzehak, and J. D. Wells, Phys. Rev. **D88**, 055024 (2013), 1305.6397.
- [90] B. Hespel, D. Lopez-Val, and E. Vryonidou, JHEP **09**, 124 (2014), 1407.0281.
- [91] J. Baglio, O. Eberhardt, U. Nierste, and M. Wiebusch, Phys. Rev. D **90**, 015008 (2014), 1403.1264.
- [92] C.-Y. Chen, S. Dawson, and I. M. Lewis, Phys. Rev. **D91**, 035015 (2015), 1410.5488.
- [93] S. Dawson, A. Ismail, and I. Low, Phys. Rev. D **91**, 115008 (2015), 1504.05596.
- [94] R. Costa, M. Mühlleitner, M. O. P. Sampaio, and R. Santos, JHEP **06**, 034 (2016), 1512.05355.
- [95] S. Dawson and I. M. Lewis, Phys. Rev. **D92**, 094023 (2015), 1508.05397.
- [96] F. Bojarski, G. Chalons, D. Lopez-Val, and T. Robens, JHEP **02**, 147 (2016), 1511.08120.
- [97] R. Grober, M. Mühlleitner, M. Spira, and J. Streicher, JHEP **09**, 092 (2015), 1504.06577.
- [98] A. Carvalho *et al.*, (2016), 1608.06578.
- [99] L. Bian and N. Chen, JHEP **09**, 069 (2016), 1607.02703.
- [100] R. Grober, M. Mühlleitner, and M. Spira, JHEP **06**, 080 (2016), 1602.05851.
- [101] M. Krause, M. Mühlleitner, R. Santos, and H. Ziesche, Phys. Rev. **D95**, 075019 (2017), 1609.04185.

- [102] S. Dawson and C. W. Murphy, Phys. Rev. D **96**, 015041 (2017), 1704.07851.
- [103] L. Di Luzio, R. Grober, and M. Spannowsky, (2017), 1704.02311.
- [104] I. M. Lewis and M. Sullivan, Phys. Rev. D **96**, 035037 (2017), 1701.08774.
- [105] P. Basler, M. Mühlleitner, and J. Wittbrodt, JHEP **03**, 061 (2018), 1711.04097.
- [106] R. Grober, M. Mühlleitner, and M. Spira, Nucl. Phys. B **925**, 1 (2017), 1705.05314.
- [107] G. Heinrich, S. P. Jones, M. Kerner, G. Luisoni, and E. Vryonidou, (2017), 1703.09252.
- [108] S. Dawson and M. Sullivan, Phys. Rev. D **97**, 015022 (2018), 1711.06683.
- [109] P. Basler, S. Dawson, C. Englert, and M. Mühlleitner, Phys. Rev. D **99**, 055048 (2019), 1812.03542.
- [110] K. S. Babu and S. Jana, JHEP **02**, 193 (2019), 1812.11943.
- [111] C.-R. Chen, Y.-X. Lin, V. Q. Tran, and T.-C. Yuan, Phys. Rev. D **99**, 075027 (2019), 1810.04837.
- [112] P. Basler, S. Dawson, C. Englert, and M. Mühlleitner, Phys. Rev. D **101**, 015019 (2020), 1909.09987.
- [113] L. Alasfar, R. Corral Lopez, and R. Gröber, JHEP **11**, 088 (2019), 1909.05279.
- [114] J. Chang, C.-R. Chen, and C.-W. Chiang, JHEP **03**, 137 (2017), 1701.06291.
- [115] T. Robens, T. Stefaniak, and J. Wittbrodt, Eur. Phys. J. C **80**, 151 (2020), 1908.08554.
- [116] A. Papaefstathiou, T. Robens, and G. Tetlalmatzi-Xolocotzi, JHEP **05**, 193 (2021), 2101.00037.
- [117] J. Park, J. Chang, K. Cheung, and J. S. Lee, Phys. Rev. D **102**, 073002 (2020), 2003.12281.
- [118] K. Cheung, A. Jueid, C.-T. Lu, J. Song, and Y. W. Yoon, Phys. Rev. D **103**, 015019 (2021), 2003.11043.
- [119] R. K. Barman, C. Englert, D. Gonçalves, and M. Spannowsky, Phys. Rev. D **102**, 055014 (2020), 2007.07295.
- [120] B. Das, S. Moretti, S. Munir, and P. Poullose, Eur. Phys. J. C **81**, 347 (2021), 2012.09587.
- [121] Q. Cao *et al.*, Phys.Lett. **B752**, 285-290 (2016), 1508.06512.
- [122] Q. Cao *et al.*, Phys. Rev. D **95**, 7 (2017), 1511.03311.
- [123] Q. Cao *et al.*, Phys. Rev. D **96**, 9 (2017), 1511.03311.
- [124] G. Li *et al.*, Phys. Lett. **B800**, 135070 (2020), 1511.03311.
- [125] G. Heinrich, S. P. Jones, M. Kerner, and L. Scyboz, JHEP **10**, 021 (2020), 2006.16877.
- [126] F. Arco, S. Heinemeyer, and M. J. Herrero, Eur. Phys. J. C **80**, 884 (2020), 2005.10576.

- [127] D. de Florian, I. Fabre, G. Heinrich, J. Mazzitelli, and L. Scyboz, (2021), 2106.14050.
- [128] F. Arco, S. Heinemeyer, and M. J. Herrero, Eur. Phys. J. C **81**, 913 (2021), 2106.11105.
- [129] J. Cao, Z. Heng, L. Shang, P. Wan, and J. M. Yang, JHEP **04**, 134 (2013), 1301.6437.
- [130] M. Brucherseifer, R. Gavin, and M. Spira, Phys. Rev. D **90**, 117701 (2014), 1309.3140.
- [131] D. T. Nhung, M. Muhlleitner, J. Streicher, and K. Walz, JHEP **11**, 181 (2013), 1306.3926.
- [132] U. Ellwanger, JHEP **08**, 077 (2013), 1306.5541.
- [133] J. Cao, D. Li, L. Shang, P. Wu, and Y. Zhang, JHEP **12**, 026 (2014), 1409.8431.
- [134] M. Muhlleitner, D. T. Nhung, and H. Ziesche, JHEP **12**, 034 (2015), 1506.03321.
- [135] Z. Heng, X. Gong, and H. Zhou, Chin. Phys. C **42**, 073103 (2018), 1805.01598.
- [136] S. Liebler, M. Muhlleitner, M. Spira, and M. Stadelmaier, Eur. Phys. J. C **79**, 65 (2019), 1810.10979.
- [137] S. Baum and N. R. Shah, JHEP **12**, 044 (2018), 1808.02667.
- [138] P. Huang and Y. H. Ng, Eur. Phys. J. Plus **135**, 660 (2020), 1910.13968.
- [139] U. Ellwanger and M. Rodriguez-Vazquez, JHEP **11**, 008 (2017), 1707.08522.
- [140] G. Chalons, A. Djouadi, and J. Quevillon, Phys. Lett. B **780**, 74 (2018), 1709.02332.
- [141] G. C. Branco *et al.*, Phys. Rept. **516**, 1 (2012), 1106.0034.
- [142] S. L. Glashow and S. Weinberg, Phys. Rev. **D15**, 1958 (1977).
- [143] A. W. El Kaffas, P. Osland, and O. M. Ogreid, Nonlin. Phenom. Complex Syst. **10**, 347 (2007), hep-ph/0702097.
- [144] J. E. Kim and H. P. Nilles, Phys. Lett. **138B**, 150 (1984).
- [145] A. Arhrib, Unitarity constraints on scalar parameters of the standard and two Higgs doublets model, in *Workshop on Noncommutative Geometry, Superstrings and Particle Physics*, 2000, hep-ph/0012353.
- [146] P. Basler, M. Krause, M. Muhlleitner, J. Wittbrodt, and A. Wlotzka, JHEP **02**, 121 (2017), 1612.04086.
- [147] M. Muhlleitner, M. O. P. Sampaio, R. Santos, and J. Wittbrodt, JHEP **08**, 132 (2017), 1703.07750.
- [148] A. Arhrib, R. Benbrik, M. El Kacimi, L. Rahili, and S. Semlali, Eur. Phys. J. C **80**, 13 (2020), 1811.12431.
- [149] D. Azevedo, P. Ferreira, M. M. Muhlleitner, R. Santos, and J. Wittbrodt, Phys. Rev. D **99**, 055013 (2019), 1808.00755.
- [150] R. Coimbra, M. O. P. Sampaio, and R. Santos, Eur. Phys. J. **C73**, 2428 (2013), 1301.2599.

- [151] R. Costa, R. Guedes, M. O. P. Sampaio, and R. Santos, SCANNERS project, 2014, <http://scanners.hepforge.org>.
- [152] M. Mühlleitner, M. O. P. Sampaio, R. Santos, and J. Wittbrodt, (2020), 2007.02985.
- [153] A. Barroso, P. M. Ferreira, I. P. Ivanov, and R. Santos, JHEP **06**, 045 (2013), 1303.5098.
- [154] I. P. Ivanov and J. P. Silva, Phys. Rev. **D92**, 055017 (2015), 1507.05100.
- [155] Gfitter Group, M. Baak *et al.*, Eur. Phys. J. **C74**, 3046 (2014), 1407.3792.
- [156] ATLAS, CMS, G. Aad *et al.*, Phys. Rev. Lett. **114**, 191803 (2015), 1503.07589.
- [157] P. Bechtle, S. Heinemeyer, O. Stål, T. Stefaniak, and G. Weiglein, Eur. Phys. J. **C74**, 2711 (2014), 1305.1933.
- [158] P. Bechtle, O. Brein, S. Heinemeyer, G. Weiglein, and K. E. Williams, Comput. Phys. Commun. **181**, 138 (2010), 0811.4169.
- [159] P. Bechtle, O. Brein, S. Heinemeyer, G. Weiglein, and K. E. Williams, Comput. Phys. Commun. **182**, 2605 (2011), 1102.1898.
- [160] P. Bechtle *et al.*, Eur. Phys. J. **C74**, 2693 (2014), 1311.0055.
- [161] ATLAS, G. Aad *et al.*, Eur. Phys. J. **C81**, 332 (2021), 2009.14791.
- [162] ATLAS collaboration, ATLAS-CONF-2020-037.
- [163] H. E. Haber and H. E. Logan, Phys. Rev. **D62**, 015011 (2000), hep-ph/9909335.
- [164] O. Deschamps *et al.*, Phys. Rev. **D82**, 073012 (2010), 0907.5135.
- [165] F. Mahmoudi and O. Stal, Phys. Rev. **D81**, 035016 (2010), 0907.1791.
- [166] T. Hermann, M. Misiak, and M. Steinhauser, JHEP **11**, 036 (2012), 1208.2788.
- [167] M. Misiak *et al.*, Phys. Rev. Lett. **114**, 221801 (2015), 1503.01789.
- [168] M. Misiak and M. Steinhauser, Eur. Phys. J. **C77**, 201 (2017), 1702.04571.
- [169] M. Misiak, A. Rehman, and M. Steinhauser, JHEP **06**, 175 (2020), 2002.01548.
- [170] S. Inoue, M. J. Ramsey-Musolf, and Y. Zhang, Phys. Rev. **D89**, 115023 (2014), 1403.4257.
- [171] ACME, J. Baron *et al.*, Science **343**, 269 (2014), 1310.7534.
- [172] J. Baglio *et al.*, Comput. Phys. Commun. **185**, 3372 (2014), 1312.4788.
- [173] S. F. King, M. Mühlleitner, R. Nevzorov, and K. Walz, Nucl. Phys. **B901**, 526 (2015), 1508.03255.
- [174] M. Mühlleitner, D. T. Nhung, H. Rzehak, and K. Walz, JHEP **05**, 128 (2015), 1412.0918.
- [175] T. N. Dao, R. Gröber, M. Krause, M. Mühlleitner, and H. Rzehak, JHEP **08**, 114 (2019), 1903.11358.

- [176] T. N. Dao, M. Gabelmann, M. Mühlleitner, and H. Rzehak, *JHEP* **09**, 193 (2021), 2106.06990.
- [177] ATLAS, ATL-PHYS-PUB-2021-019.
- [178] CMS, [https://twiki.cern.ch/twiki/bin/view/CMSPublic/PhysicsResultsSUS#Run\\_2\\_Summary\\_plots\\_13\\_TeV](https://twiki.cern.ch/twiki/bin/view/CMSPublic/PhysicsResultsSUS#Run_2_Summary_plots_13_TeV).
- [179] M. Spira, <http://tiger.web.psi.ch/proglist.html>.
- [180] S. Dulat *et al.*, *Phys. Rev. D* **93**, 033006 (2016), 1506.07443.
- [181] R. V. Harlander, S. Liebler, and H. Mantler, *Comput. Phys. Commun.* **184**, 1605 (2013), 1212.3249.
- [182] S. Liebler, *Eur. Phys. J. C* **75**, 210 (2015), 1502.07972.
- [183] R. V. Harlander, S. Liebler, and H. Mantler, *Comput. Phys. Commun.* **212**, 239 (2017), 1605.03190.
- [184] A. Djouadi, J. Kalinowski, and M. Spira, *Comput. Phys. Commun.* **108**, 56 (1998), hep-ph/9704448.
- [185] A. Djouadi, J. Kalinowski, M. Mühlleitner, and M. Spira, (2018), 1801.09506.
- [186] A. Djouadi, M. M. Mühlleitner, and M. Spira, *Acta Phys. Polon. B* **38**, 635 (2007), hep-ph/0609292.
- [187] ATLAS, M. Aaboud *et al.*, *JHEP* **01**, 030 (2019), 1804.06174.
- [188] ATLAS, M. Aaboud *et al.*, *Phys. Rev. Lett.* **121**, 191801 (2018), 1808.00336, [Erratum: *Phys.Rev.Lett.* 122, 089901 (2019)].
- [189] ATLAS, G. Aad *et al.*, *JHEP* **11**, 163 (2020), 2007.14811.
- [190] ATLAS, M. Aaboud *et al.*, *JHEP* **11**, 040 (2018), 1807.04873.
- [191] ATLAS, M. Aaboud *et al.*, *JHEP* **04**, 092 (2019), 1811.04671.
- [192] CMS, A. M. Sirunyan *et al.*, *Phys. Rev. D* **102**, 032003 (2020), 2006.06391.
- [193] ATLAS, M. Aaboud *et al.*, *Eur. Phys. J. C* **78**, 1007 (2018), 1807.08567.
- [194] ATLAS, M. Aaboud *et al.*, *JHEP* **05**, 124 (2019), 1811.11028.
- [195] CMS, A. M. Sirunyan *et al.*, *Phys. Rev. Lett.* **122**, 121803 (2019), 1811.09689.
- [196] ATLAS Collaboration, ATLAS-CONF-2021-035.
- [197] CMS Collaboration, CMS-PAS-B2G-20-004.
- [198] ATLAS Collaboration, ATLAS-CONF-2021-030.
- [199] ATLAS Collaboration, ATLAS-CONF-2021-016.
- [200] CMS, V. Khachatryan *et al.*, *Phys. Rev. D* **94**, 052012 (2016), 1603.06896.

- [201] CMS, A. M. Sirunyan *et al.*, JHEP **01**, 054 (2018), 1708.04188.
- [202] CMS Collaboration, CMS-PAS-HIG-17-008.
- [203] D. Fontes, J. C. Romão, R. Santos, and J. a. P. Silva, Phys. Rev. D **92**, 055014 (2015), 1506.06755.
- [204] ATLAS, G. Aad *et al.*, Phys. Rev. Lett. **125**, 061802 (2020), 2004.04545.
- [205] CMS, A. M. Sirunyan *et al.*, Phys. Rev. Lett. **125**, 061801 (2020), 2003.10866.
- [206] CMS, A. Tumasyan *et al.*, (2021), 2110.04836.
- [207] P. Z. Skands *et al.*, JHEP **07**, 036 (2004), hep-ph/0311123.
- [208] B. C. Allanach *et al.*, Comput. Phys. Commun. **180**, 8 (2009), 0801.0045.
- [209] L. Berthier and M. Trott, JHEP **05**, 024 (2015), 1502.02570.
- [210] M. Ghezzi, R. Gomez-Ambrosio, G. Passarino, and S. Uccirati, JHEP **07**, 175 (2015), 1505.03706.
- [211] I. Brivio and M. Trott, JHEP **07**, 148 (2017), 1701.06424, [Addendum: JHEP 05, 136 (2018)].
- [212] J. Ellis, C. W. Murphy, V. Sanz, and T. You, JHEP **06**, 146 (2018), 1803.03252.
- [213] F. Feruglio, Int. J. Mod. Phys. A **8**, 4937 (1993), hep-ph/9301281.
- [214] J. Bagger *et al.*, Phys. Rev. D **49**, 1246 (1994), hep-ph/9306256.
- [215] V. Koulovassilopoulos and R. S. Chivukula, Phys. Rev. D **50**, 3218 (1994), hep-ph/9312317.
- [216] C. P. Burgess, J. Matias, and M. Pospelov, Int. J. Mod. Phys. A **17**, 1841 (2002), hep-ph/9912459.
- [217] L.-M. Wang and Q. Wang, (2006), hep-ph/0605104.
- [218] B. Grinstein and M. Trott, Phys. Rev. D **76**, 073002 (2007), 0704.1505.
- [219] R. Contino, C. Grojean, M. Moretti, F. Piccinini, and R. Rattazzi, JHEP **05**, 089 (2010), 1002.1011.
- [220] R. Contino, The Higgs as a Composite Nambu-Goldstone Boson, in *Theoretical Advanced Study Institute in Elementary Particle Physics: Physics of the Large and the Small*, pp. 235–306, 2011, 1005.4269.
- [221] R. Alonso, M. B. Gavela, L. Merlo, S. Rigolin, and J. Yepes, Phys. Lett. B **722**, 330 (2013), 1212.3305, [Erratum: Phys.Lett.B 726, 926 (2013)].
- [222] G. Buchalla, O. Catà, and C. Krause, Nucl. Phys. B **880**, 552 (2014), 1307.5017, [Erratum: Nucl.Phys.B 913, 475–478 (2016)].
- [223] R. L. Delgado, A. Dobado, and F. J. Llanes-Estrada, JHEP **02**, 121 (2014), 1311.5993.

- [224] G. Buchalla, O. Catá, and C. Krause, Phys. Lett. B **731**, 80 (2014), 1312.5624.
- [225] G. Buchalla, O. Cata, A. Celis, and C. Krause, Eur. Phys. J. C **76**, 233 (2016), 1511.00988.
- [226] J. de Blas, O. Eberhardt, and C. Krause, JHEP **07**, 048 (2018), 1803.00939.
- [227] A. Crivellin, M. Ghezzi, and M. Procura, JHEP **09**, 160 (2016), 1608.00975.
- [228] S. De Curtis, L. Delle Rose, S. Moretti, and K. Yagyu, JHEP **12**, 051 (2018), 1810.06465.
- [229] S. De Curtis, S. Moretti, R. Nagai, and K. Yagyu, JHEP **10**, 040 (2021), 2107.08201.
- [230] A. Azatov, R. Contino, G. Panico, and M. Son, Phys. Rev. **D92**, 035001 (2015), 1502.00539.
- [231] R. Contino *et al.*, JHEP **08**, 154 (2012), 1205.5444.
- [232] C.-R. Chen and I. Low, Phys. Rev. D **90**, 013018 (2014), 1405.7040.
- [233] F. Goertz, A. Papaefstathiou, L. L. Yang, and J. Zurita, JHEP **04**, 167 (2015), 1410.3471.
- [234] L. Edelh user, A. Knochel, and T. Steeger, JHEP **11**, 062 (2015), 1503.05078.
- [235] D. de Florian, I. Fabre, and J. Mazzitelli, JHEP **10**, 215 (2017), 1704.05700.
- [236] G. Buchalla, M. Capozzi, A. Celis, G. Heinrich, and L. Scyboz, JHEP **09**, 057 (2018), 1806.05162.
- [237] P. Nason, JHEP **11**, 040 (2004), hep-ph/0409146.
- [238] S. Frixione, P. Nason, and C. Oleari, JHEP **11**, 070 (2007), 0709.2092.
- [239] S. Alioli, P. Nason, C. Oleari, and E. Re, JHEP **06**, 043 (2010), 1002.2581.
- [240] D. Fontes *et al.*, (2017), <http://porthos.tecnico.ulisboa.pt/arXiv/C2HDM/>.